Alaska Department of Transportation & Public Facilities

Research & Technology Transfer

Testing of Novel Technologies for Monitoring Aufeis Under Bridges in Alaska



Jack River Bridge near Cantwell, AK

Prepared by:
Jessica Cherry

Date: August 26, 2021

Prepared for:
Alaska Department of Transportation & Public Facilities
Statewide Research Office
3132 Channel Drive
Juneau, AK 99801-7898

Publication Number: FHWA-AK-RD-4000(182)

REPORT DOCUMENTATION PAGE	Form approved OMB No.

Public reporting for this collection of information is estimated to average 1 hour per response, including the time for reviewing instructions, searching existing data sources, gathering and maintaining the data needed, and completing and reviewing the collection of information. Send comments regarding this burden estimate or any other aspect of this collection of information, including suggestion for reducing this burden to Washington Headquarters Services, Directorate for Information Operations and Reports, 1215 Jefferson Davis Highway, Suite 1204, Arlington, VA 22202-4302, and to the Office of Management and Budget, Paperwork Reduction Project (0704-1833), Washington, DC 20503

1. AGENCY USE ONLY (LEAVE BLANK)	2. REPORT DATE	3. REPORT TYPE AND DATES COVERED
FHWA-AK-RD-4000(182)		5/15/19-6/30/21

4. TITLE AND SUBTITLE	5. FUNDING NUMBERS
Testing of Novel Technologies for Monitoring Aufeis Under Bridges in Alaska	ADN# 2598036, 2518036
6. AUTHOR(S) Cherry, Jessica	
7. PERFORMING ORGANIZATION NAME(S) AND ADDRESS(ES) Institute of Northern Engineering University of Alaska Fairbanks	8. PERFORMING ORGANIZATION REPORT NUMBER INE 21.01
9. SPONSORING/MONITORING AGENCY NAME(S) AND ADDRESS(ES) State of Alaska, Alaska Dept. of Transportation and Public Facilities Research and Technology Transfer 3132 Channel Drive Juneau, AK 99801-7898	10. SPONSORING/MONITORING AGENCY REPORT NUMBER FHWA-AK-RD-4000(182) HFHWY00124
11. SUPPLEMENTARY NOTES	
12a. DISTRIBUTION / AVAILABILITY STATEMENT No restrictions	12b. DISTRIBUTION CODE

13. ABSTRACT (Maximum 200 words)

This study evaluated multiple technologies for imaging aufeis features in the vicinity of bridge structures in Alaska. Aufeis is a layered ice feature formed from the freezing of successive flows of water over the top of previously formed ice. For this study, imagery was collected at twenty-one different bridge sites. An uncrewed aerial system (UAS), a crewed aircraft and camera, a handheld field camera, and a fixed field camera were all tested. No single technology was appropriate for all sites, but in general, the UAS was better for small creeks and the crewed aircraft was better for larger rivers. The crewed aircraft was more efficient at collecting a large number of sites in one day, while the UAS was better at seeing under the bridges (a data gap problem identified in the crewed aircraft dataset). The crewed aircraft had a larger operating range in terms of temperature and wind, while the UAS was limited in cold temperatures and high winds. The handheld field camera could capture significant detail, but with distorted optics. The fixed field camera was susceptible to moisture buildup that obscured the lens on many days. More research is recommended that investigates connections between groundwater, aufeis, and changes in sediment and scouring in the vicinity of bridges.

14- KEYWORDS: Aufeis, icings, groundwater, cold region hydrology, permafrost, ice effects on bridges	15. NUMBER OF PAGES
	16. PRICE CODE N/A

17. SECURITY CLASSIFICATION OF REPORT	18. SECURITY CLASSIFICATION OF THIS PAGE	19. SECURITY CLASSIFICATION OF ABSTRACT	20. LIMITATION OF ABSTRACT
Unclassified	Unclassified	Unclassified	N/A

NSN 7540-01-280-5500

STANDARD FORM 298 (Rev. 2-98) Prescribed by ANSI Std. 239-18 298-102

Notice

This document is disseminated under the sponsorship of the U.S. Department of Transportation in the interest of information exchange. The U.S. Government assumes no liability for the use of the information contained in this document. The U.S. Government does not endorse products or manufacturers. Trademarks or manufacturers' names appear in this report only because they are considered essential to the objective of the document.

Quality Assurance Statement

The Federal Highway Administration (FHWA) provides high-quality information to serve Government, industry, and the public in a manner that promotes public understanding. Standards and policies are used to ensure and maximize the quality, objectivity, utility, and integrity of its information. FHWA periodically reviews quality issues and adjusts its programs and processes to ensure continuous quality improvement.

Author's Disclaimer

This report reflects the views of the authors, who are responsible for the facts and the accuracy of the information presented herein. The information is disseminated under the sponsorship of one or more of the following agencies: U.S. Department of Transportation's University Transportation Centers Program, FHWA, University of Alaska Fairbanks, and/or the Alaska Department of Transportation and Public Facilities, in the interest of information exchange. The University of Alaska Fairbanks, the U.S. Government and matching sponsor(s) assume no liability for the contents or use thereof. Opinions and conclusions expressed or implied in the report are those of the author(s) and not necessarily those of the Alaska DOT&PF or funding agencies.

METRIC (SI*) CONVERSION FACTORS

APPROXIMATE CONVERSIONS TO SI UNITS

Symbol	When You Know	Multiply By	To Find	Symbol
		LENGTH		
in	inches	25.4		mm
ft	feet	0.3048		m
yd	yards	0.914		m
mi	Miles (statute)	1.61		km
		AREA		
in^2	square inches	645.2	millimeters squared	cm^2
ft^2	square feet	0.0929	meters squared	m^2
yd^2	square yards	0.836	meters squared	m^2
mi^2	square miles	2.59	kilometers squared	km^2
ac	acres	0.4046	hectares	ha
		MASS (weight)		
oz	Ounces (avdp)	28.35	grams	g
lb	Pounds (avdp)	0.454	kilograms	kg
T	Short tons (2000 lb)	0.907	megagrams	mg
		VOLUME		
fl oz	fluid ounces (US)	29.57	milliliters	mL
gal	Gallons (liq)	3.785	liters	liters
ft^3	cubic feet	0.0283	meters cubed	m^3
yd^3	cubic yards	0.765	meters cubed	m^3

Note: Volumes greater than 1000 L shall be shown in m^3

		TEMPERATURE (exact)		
ºF	Fahrenheit temperature	5/9 (ºF-32)	Celsius temperature	ºC
		ILLUMINATION		
fc	Foot-candles	10.76	lux	lx
fl	foot-lamberts	3.426	candela/m^2	cd/cm^2
		FORCE and PRESSURE or STRESS		
lbf	pound-force	4.45	newtons	N
psi	pound-force per square inch	6.89	kilopascals	kPa

//

These factors conform to the requirement of FHWA Order 5190.1A *SI is the symbol for the International System of Measurements

APPROXIMATE CONVERSIONS FROM SI UNITS

Symbol	When You Know	Multiply By	To Find	Symbol
		LENGTH		
mm	millimeters	0.039	inches	in
m	meters	3.28	feet	ft
m	meters	1.09	yards	yd
km	kilometers	0.621	Miles (statute)	mi
		AREA		
mm^2	millimeters squared	0.0016	square inches	in^2
m^2	meters squared	10.764	square feet	ft^2
km^2	kilometers squared	0.39	square miles	mi^2
ha	hectares (10,000 m^2)	2.471	acres	ac
		MASS (weight)		
g	grams	0.0353	Ounces (avdp)	oz
kg	kilograms	2.205	Pounds (avdp)	lb
mg	megagrams (1000 kg)	1.103	short tons	T
		VOLUME		
mL	milliliters	0.034	fluid ounces (US)	fl oz
liters	liters	0.264	Gallons (liq)	gal
m^3	meters cubed	35.315	cubic feet	ft^3
m^3	meters cubed	1.308	cubic yards	yd^3

		TEMPERATURE (exact)		
ºC	Celsius temperature	9/5 ºC+32	Fahrenheit temperature	ºF
		ILLUMINATION		
lx	lux	0.0929	foot-candles	fc
cd/cm^2	candela/m^2	0.2919	foot-lamberts	fl
		FORCE and PRESSURE or STRESS		
N	newtons	0.225	pound-force	lbf
kPa	kilopascals	0.145	pound-force per square inch	psi

Table of Contents

List of Figures v
List of Tables vi
Acknowledgments vi
Executive Summary vii
CHAPTER 1 – INTRODUCTION 1
1.1 Problem Statement and Motivation 1
1.2 Background 2
1.3 Objectives and Scope 8
1.4 Methodology 8
1.5 Detailed Case Study Site Maps 12
CHAPTER 2 – FINDINGS 17
2.1 Detailed Case Study Sites 17
2.2 Other Study Sites 27
CHAPTER 3 – INTERPRETATION, APPRAISAL, AND APPLICATIONS 31
CHAPTER 4 – CONCLUSIONS AND SUGGESTED RESEARCH 35
REFERENCES 37
APPENDIX A: Additional Images of Case Study Bridges
APPENDIX B: Sample Images of Other Bridges

List of Figures

Figure 1: Imagery-derived point clouds collected from crewed aircraft in a nadir configuration have a data gap under the bridges. 1
Figure 2: Numbered bridge sites in Interior and Southcentral Alaska that were flown with the UAS or imaged with field cameras. Findings for sites indicated in pink were chosen as a subset of case studies for detailed analysis. 2
Figure 3: Alaska's permafrost distributions from Callegary et al. (2013) based on Jorgenson et al. (2008). 5
Figure 4: Location of Alaska's current glaciers, maximum extent of Pleistocene glaciation, surficial unconsolidated material, and mountainous or hilly terrain with bedrock exposures and associated rubbly deposits (Arnold et al., 2008; Karlstrom, 1964), reproduced from Callegary et al. (2013). 6
Figure 5: Schematic representation of recharge and circulation of groundwater and the growth of aufeis. Reproduced from Clark and Lauriol (1997). 7
Figure 6: Satellite imagery of the Jack River near Cantwell, Alaska. 12
Figure 7: Hydrography of Jack River near Cantwell, Alaska. 12
Figure 8: Satellite image of O'Connor Creek north of Fairbanks, Alaska. 13
Figure 9: Hydrography of O'Connor Creek north of Fairbanks, Alaska. 13
Figure 10: Satellite image of the Robertson River near Dot Lake, Alaska. 14
Figure 11: Hydrography of the Robertson River near Dot Lake, Alaska. 14
Figure 12: Satellite image of Peters Creek near Chugiak, Alaska. 15
Figure 13: Hydrography of Peters Creek near Chugiak, Alaska. 15
Figure 14: Satellite image of Anchor River near Homer, Alaska. 16
Figure 15: Hydrography of Anchor River near Homer, Alaska. 16
Figure 16: Jack River detail of orthomosaic derived from UAS imagery collected in April 2020. 17
Figure 17: Jack River detail of orthomosaic derived from crewed aircraft collection in April 2017. 18
Figure 18: Jack River single frame from handheld field camera collected in April 2020. 18
Figure 19: O'Connor Creek orthomosaic derived from UAS collection in November 2020. 19
Figure 20: O'Connor Creek orthomosaic derived from UAS collection in March 2020. 20
Figure 21: O'Connor Creek point cloud from data collected by UAS in November 2020. 20
Figure 22: O'Connor Creek point cloud from data collected by UAS in March 2020. 21
Figure 23: O'Connor Creek orthomosaic from data collected by crewed aircraft in April 2019. 22
Figure 24: O'Connor Creek detail of orthomosaic from data collected by crewed aircraft in April 2019. 22
Figure 25: O'Connor Creek point cloud from data collected by crewed aircraft in April 2019. 23
Figure 26: Robertson River orthomosaic from UAS data collection in April 2020. 24
Figure 27: Robertson River point cloud detail from UAS data collection in April 2020. 24
Figure 28: Robertson River orthomosaic from imagery collected by crewed aircraft in April 2019. 25
Figure 29: Robertson River single frame from UAS collection in April 2020. 25

Figure 30: Peters Creek detail from orthomosaic of data collected by UAS in November 2020..... 26
Figure 31: Anchor River example of stationary mounted field camera..... 27

List of Tables

Table 1: Summary of bridge data collection dates..... 11

Acknowledgments

The author acknowledges the support of the Alaska Department of Transportation and Public Facilities (DOT&PF). Tim Smith collected much of the data from the uncrewed aerial system and handheld field camera during the start of the COVID-19 outbreak and patiently adapted to changing field safety protocols. Joan Welc-Lepain provided budgetary project administration at the University of Alaska Fairbanks (UAF). Fran Pedersen helped edit the report. Deb Gonzales oversaw contracting at UAF. DOT&PF program managers Anna Bosin, Ian Grant, and Shane Moller and technical advisor Michael Knapp provided oversight. Ryan Marlow and Jesse Escamilla organized the oral presentation within a great peer-exchange meeting of other bridge inspection experts.

Executive Summary

This study evaluated multiple technologies for imaging aufeis features in the vicinity of bridge structures in Alaska. Aufeis is a layered ice feature formed from the freezing of successive flows of water over the top of previously formed ice. For this study, imagery was collected at twenty-one different bridge sites in Alaska where aufeis buildup or other types of related flooding are common. An uncrewed aerial system (UAS), a crewed aircraft and camera, a handheld field camera, and a fixed field camera were all tested for their ability to characterize ice-bridge interaction and the presence of aufeis. No single technology was appropriate for all sites, but in general, the UAS was better for small creeks and the crewed aircraft was better for larger rivers. The crewed aircraft was more efficient at collecting a large number of sites in one day, while the UAS was better at seeing under bridges (a data gap problem identified in the crewed aircraft dataset). The crewed aircraft had a larger operating range in terms of temperature and wind, while the UAS was limited in cold temperatures and high winds. The handheld field camera could capture significant detail, but with distorted optics. The fixed field camera was susceptible to moisture buildup that obscured the lens on many days. More research is recommended to investigate connections between groundwater, aufeis, and changes in sediment and scouring in the vicinity of bridges. The author suggests that imagery is one of the more effective forms of data collection for aufeis, but whether the imagery is best collected with a crewed aircraft, a UAS, or fixed-or handheld field cameras depends on the river size and its location. The best time to collect imagery seems to be just prior to ice breakup, typically in mid- to late April, and overcast conditions are best for image quality. In situ instrumentation on the bridge or in the water could provide additional information on water temperatures, upwelling rates, or stresses on the bridge, but are highly susceptible to damage from ice.

CHAPTER 1 – INTRODUCTION

1.1 Problem Statement and Motivation

Prior to the start of this project, several years of data were collected for DOT&PF to monitor the relationship between bridge structures and abutments, and underlying aufeis. Aufeis is a layered ice feature formed from the freezing of successive flows of water over the top of previously formed ice. It is found in rivers and streams in Alaska and other cold regions. Aufeis can form naturally from the upwelling of groundwater in winter, but it may also form when bridge structures such as piles and piers block subsurface flow. Aufeis can be stronger than some other river ice features and may exert forces on bridge and road infrastructure.

The data shown in Figure 1 is an example of what was acquired with crewed aircraft shooting straight downward from about 1000 feet above a bridge. Many single frame photos of each bridge were processed into elevation point-cloud datasets, from which elevation profiles of the river ice both upstream and downstream of the bridge can be extracted, as well as digital surface models and orthomosaics. These data collected by the crewed aircraft in a nadir position, although valuable for learning more about the impact of aufeis on bridges, are unable to capture conditions directly under a bridge: the bridge deck simply blocks this area of the image. Filling in that data gap is one problem addressed by this project, as well as the larger objective of determining optimal technologies for aufeis monitoring.

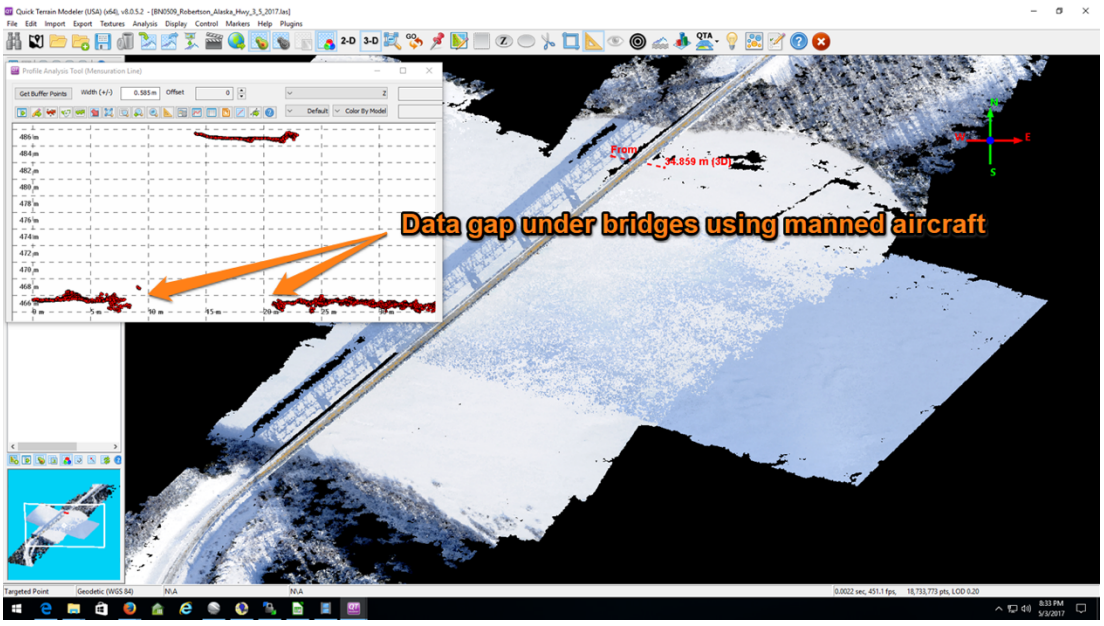

Figure 1: Imagery-derived point clouds collected from crewed aircraft in a nadir configuration have a data gap under the bridges.

This new research project uses multiple photographic methods from the ground and an uncrewed aerial system (UAS) to capture imagery of the direct contact between ice and structures underlying a selection of aufeis-prone bridges in Alaska, shown in Figure 2. The older data from the crewed aircraft were compared to data collected by UAS and mounted and handheld field cameras. Besides the identification of potential aufeis forces on bridge structures, this work is important because

bridge decks, in addition to blocking imagery collection from a plane, also intercept snow and light, creating an insulation factor that differs from conditions upstream or downstream of the bridge. The piers, abutments, or other structures of the bridge may cause changes in sedimentation, channel dynamics, and groundwater flow. Furthermore, a bridge pier can have a thermodynamic effect on the ice around it. None of these phenomena are fully captured from the nadir crewed aircraft aerial photography collected in 2016–2019. Exploring the best solutions for imaging under a bridge will benefit these other research topics as well.



Figure 2: Numbered bridge sites in Interior and Southcentral Alaska that were flown with the UAS or imaged with field cameras. Findings for sites indicated in pink were chosen as a subset of case studies for detailed analysis.

1.2 Background

The National Research Council of Canada defines aufeis as a “sheet-like mass of layered ice formed on the ground surface, or on river or lake ice, by freezing of successive flows of water that may seep from the ground, flow from a spring or emerge from below river ice through fractures”

(Daly, 2017). Aufeis is a German term for what is called a "naled" in Russian. In Alaska, aufeis is also called overflow, and liquid water may be present, even in very cold conditions, since it is derived from warm subsurface sources. The term aufeis or "icing" refers to not just the formation process, but the resulting body of ice as well (Harden et al., 1977). The required components for formation are a source of flowing water beneath a frozen surface and a barrier to flow of water that causes upwelling to the surface.

Bridge piers and abutments are locations where this liquid/solid water interaction may influence a structure's integrity and lead to an ice height and pressure gradient upstream and downstream of a bridge. However, little research or monitoring of bridge/aufeis interactions has been conducted in Alaska, which was the motivation behind commissioning monitoring with crewed aircraft. The proposed research would seek out the best technology for monitoring ice conditions under bridges and against piers and abutments.

Over the past decade or so, the science of photogrammetry has changed considerably. Digital single lens reflex (DSLR) cameras have replaced large format aerial film cameras, and new computer vision software techniques have enabled the processing of overlapping images into point clouds and three-dimensional surfaces. These same software techniques, known as structure from motion (SfM), can be used to create similar imagery and models from uncrewed aerial systems and side-by-side field cameras. Crewed aircraft can also be used to create under-bridge models, if flown low with the photographer shooting out the side window, as opposed to 1000 feet above the bridge. It is anticipated that each of these various methods will have pros and cons and be matched better at some types of bridges and settings than others.

We know little about aufeis in Alaska and the circumpolar north. In fact, what we know about groundwater in Alaska is also quite limited. Work by Harden et al. (1977) describes the distribution and properties of aufeis formation on Alaska's North Slope. Aufeis there tends to form in the same places from year to year. The formation of aufeis can also be related to changes in stream gradients, or changes in soils or soil permeability (Harden et al., 1977), which could include permafrost. The characteristically wide nature of arctic rivers relates to water flowing around in-place ice features like aufeis, which can grow as thick as 5–6 meters. Aufeis formations can link directly to flooding by ice damming during breakup, and moving sediment may cause further changes (Turcotte et al., 2017).

Harden et al. (1977) describe climate as a controlling factor for variability in aufeis formation, particularly the preceding summer precipitation leading into freeze-up. Snow depth and its insulating power in early winter may also have an effect. These authors show the co-location of springs on the North Slope with areas of aufeis formation suggesting that in areas of continuous permafrost distribution, springs are a likely source of water for aufeis in this region. Veillette and Thomas (1978) published a study of sites in Keewatin, Nunavut, Canada. They also conclude that source waters are likely spring fed from taliks (voids) in the otherwise continuous permafrost.

Kane (1981) studied the aufeis growth mechanics of a small, subarctic research watershed just north of Fairbanks, Alaska, as well as at Goldstream Creek near the University of Alaska Fairbanks. There, direct measurements of pore water pressure showed that the source water for aufeis formation was groundwater below the permafrost or from non-permafrost regions: source water was not from moisture in the local soil active layer. One exception to this is when the slope

adjacent to the stream is quite steep. However, this study was performed at two small creeks surrounded by boreal forest, not the wide-open tundra of the Arctic Coastal Plain. Yoshikawa et al. (2007) focused their study on the Brooks Range and concluded that the most productive source water springs for aufeis were associated with limestone areas in the foothills, in a region of glacial morphology. Clark and Lauriol (1997) made an earlier geochemical study showing similar results in the Firth River Basin in northern Yukon, Canada: aufeis source water tends to come from deep taliks, not the annual layer of freeze-thaw in soil.

While Yoshikawa et al. (2007) examined synthetic aperture radar data from 1996–2005 and found no trend in aufeis development on the Kuparuk River during that period, Pavelsky and Zarnetske (2017) reported a rapid decline in aufeis detected in Arctic Alaska from NASA's Moderate Resolution Imaging Spectrometer (MODIS) over the period 2000–2015. It could be that there was a step-change in climate conditions during that period, but more likely the larger study area covered by Pavelsky and Zarnetske (2017) was the more significant factor.

Of these studies cited above, none occurred south of the Alaska Range. For an understanding of aufeis there, we must look to a broader view of groundwater, permafrost, and soil properties in that region. Callegary et al. (2013) provide a convenient and relatively recent review of what is known about groundwater in Alaska. Figure 3 is reproduced from their study based on the permafrost map by Jorgenson (2008). The field sites covered by UAS data collection for the present study were characterized by discontinuous, sporadic, and isolated permafrost areas, unlike most field sites studied in the literature cited above, from the continuous permafrost part of the state.

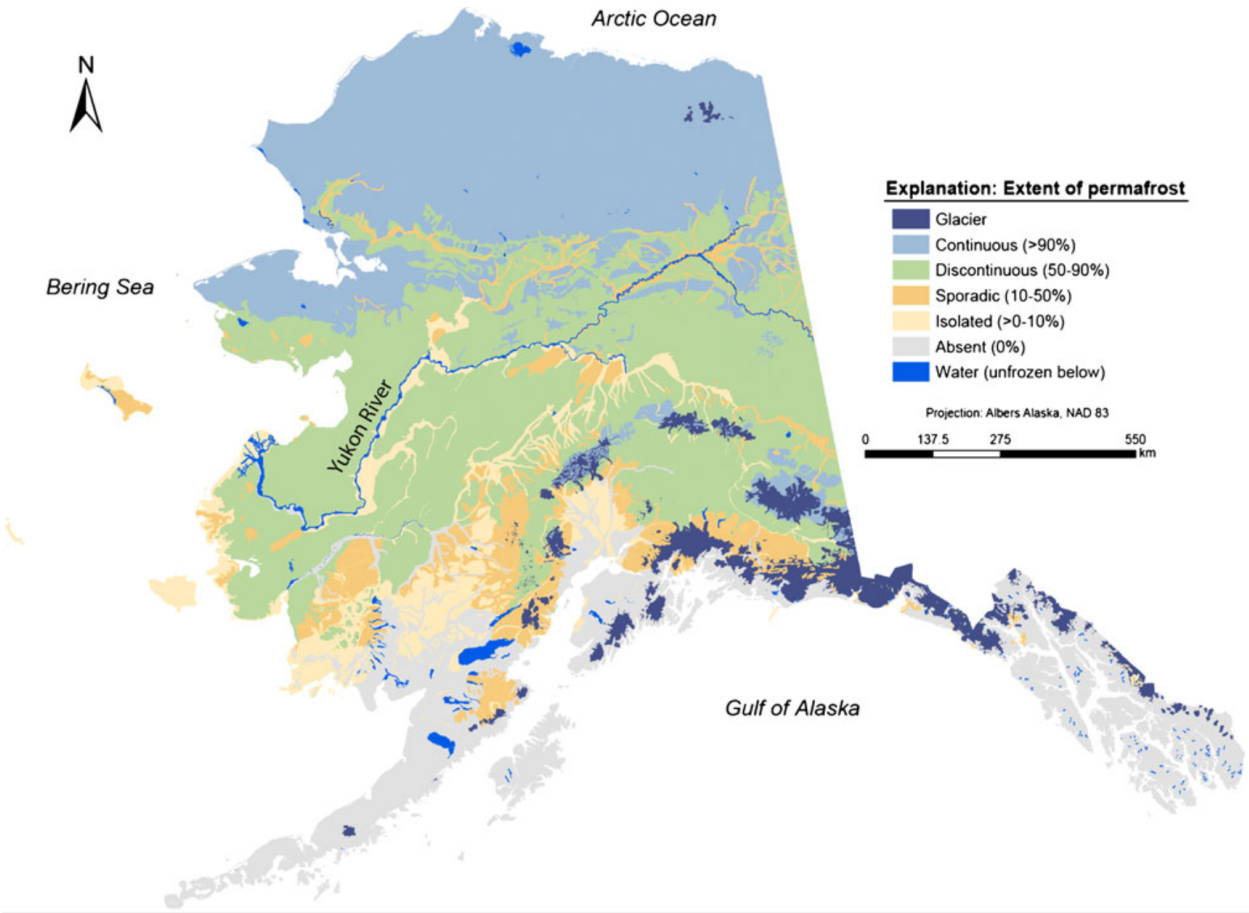

Figure 3: Alaska's permafrost distributions from Callegary et al. (2013) based on Jorgenson et al. (2008).

Figure 4 shows a map of broad characteristics of Alaska's surface geology, from Callegary et al. (2013). According to the map, all study sites included in this project could be characterized as having unconsolidated material flanked by moderate to steep mountainous areas. Our study sites vary as to whether they were glaciated during the Pleistocene, but the aufeis formation mechanism described by Clark and Lauriol (1997) is possible at all sites. A schematic of this is shown in Figure 5. Where sites lack limestone karst geology or taliks, other types of voids such as within unconsolidated gravels—many of which are glacial alluvium—provide ample openings for groundwater recharge. Of course, frozen ground is only one type of barrier that can generate aufeis. Others could include rock, transient tree litter, and bridge piles and piers.

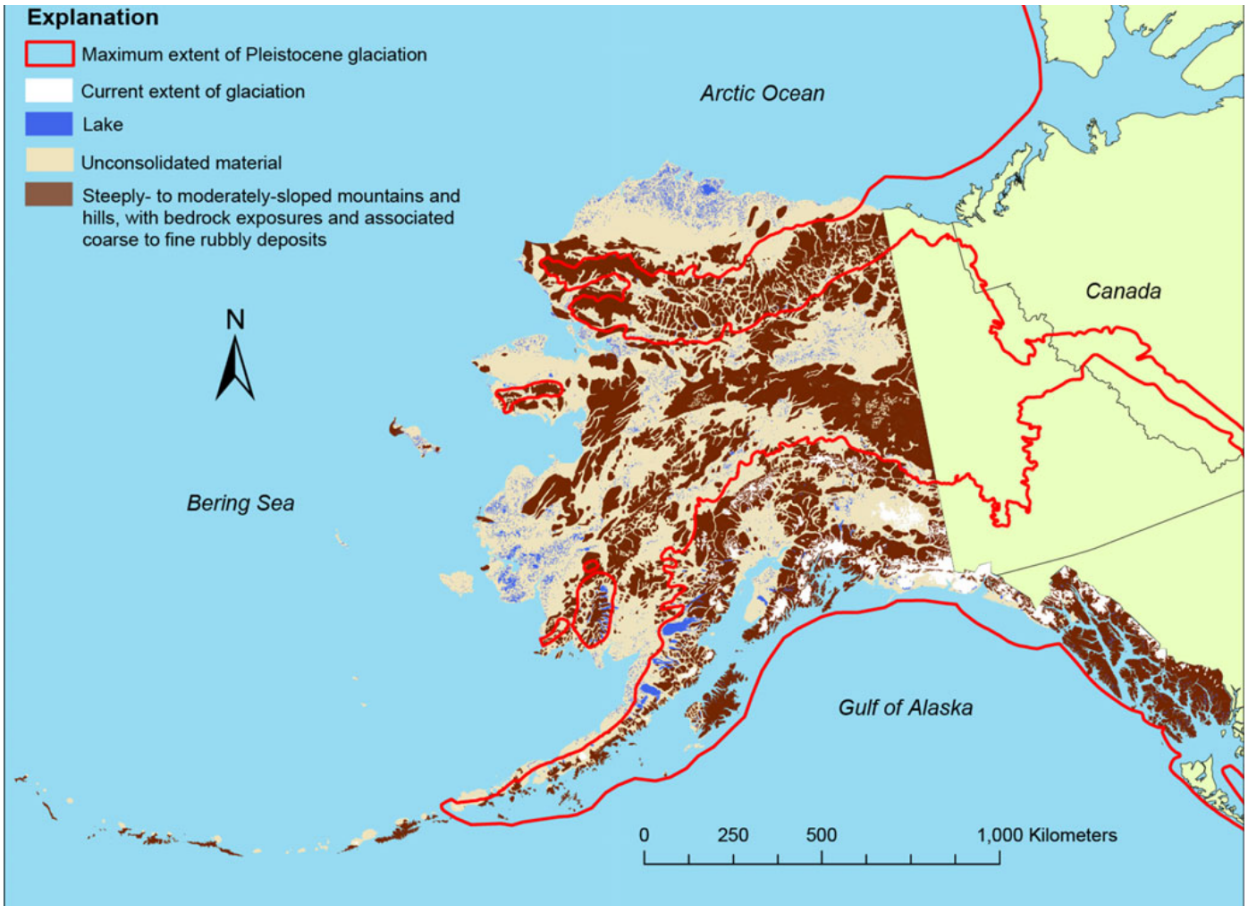

Figure 4: Location of Alaska's current glaciers, maximum extent of Pleistocene glaciation, surficial unconsolidated material, and mountainous or hilly terrain with bedrock exposures and associated rubbly deposits (Arnold et al., 2008; Karlstrom, 1964), reproduced from Callegary et al. (2013).

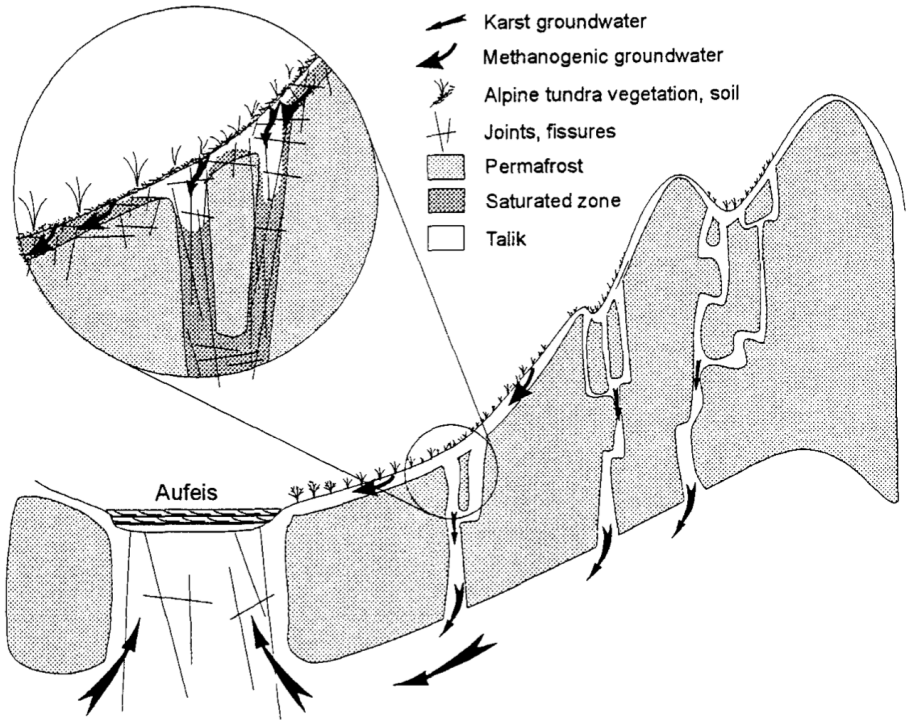

Figure 5: Schematic representation of recharge and circulation of groundwater and the growth of aufeis. Reproduced from Clark and Lauriol (1997).

The literature with respect to aufeis modeling generally falls into early mathematical approaches—largely from Russia including Korzhavin (1962) and discussed by Carey et al. (1975) and Yoshikawa et al. (2008)—and more recent approaches involving adaption of modern hydraulic models. The approach used by Zufelt et al. (2006) is an example of the latter, applied to the Jarvis Creek aufeis field in Alaska's Interior. That study was performed simply to estimate potential flood zones for military land use and did not focus on impacts on the Jarvis Creek Bridge, which is a considerable distance downstream.

While there are studies such as Beltaos et al. (2003) that discuss hydraulic interactions between ice and bridges, they do not focus on aufeis in particular. Still, some of the findings are relevant. For example, those authors discuss possible effects during river breakup: "horizontal and vertical ice forces can damage piers, while local scour can undermine a pier and cause it to fail." There is certainly a need for an appropriate expert to study the exact forces at play on, say, bridge piers and how the forces of aufeis and ice formed by simply freezing over differ. Due to the laminated structure of aufeis and its ongoing thickening throughout winter, there are reasons to believe that aufeis might be stronger than river ice formed during a single freezing event. It could be that the dataset generated by the present study is useful for that effort. Detailed measurement of sediment change and scouring related to aufeis could also be valuable for understanding whether aufeis transports sediment in a different manner from other types of river ice. Hains and Zabilansky (2006) and Zabilansky et al. (2006) describe how ice contributes to bed scour and how that can lead to bridge failure.

In terms of engineering mitigation studies, Carey et al. (1975) recognized the problem of aufeis formation at stream crossings and performed studies during the 1960s and 1970s on various mitigation techniques for culvert icings, such as electrically heated cables, channel covers, and channel improvements. The prevailing approach with the DOT&PF since that period has been to use steaming pipes to clear winter ice buildup in culverts and at smaller bridges, whether or not that ice is groundwater derived.

1.3 Objectives and Scope

The objectives of this study were to evaluate several different techniques for capturing imagery under bridges in Alaska during the cold season to see how well they could identify potential interaction between groundwater processes and structures, under and around the bridge. These techniques included imagery from UAS, rugged field cameras, and crewed aircraft collections. To meet these objectives, the specific tasks laid out in the project proposal were as follows:

Task 1: Conduct background research on appropriate UAS and payload, procure and test
Task 2: Design and procure in-situ field camera system
Task 3: Collect and process oblique data from crewed aircraft
Task 4: Deploy in-situ field camera system, collect and process data
Task 5: Train on the UAS, deploy the UAS to field sites, collect and process data
Task 6: Write intermediate and final reports comparing these methods
Task 7: Make presentation or conduct mini-workshop on "cold season use of UAS in Alaska"

The outcomes of these specific tasks are described in the following Methodology sub-section, and the results and analysis of the data collected are presented in Chapter 2 – Findings.

1.4 Methodology

At the start of the crewed aircraft data collection (a separately funded project), DOT&PF technical advisor Michael Knapp provided a list of bridges susceptible to aufeis formation. A subset of these was chosen based on available aviation fuel and a logistical loop that could be completed in two days. In the present project, as many of those same sites were re-occupied with the UAS and/or field cameras if and when it was safe to operate at these sites. A lack of pedestrian walkways, declining light conditions, cold temperatures limiting battery life, and other logistical concerns guided the site choices. Some very wide rivers were too far for the UAS to fly in cold temperatures and some very small creeks were too narrow or far off the flight path to capture with the crewed aircraft.

Task 1: Conduct background research on appropriate UAS and payload, procure and test

Project team members Cherry and Smith performed a market analysis in 2019 of available systems and chose the DJI Mavic 2 Zoom for its affordability and ease of use. Cherry and Smith examined another system, Skydio, but the system was extremely difficult to procure at that time. While the Mavic 2 Zoom does not have a survey-grade kinematic GPS, we found it to be a reliable and robust tool for this project, flying during Alaska's cold season.

Task 2: Design and procure in-situ field camera system

We evaluated several field cameras for properties such as durability in weather, heating, power consumption, connection to communication systems (cellular and satellite). Due to the constraints on fieldwork during the COVID-19 pandemic, we ended up using data from an existing camera on the Anchor River, as well as from a handheld field camera on an extendable monopod. The camera on the Anchor River was a Moultrie Wingscapes TimelapseCam Pro managed by a partnership between Cook Inletkeeper and the National Weather Service. In January 2021, this camera was removed and later replaced by DOT&PF's own EarthCam to oversee construction on the new Anchor River Bridge on the Old Sterling Highway. The handheld field camera was a GoPro 7. The changes to this task were reflected in the approved re-budget requests.

Task 3: Collect and process oblique data from crewed aircraft

Due to the fieldwork constraints during the COVID-19 pandemic and the challenge of a pilot and a photographer sharing a cockpit prior to the development of the vaccine, the existing nadir data from the crewed aircraft was mined for evidence of aufeis around bridge structures. This decision turned out to be a productive use of the existing data: many such features were identified. The camera used was a Nikon D3s, and the DGPS system was a Trimble NetR9. The change to this task was reflected in the approved re-budget requests.

Task 4: Deploy in-situ field camera system, collect and process data

Data from the existing webcam at Anchor River was downloaded and analyzed, and the handheld field camera was used in conjunction with the UAS acquisitions described in Task 5. Single frame shots were used from the GoPro, and many of the scenes were also processed using the same techniques used on the UAS data.

Task 5: Train on the UAS, deploy the UAS to field sites, collect and process data

After initial training, fieldwork efforts were focused on this UAS data collection task, and much more data were collected than originally planned. Nearly every bridge was imaged which also appeared in the longer-term data collected by the crewed aircraft team during the 2016–2019 project period. Many bridges were imaged more than once, showing the river ice in varying conditions around the bridge structures. Table 1 shows a summary of the collection times for data from the UAS, handheld field camera, and crewed aircraft. These data were then processed with the SfM technique, which uses computer vision and tie points between overlapping image frames to generate a three-dimensional point cloud. Different processing software was tested including Agisoft Metashape, Pix4D, and Bentley. Ultimately, Agisoft Metashape was used to process all the data into a sparse point cloud, a dense point cloud, a digital surface model, and an orthomosaic. The single frames, dense point clouds, and orthomosaics were used to describe the findings in this report. The field sites flown are shown in Figure 2.

Task 6: Write intermediate and final reports comparing these methods

Quarterly reports were submitted throughout the project period. The present report is the final product of our efforts.

Task 7: Make presentation or conduct mini-workshop on "cold season use of UAS in Alaska"

Cherry presented the project findings during a peer-exchange workshop organized by DOT&PF during February 2021. The recording and slide deck from this meeting are available to agency employees and partners who could not attend.

DOT Aufeis Photo Record																						
		UAS					Handheld field camera					Crewed Aircraft										
		2019		2020			2019		2020			2016		2017				2018		2019		
		Oct/Nov	Dec19/Jan20	Mar	Apr	Nov	Oct	Nov	Mar	Apr	Oct	Dec	Mar	Apr	Oct	Nov	Mar	Apr	Mar	Apr	Oct
Site																						
BN0302	Jack River nr Cantwell			Y	Y				Y	Y	Y	Y*		Y		Y	Y	Y			
BN0303	O'Conner Crk nr Goldstream Valley	Y		Y					Y		Y	Y	Y	Y	Y		Y	Y	Y	Y	Y
BN0509	Robertson River on Alaska Hwy				Y						Y	Y	Y	Y		Y	Y	Y	Y*	Y	
BN0518	Johnson River on Alaska Hwy				Y						Y		Y	Y		Y	Y	Y	Y	Y	
BN0520	Gerstle River on Alaska Hwy				Y						Y	Y	Y	Y	Y	Y	Y	Y	Y	Y	
BN0526	Banner Crk on Richardson Hwy				Y			Y		Y	Y	Y	Y	Y	Y	Y	Y			Y	
BN0574	Gulkana			Y	Y				Y		Y	Y		Y		Y	Y	Y			
BN0590	Gunnysack Creek on Richardson				Y			Y	Y	Y	Y			Y							
BN0594	Ruby Creek on Richardson Hwy				Y			Y		Y	Y	Y*	Y*								
BN0595	Jarvis Creek								Y	Y	Y	Y	Y	Y	Y		Y	Y	Y	Y	
BN0646	Gakona	Y			Y			Y			Y	Y		Y		Y	Y	Y			
BN0648	Sinona Creek Tok Cutoff				Y					Y						Y	Y	Y			
BN0663	Tok River				Y					Y	Y	Y*		Y			Y	Y			
BN0690	Seattle Cr Denali Hwy				Y					Y	Y	Y		Y		Y	Y	Y			
BN0693	Carlo Creek Parks Hwy			Y	Y				Y	Y	Y	Y		Y		Y*	Y	Y			
BN0697	Kingfisher Creek Parks Hwy			Y	Y				Y	Y				Y		Y	Y	Y			
BN1009	Goldstream Creek at Ballaine			Y				Y	Y		Y	Y	Y	Y	Y		Y	Y	Y	Y	Y
BN1075	Dragonfly Creek Parks			Y	Y				Y	Y				Y			Y				
BN1144	Fox Creek Parks			Y	Y				Y	Y						Y					
BN1250	Tulsona Creek Tok Cutoff	Y			Y			Y		Y	Y			Y		Y	Y	Y			
BN1031	Peters Creek at Stoltze	M	M			M	Y														

Table 1: Summary of bridge data collection dates. "Y" indicates that images were collected and processed into an orthomosaic. "Y*" indicates that images were collected but not processed into an ortho (typically because not enough overlap or sidelap), and "M" indicates images were collected on multiple dates in this month. "Y" for the handheld field cameras indicates that images were collected, but most were not processed all the way into orthomosaics because of lens distortion.

1.5 Detailed Case Study Site Maps

Jack River Bridge on the Parks Highway near Cantwell (BN0302)

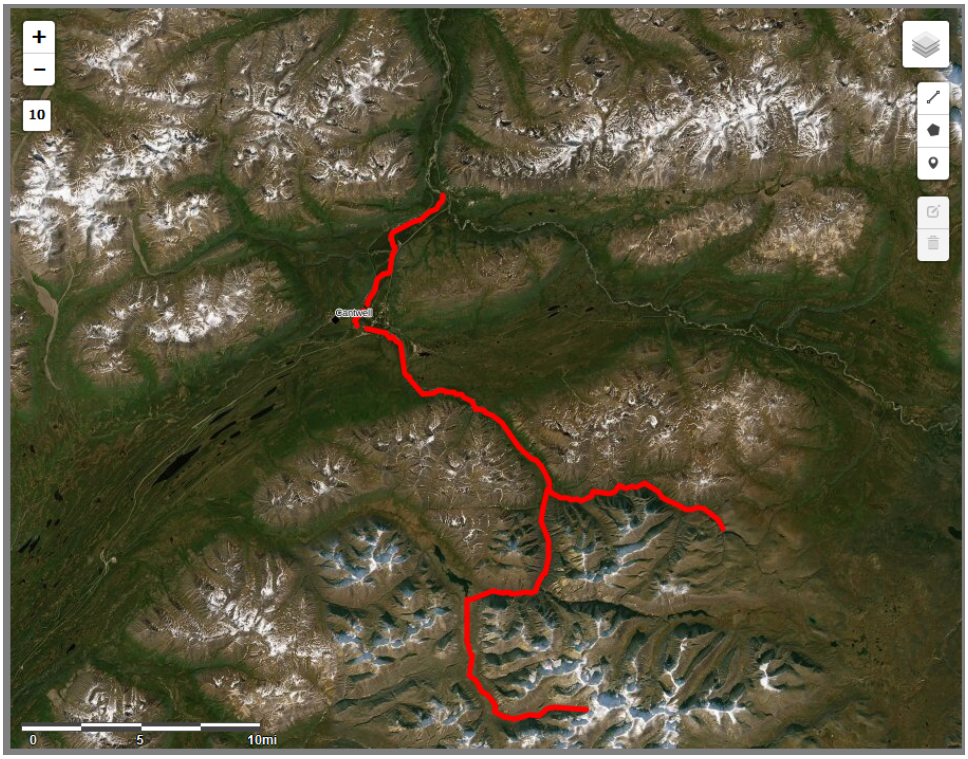

Figure 6: Satellite imagery of the Jack River near Cantwell, Alaska.

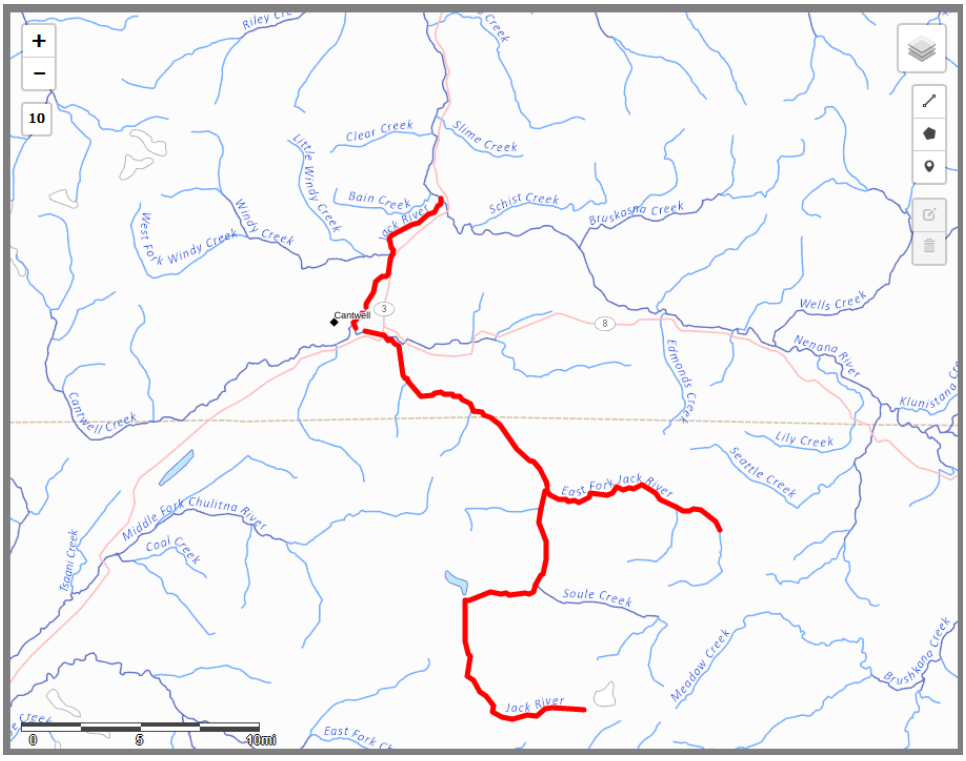

Figure 7: Hydrography of Jack River near Cantwell, Alaska.

O'Connor Creek Bridge on Goldstream Road near Fairbanks (BN0303)



Figure 8: Satellite image of O'Connor Creek north of Fairbanks, Alaska.

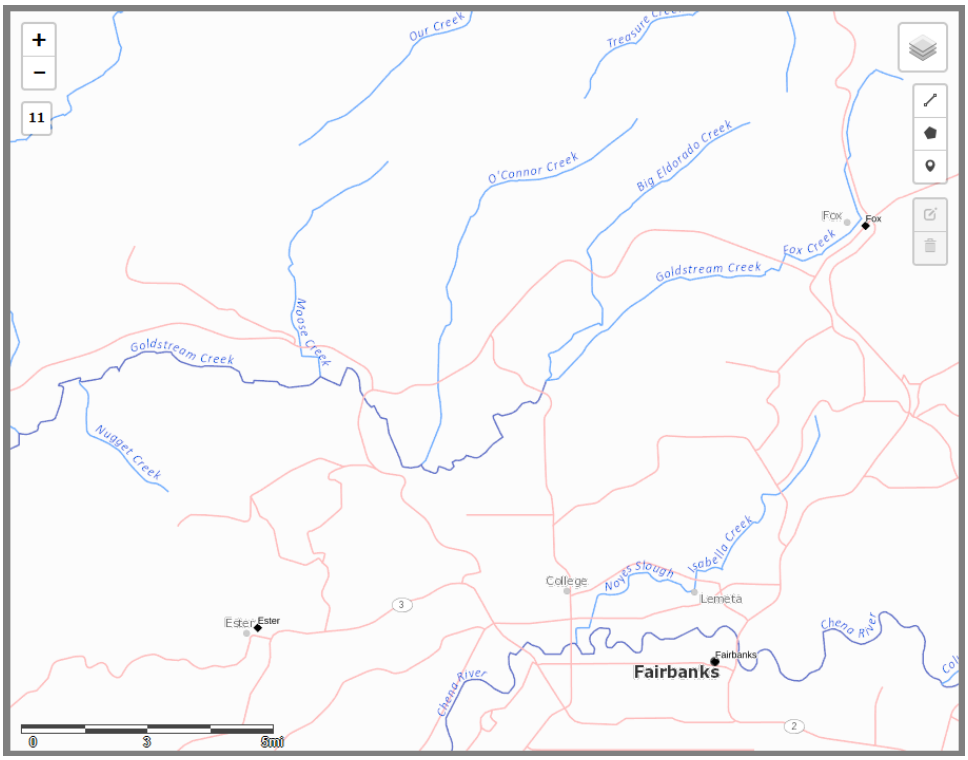

Figure 9: Hydrography of O'Connor Creek north of Fairbanks, Alaska.

Robertson River Bridge on the Alaska Highway near Dot Lake (BN0509)

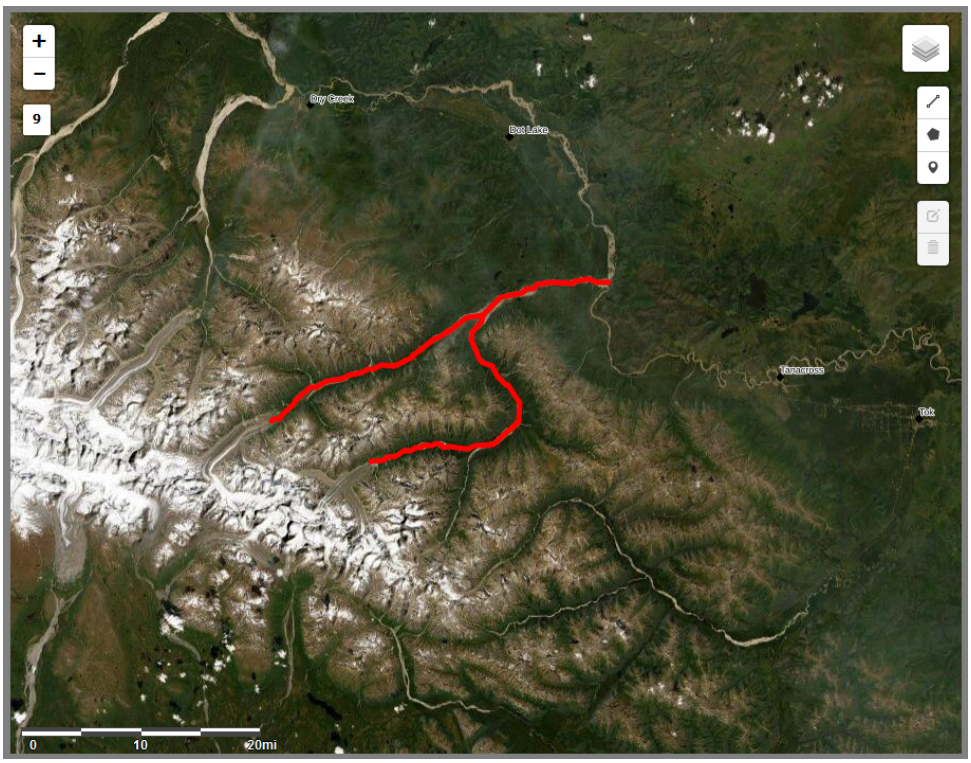

Figure 10: Satellite image of the Robertson River near Dot Lake, Alaska.

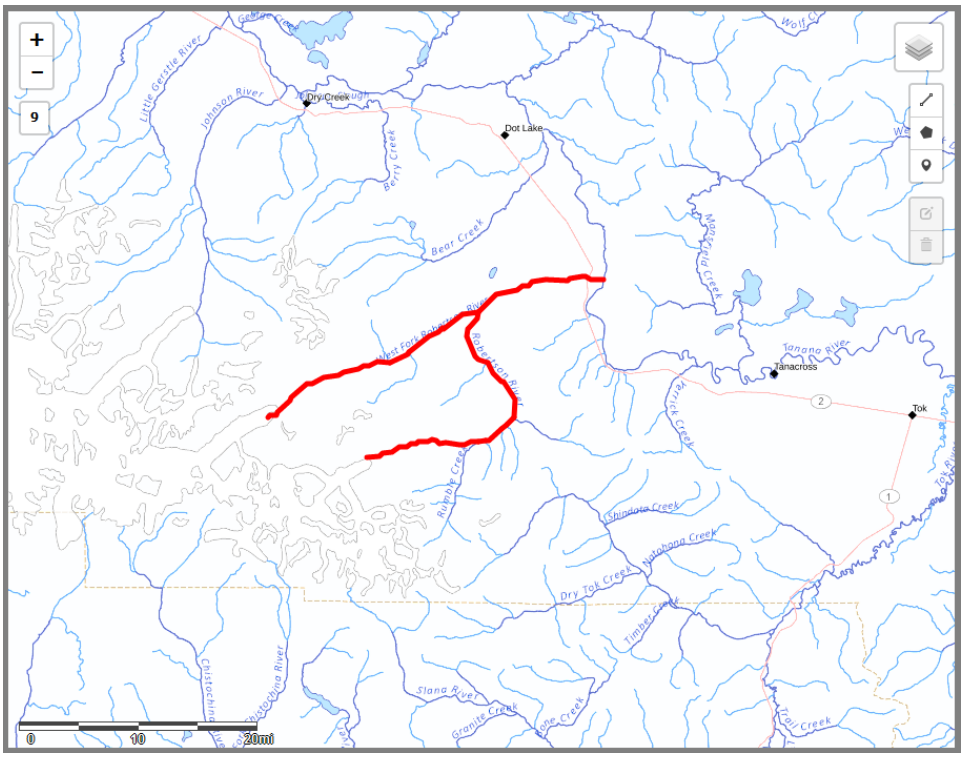

Figure 11: Hydrography of the Robertson River near Dot Lake, Alaska.

Peters Creek at Stoltze Road (BN1031)

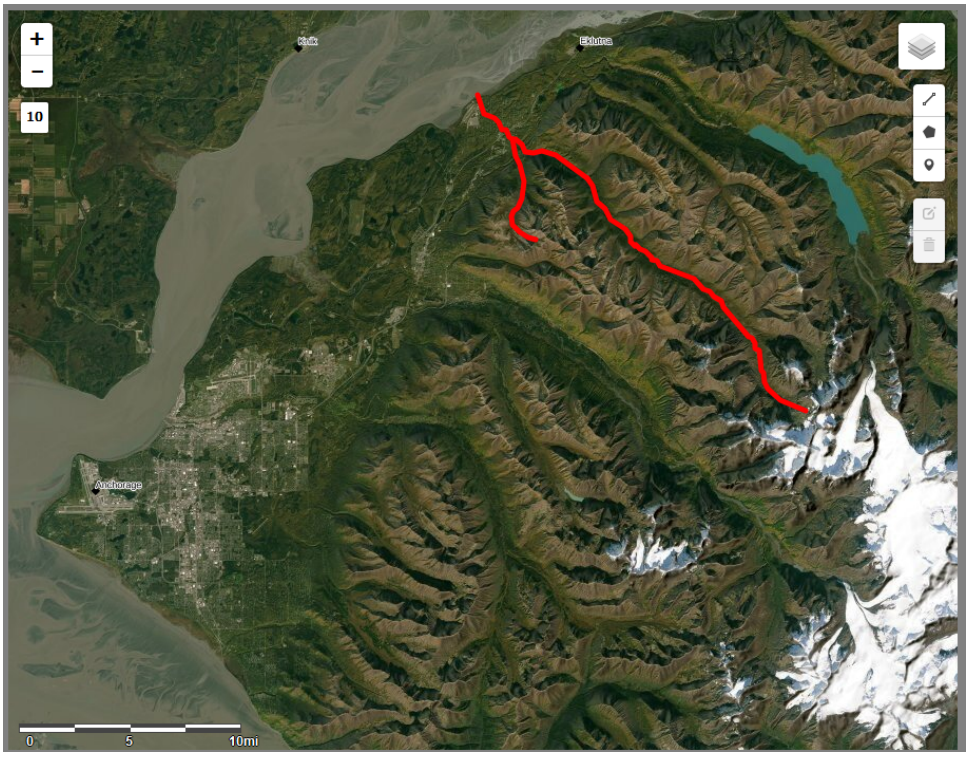

Figure 12: Satellite image of Peters Creek near Chugiak, Alaska.

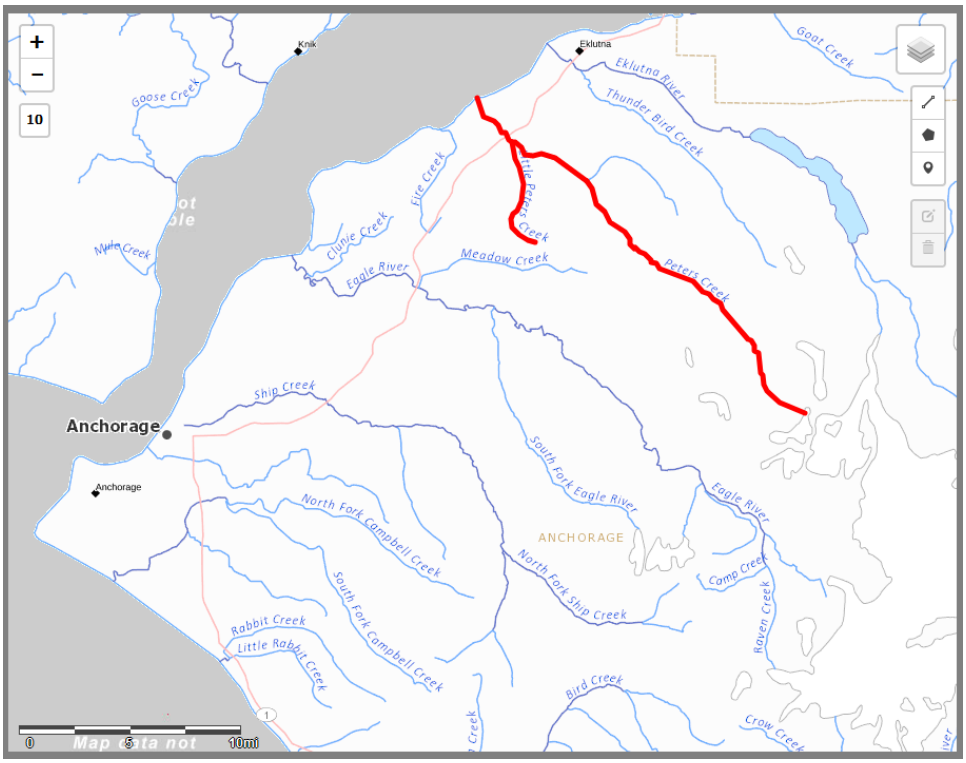

Figure 13: Hydrography of Peters Creek near Chugiak, Alaska.

Anchor River Bridge on the Old Sterling Highway (BN0910)



Figure 14: Satellite image of Anchor River near Homer, Alaska.

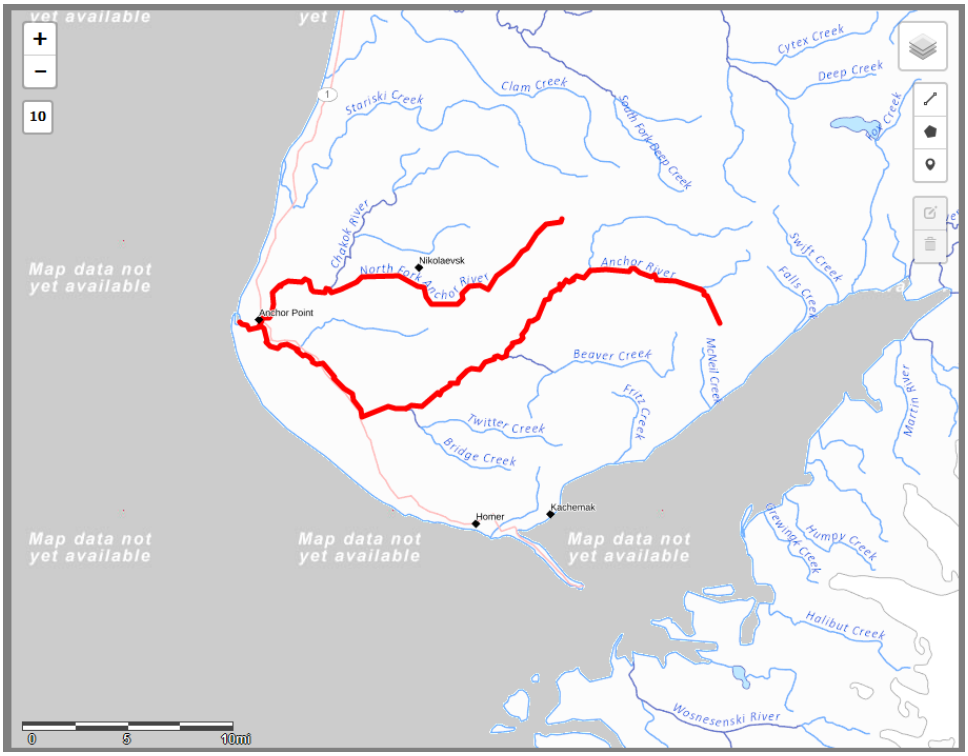

Figure 15: Hydrography of Anchor River near Homer, Alaska.

CHAPTER 2 – FINDINGS

The results that follow are described for the rivers and creeks captured by UAS, and handheld and fixed field cameras. If imagery from crewed aircraft also exist, these data will also be described in comparison. The most interesting sites will then be interpreted in more detail in Chapter 3.

2.1 Detailed Case Study Sites

Jack River Bridge on the Parks Highway near Cantwell (BN0302)

This site was flown with the UAS in March and April 2020 and captured by the handheld field camera on the same dates. This bridge was photographed from the crewed aircraft in October and December 2016; April and November 2017; and March and April 2018. Examples of these images are shown here and in Appendix A. Results from the imagery collected show what is most likely direct interaction between bridge piers and groundwater. The structures themselves appear to be causing local upwelling and formation of aufeis. This process was more evident at this site than at any other in our study area. The handheld field camera was particularly helpful at recording small-scale groundwater upwelling at Jack River Bridge in real time. Evidence of aufeis formation around the bridge piers is also clear from both the UAS and the crewed aircraft imagery. The Jack River site, which displays many of the processes that motivated this study, is explored in more detail in Chapter 3.



Figure 16: Jack River detail of orthomosaic derived from UAS imagery collected in April 2020.

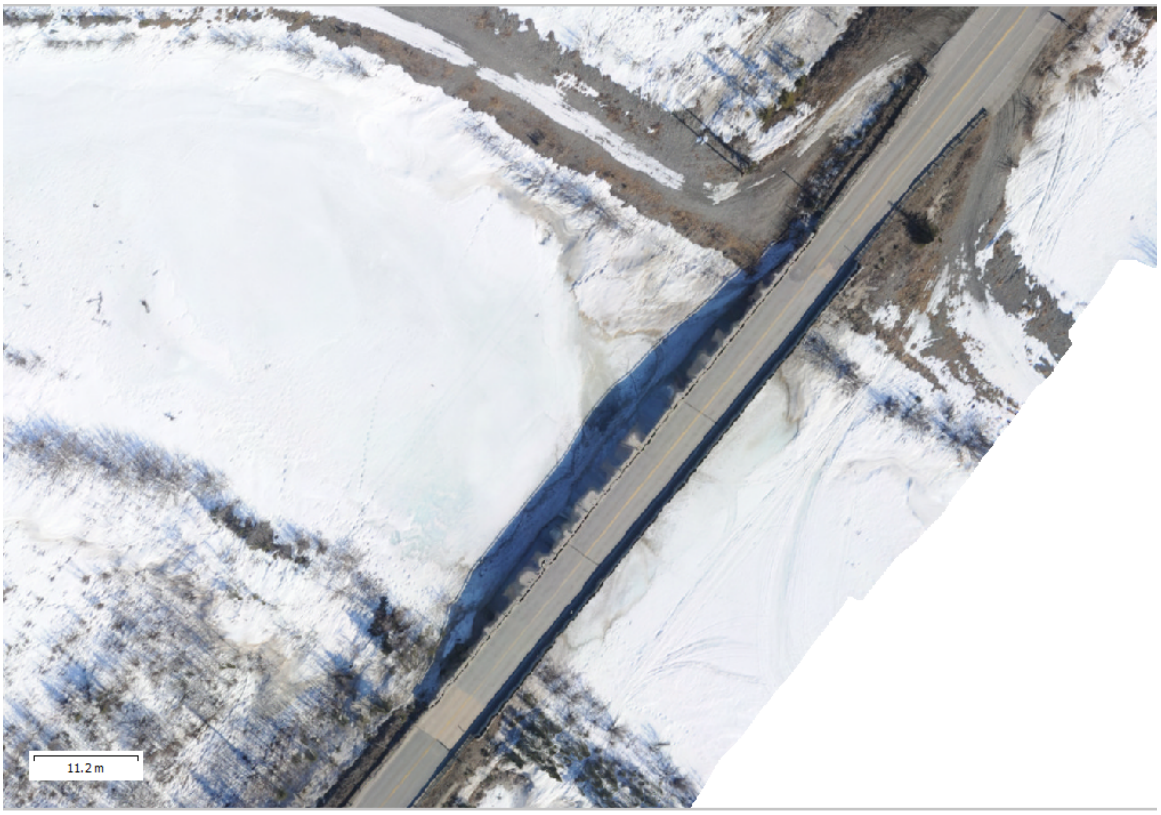

Figure 17: Jack River detail of orthomosaic derived from crewed aircraft collection in April 2017.



Figure 18: Jack River single frame from handheld field camera collected in April 2020.

O'Connor Creek Bridge on Goldstream Road near Fairbanks (BN0303)

This site was flown with the UAS in November 2019 and March 2020 and was imaged with the handheld field camera in March 2020. The site was also flown with the crewed aircraft in October and December 2016; March, April, and October 2017; March and April 2018; and March, April, and October 2019. Examples of these images are shown here and in Appendix A. Results from these images show aufeis formation and impoundment by the bridge abutments. These processes may impact soil moisture and stability in the surrounding area. Aufeis at this site can be seen well into the summer in many years. Interpretation of processes and the site history are discussed in more detail in Chapter 3.

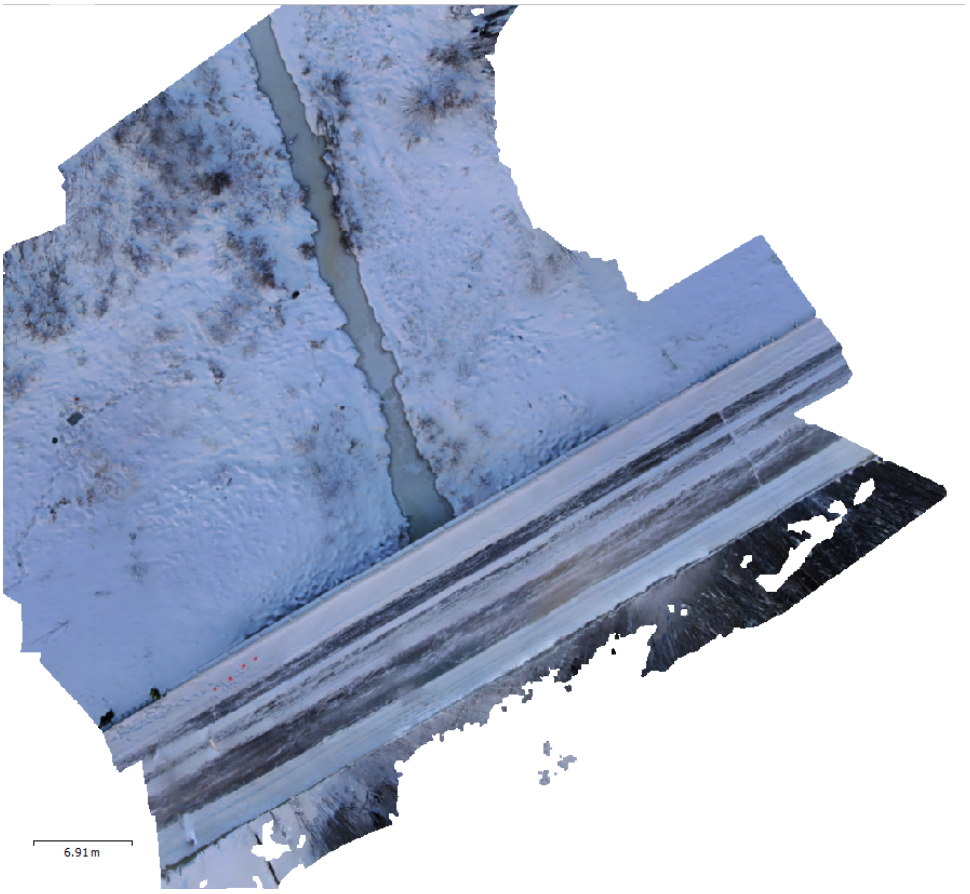

Figure 19: O'Connor Creek orthomosaic derived from UAS collection in November 2020.

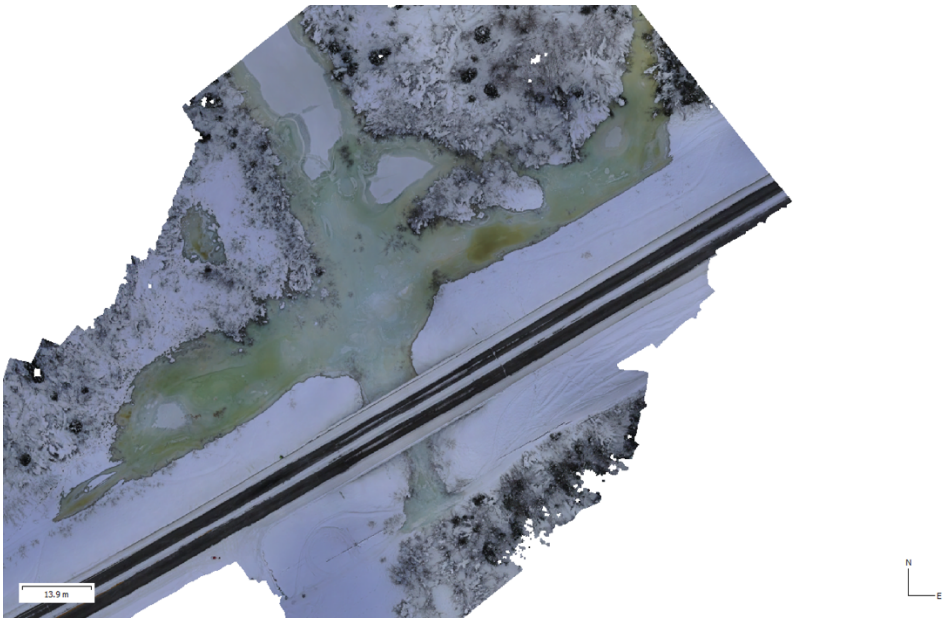

Figure 20: O'Connor Creek orthomosaic derived from UAS collection in March 2020.



Figure 21: O'Connor Creek point cloud from data collected by UAS in November 2020.

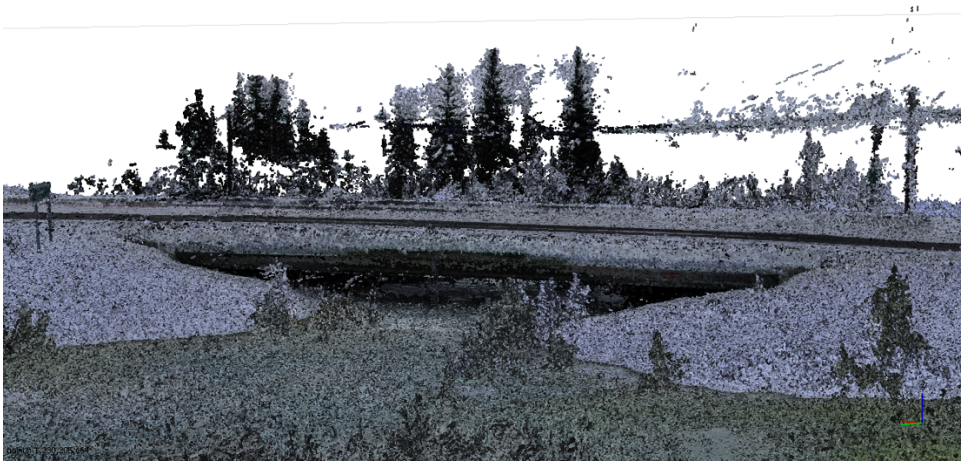

Figure 22: O’Connor Creek point cloud from data collected by UAS in March 2020.



Figure 23: O'Connor Creek orthomosaic from data collected by crewed aircraft in April 2019.



Figure 24: O'Connor Creek detail of orthomosaic from data collected by crewed aircraft in April 2019.

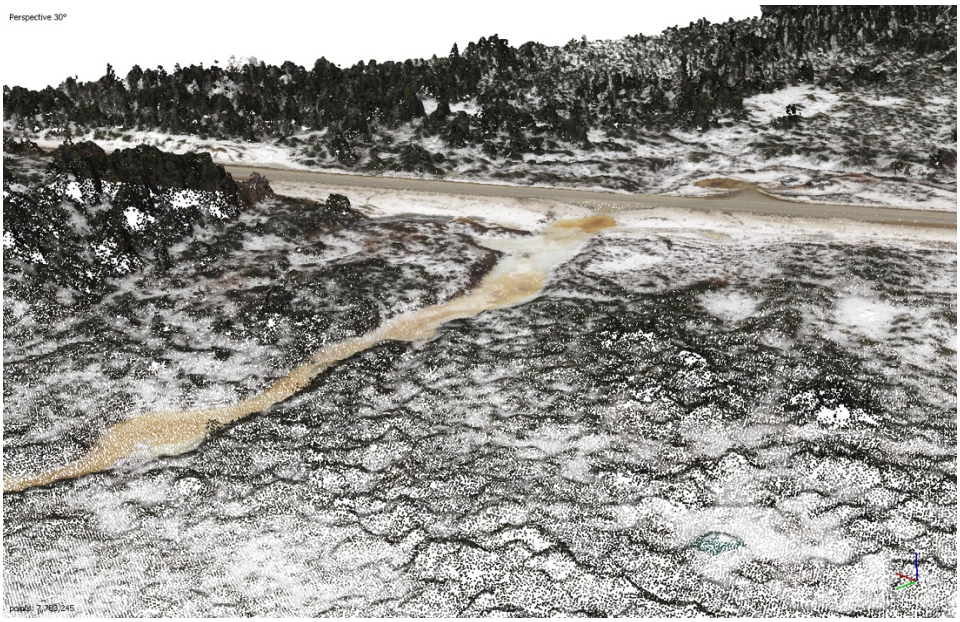

Figure 25: O'Connor Creek point cloud from data collected by crewed aircraft in April 2019.

Robertson River Bridge on the Alaska Highway near Dot Lake (BN0509)

This site was flown with the UAS in April 2020 and for safety reasons was not imaged with the handheld field camera (as there is no pedestrian walkway). It was also flown with the crewed aircraft in October and December 2016; March, April and November 2017; March and April 2018; and March and April 2019. Examples of these images are shown here and in Appendix A. This site shows evidence of large-scale overflow and aufeis formation, but direct evidence of interaction with the bridge piers is less obvious. Interpretation of processes at this site are discussed in detail in Chapter 3.

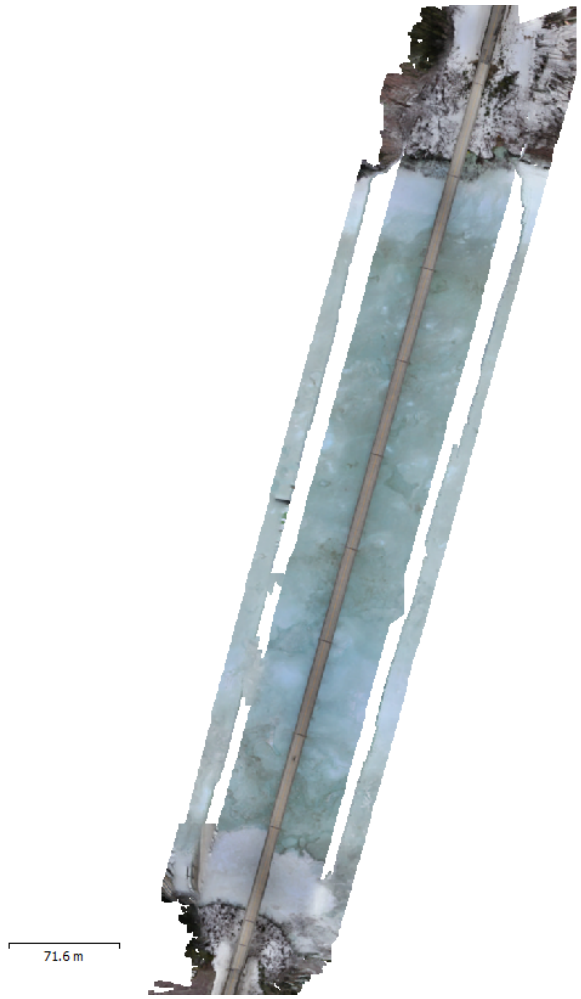

Figure 26: Robertson River orthomosaic from UAS data collection in April 2020.

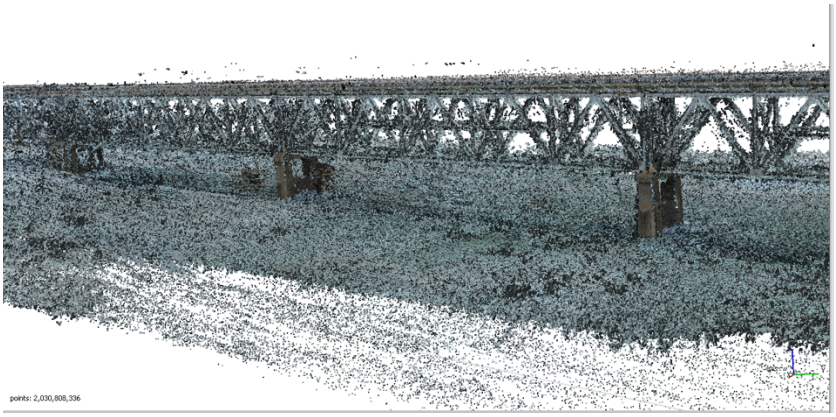

Figure 27: Robertson River point cloud detail from UAS data collection in April 2020.



Figure 28: Robertson River orthomosaic from imagery collected by crewed aircraft in April 2019.



Figure 29: Robertson River single frame from UAS collection in April 2020.

Peters Creek at Stoltze Road (BN1031)

This site was flown more than any other, due to its close proximity to the field team based out of Anchorage. Peters Creek is narrow, and freeze-up flooding frequently occurs, sometimes with minor impacts to nearby roads and private property. The site was flown by the project team in October 2019, five times between December 19 and 30, 2019, and three times in November 2020. These closely spaced flights captured freeze-up processes such as anchor ice formation, shelf ice formation, and ice damming. Data show water and ice interacting with the bridge during freeze-up, mostly in that freeboard between the water level and bridge deck is relatively minimal; sedimentation and beaver habitat may also play a role in exacerbating flood risk at this site. While

this study was not focused on flooding, groundwater may play a role in what is happening at Peters Creek, and it is a good site to watch for processes that are harder to capture at remote sites.



Figure 30: Peters Creek detail from orthomosaic of data collected by UAS in November 2020.

Anchor River Bridge on the Old Sterling Highway (BN0910)

A field camera was mounted on the Anchor River Bridge at Anchor Point on the Old Sterling Highway looking upstream, attached to a wing-wall I-beam. These data provided an example of the type of imagery that can be collected by a field camera mounted to a bridge in winter. Data were collected from November 6, 2020, to January 14, 2021, hourly between 8 a.m. and 5 p.m. by Cook Inletkeeper and its partners at the National Weather Service. Both freeze-up flooding and breakup flooding are common at this site. Many of the photos show low light conditions and moisture buildup on the lens, but several images per week show current river conditions clearly. In these images, it is possible to see whether the river is open or ice-covered and the approximate extent of shelf-ice development. However, no detail can be seen with respect to water or ice interacting with the bridge abutments. Lens heaters can help with moisture and frost build up on in situ field cameras but these heaters typically consume too much power to be used at remote sites away from an accessible municipal power grid. To capture potential aufeis development, the lens would need to point downward and thus the camera imagery would not be useful for detecting ice jams or other purposes. One would also essentially need to already know where the aufeis forms. In that sense, the UAS and crewed aircraft imagery at the Jack River, for example, could guide the placement of a field camera, if DOT&PF determined they wanted more imagery.



Figure 31: Anchor River example of stationary mounted field camera.

2.2 Other Study Sites

Sample imagery from these sites is shown in Appendix B.

Johnson River Bridge on the Alaska Highway (BN0518)

This site was imaged once with the UAS in April 2020 as well as with the crewed aircraft in October 2016; March, April, and November 2017; March and April 2018; and March and April 2019. The site was not imaged with the handheld field camera for safety reasons. Like the Robertson River Bridge, the Johnson River Bridge is relatively long at about 900 feet, but imagery does not show as much aufeis development at this site as it does at the Robertson River, although it does show some. This truss bridge imagery also shows accumulation of trees and brush downstream of the piers. The point cloud generated from the UAS acquisition shows all dimensions of the bridge clearly, including under and through each side and the superstructure, but due to the bridge size this dataset contains nearly a billion points and is somewhat unwieldy. The Johnson River is braided and gravel-rich with low water levels during freeze-up and winter. Comparisons with the longer-term crewed aircraft dataset show significant differences in the location of the river channel from year to year.

Gerstle River Bridge on the Alaska Highway (BN0520)

This site was imaged once with the UAS in April 2020 as well as with the crewed aircraft in October and December 2016; March, April, October, and November 2017; March and April 2018; and March and April 2019. The site was not imaged with the handheld field camera for safety reasons. The UAS imagery shows much of the snow having melted at this site by the acquisition date (April 17) and what are likely aufeis features still intact. There appears to be one or more channels under this ice and evidence of sediment buildup at some piers and scouring at others. Note that the processed orthomosaics for these long bridges show distortions as the viewer gets further from the bridge. The model and orthomosaic for this bridge (about 1700 feet long) included

over 2000 single frames, so like the other long bridges, this point cloud and model are difficult to work with and took several days to process. The UAS did capture well the area under the bridge and around the piers.

Banner Creek Bridge on the Richardson Highway (BN0526)

This site was imaged once with the UAS in April 2020, twice with the handheld field camera in April and November 2020, as well as with the crewed aircraft in October and December 2016; March, April, October, and November 2017; March 2018; and April 2019. Comparison between the field camera and the UAS shows the significant advantage of the UAS at some sites. Low light conditions hampered the November field camera acquisition, but the crewed aircraft and UAS show overflow and aufeis features at this site. No interaction with bridge structures is obvious from the imagery.

Gulkana River Bridge on the Richardson Highway (BN0574)

This site was imaged in both March and April 2020 with the UAS and in March 2020 with the handheld field camera. It was flown with the crewed aircraft in October and December 2016; April and November 2017; and March and April 2018. The orthomosaics generated by the UAS imagery in March and April 2020 are both distorted this is a sign that the pilot did not cover enough area around the bridge. The features there appear in the point cloud in nearly two-dimensional manner instead of three, but the products are still sufficient to show what is going on. In March of that year, the scene is snow-covered, but ridged ice features below the snow are apparent, showing aufeis forming and flowing around the bridge piers. In April, the river had begun to break up, but the image shows remnant "backwaters" of aufeis upstream of the bridge. The crewed aircraft data also show aufeis flowing around the bridge piers in March and April 2018 and in April 2017. The October 2016 and November 2017 images nicely capture the freeze-up processes and formation of shelf ice between the bank and the piers.

Gunnysack Creek Bridge on the Richardson Highway (BN0590)

This site was imaged in April 2020 with both the UAS and the handheld field camera. The imagery shows very deep, compacted snowdrifts covered in dust. Aufeis is not apparent. The site was also imaged in November 2019 and March 2020 with the handheld field camera only. These scenes are also snow packed, and aufeis is not apparent. The imagery from the crewed aircraft is similar.

Ruby Creek Bridge on the Richardson Highway (BN0594)

This site was imaged with the UAS in April 2020, with the field camera in November 2019, and with the crewed aircraft in October 2016. The November imagery shows a frozen creek, but whether aufeis is a factor is not clear. The October scene is snow-covered with no obvious signs of groundwater or aufeis. The April imagery and point cloud show some meltwater and deep snowpack, and it is not clear if groundwater is a factor here.

Jarvis Creek Bridge on the Richardson Highway (BN0595)

Jarvis Creek Bridge was not imaged with the UAS because it is inside military airspace, but it was imaged with the handheld field camera in March and April 2020 and from the crewed aircraft in

October and December 2016; March, April, and October 2017; March and April 2018; and March and April 2019. While the field camera data from 2020 was processed into orthomosaics, the point clouds are overly noisy. The April data show meltwater and ice, but their origin is uncertain. In the crewed aircraft datasets, the October 2017 data show snow conditions of the creek going into freeze-up and the location of the channel at that time. The April 2019 scene shows mostly gravel with snow filling in flow paths within the gravel, which is interesting. While further up Jarvis Creek there are large fields of aufeis, it is not clear from the imagery that buildup occurs at this bridge.

Gakona River Bridge on the Tok Cutoff (BN0646)

UAS imagery was collected in November 2019 and April 2020. Handheld field camera data were collected in November 2019, and the crewed aircraft collected data in October and December 2016; April and November 2017; and March and April 2018. Overflow and aufeis are apparent in many of these winter and spring scenes. The main channel shifts between years at this site. The April 2020 UAS imagery shows clear under the bridge and suggests aufeis may be building up on the upstream side of the piers.

Sinona Creek Bridge on the Tok Cutoff (BN0648)

UAS and handheld field camera data were collected at this site in April 2020. Data from crewed aircraft were collected in November 2017 and in March and April 2018. Presence of aufeis at this site is most apparent in the UAS imagery, although this site has impacts from snow machine travel that may have depressed the natural ice sheet against the stream bed. No impact on the bridge structure is apparent in any of the photos.

Tok River Bridge on the Alaska Highway (BN0663)

Images were collected on the Tok River by UAS and handheld camera in April 2020. The crewed aircraft collected imagery in October and December 2016; April 2017; and March and April 2018. The October scene shows the freeze-up configuration of the river that year, and the spring scenes all show a very large field of aufeis at this site. Inspection of the piers in the point cloud does not show obvious interaction with the aufeis.

Seattle Creek Bridge on the Denali Highway (BN0690)

Images were collected on the Denali Highway at the Seattle Creek Bridge by UAS and field camera in April 2020. The crewed aircraft captured data at this site in October and December 2016; in April and November 2017, and March and April 2018. The imagery suggests groundwater keeps leads open year-round at this site, despite the extremely cold temperatures in this region. Aufeis is difficult to determine from these data.

Carlo Creek Bridge on the Parks Highway (BN0693)

The UAS and handheld camera were used to collect data here in March and April 2020. The crewed aircraft collected imagery in October and December 2016; April 2017; and March and April 2018. As with some of the other small creeks (Gunnysack and Ruby), aufeis development is not apparent from these images. Deep snow seems to pack into these sites.

Kingfisher Creek Bridge on the Parks Highway (BN0697)

The UAS and handheld camera collected data here in March and April 2020. Data were collected from the crewed aircraft in April and November 2017 and March and April 2018. The March 2020 UAS data show a large volume of aufeis developing at this site, but no obvious interaction with the bridge infrastructure is apparent.

Goldstream Creek Bridge on Ballaine Road (BN1009)

Data were collected with the UAS at this site in March 2020 and with the handheld camera in November 2019 and March 2020. Data were collected from the crewed aircraft in October and November 2016; March, April, and October 2017; March and April 2018; and March, April, and October 2019. The UAS data do not show aufeis, but they do show snow packed to the bottom of the bridge deck on both the upstream and downstream sides. The crewed airborne data show the way that groundwater and overflow pool on the upstream side of this bridge in late winter and spring, before breakup. Most likely, groundwater impacts the road and abutment structures, and breakup could be affected by aufeis laminations in the creek.

Dragonfly Creek Bridge on the Parks Highway (BN1075)

Data were collected at this site with the UAS and handheld camera in March and April 2020. Data were captured by the crewed aircraft in April 2017 and March 2018. The crewed aircraft imagery shows considerable snowpack around this bridge. The UAS imagery and point clouds suggest some aufeis development, but they do not show it interacting with the bridge abutments in this case. This small bridge in rough terrain was better suited to photography with the UAS than with the crewed aircraft.

Fox Creek Bridge on the Parks Highway (BN1144)

Imagery was collected at this site with the UAS and handheld camera in March and April 2020. Imagery was captured by the crewed aircraft only in November 2017. The March UAS data show groundwater seepage and aufeis formation, and in the April imagery, laminated ice can be seen as it breaks apart. It is unclear as to how much the water interacts with the bridge abutments, but that effect seems possible.

Tulsona Creek Bridge on the Tok Cutoff (BN1250)

Imagery was collected at this site with the UAS and handheld camera in November 2019 and April 2020. The November data show open water, and the April images show rotten ice and meltwater. Crewed aircraft collections at this site include October 2016; April and November 2017; and March and April 2018. The crewed aircraft data show aufeis present in early winter through March and April. Impacts on the bridge, if any, are unclear.

CHAPTER 3 – INTERPRETATION, APPRAISAL, AND APPLICATIONS

Only the detailed case study sites are discussed in this chapter. These sites are located in two different hydrologic zones in the state of Alaska (Callegary et al., 2013): the Interior region and the Southcentral region, with the Alaska Range separating the two.

Jack River Bridge over the Parks Highway near Cantwell (BN0302)

The Jack River Bridge over the Parks Highway is in an area of disturbed soils. This watershed, an upper tributary of the Nenana River, probably contains at least sporadic (if not discontinuous) permafrost and was glaciated during the last glacial period. The river is situated in a low-gradient area known as Broad Pass, a wide valley between the Talkeetna Mountains and the Alaska Range, and its soils are unconsolidated. The area has seen considerable mineral- and gravel-mining activity over the past century and shows evidence of disturbance in the vicinity of the bridge. It appears that various mitigation structures have been deployed to control erosion on the riverbanks near the bridge, and in satellite imagery shown in Appendix A, water can be seen impounded outside of the channel, against the road.

The Jack River Bridge is approximately 180 feet long with two piers in the riverbed. Its size and location are ideally suited for nadir airborne imaging with both the UAS and the crewed aircraft, but the short distance between the bridge deck and the river also made the handheld field camera an effective tool. In imagery shown in Chapter 2 and in Appendix A, aufeis formations can be noted in collections from all three imaging platforms. Because of the low height of this bridge, the crewed aircraft cannot see under the deck, and the UAS and handheld field cameras in oblique view angles are the right tools for doing this. However, even the nadir data shown in Chapter 2 display refrozen plumes of aufeis where we know the piers to be located. The handheld field camera and the UAS both captured imagery (stills and video) of water actively upwelling through holes in the ice around the piers in April 2020. The hole shapes suggest that this is spring or groundwater, warmer than surface meltwater.

The crewed aircraft collection does show more of the river upstream and downstream of the bridge, and when visible, gives a better sense than the UAS of how widespread aufeis may be at this site. The UAS is limited to flight at 400 feet above the bridge at most and must remain in visual line of site. Advantages of the UAS are that it can achieve higher image resolution at this height and, of course, its ability to collect oblique imagery looking under the bridge. The data from the handheld field camera are valuable as is, and the resolution is actually too high to easily process into point clouds from overlapping stills. There also is considerable lens distortion in the handheld camera, which has a fisheye lens.

It could be that the mechanism described in Figure 5 is at play at this site due to the steep mountains on either side of Broad Pass, but the low-gradient flow of the Jack River in the vicinity of this bridge, and potential barriers from permafrost or bedrock, may help drive susceptibility to aufeis formation at this site. The bridge piers and piles appear to create another such barrier, and groundwater is forced to upwell and flow around these structures.

O'Connor Creek Bridge on Goldstream Road near Fairbanks (BN0303)

The soils on O'Connor Creek in the Goldstream Valley north of Fairbanks are also disturbed by mining activities and are silty loam (not gravel like on the Jack and Robertson rivers). They probably contain ice-rich permafrost or used to and were not glaciated. The watershed is on the south side of a boreal hillslope of a small mountain called Murphy Dome and flows into Goldstream Creek. Nearby vegetation includes black spruce, alders, and birch trees. The bridge is approximately 100 feet long and has a steaming pipe to help control ice buildup between the creek and the bridge deck.

All three technologies (UAS, crewed aircraft, and field camera) are useful for imaging O'Connor Creek in winter. The UAS and field camera can capture approximately the same view from the oblique, near-ground perspective, but the optics of the UAS are much higher quality. Trying to create a point cloud from the field camera is noisy and too computationally intensive due to the distorted lens and the high resolution of the sensor; however, single frame photography or video from the field camera may be perfectly sufficient for this application. From the air, the crewed aircraft can get a better perspective on the whole creek, whereas the line of sight of the UAS is more limited for a pilot on the ground. It would not be possible for a UAS pilot to image the whole watershed by standing near the bridge. The advantage of the UAS over the crewed aircraft is the ability to get more detail under the bridge and the areas on the north slide of the bridge where aufeis tends to build up against the abutments and roadway.

Other limitations of the UAS are the Class D airspace of Fairbanks International Airport. The O'Connor Creek Bridge site is just outside of controlled airspace and in a relatively congested area where pilots of incoming crewed aircraft report their position. The Ballaine Road Bridge over Goldstream Creek nearby is outside of the Class D airspace but under the Class E airspace, which has a floor at 700 feet. In addition to the International Airport, there are small, private airstrips throughout the Goldstream Valley where aircraft are taking off and operating within 400 feet of the ground. Because of this potential conflict and limited line of sight, it may be best to use UAS within 100 feet of the ground in this area and listen on the Community Traffic Advisory Frequency (CTAF) on an aviation radio. This low-level flying requires the pilot to avoid power lines, which are not just a physical obstacle, but may also cause electro-magnetic interference with the UAS GPS and compass. Caution is recommended.

Robertson River Bridge on the Alaska Highway near Dot Lake (BN0509)

The Robertson River Bridge is quite different from the O'Connor Creek site. The Robertson River is a wide, braided river that originates from glaciers on the north side of the Alaska Range. Discontinuous permafrost is likely in this basin. Soils are unconsolidated and gravel-rich, the product of glacial movement in steep terrain, as at the Jack River. Any anthropogenic soil disturbances are small relative to the size of the basin. The Alaska Highway bridge over the Robertson River is quite long: about 1,600 feet with at least nine piers. The Robertson River goes into freeze-up during low flows, spread over a wide bed with only one small active channel. Like the Jack River, proximity to a steep mountain range may help drive aufeis buildup at this site.

Photography from the crewed aircraft between 2016 and 2019 and with the UAS in 2020 showed considerable aufeis. The lateral field-of-view that is practical to cover with the UAS is small, which accounts for the corridor-type orthomosaic generated from that acquisition. The battery life of the

DJI Mavic in cold temperatures (0–20°F) was limited to less than 20 minutes, so it was a risk to the aircraft to fly it far from its home point. The orthomosaic generated from the crewed aircraft, especially in later years as the acquisition maneuvers improved, shows a far clearer picture of the extent of aufeis buildup in this river. On the other hand, the UAS imagery shows incredible detail, including small holes in the ice potentially associated with groundwater upwelling under the bridge. Unfortunately, because of the narrow survey from the UAS, it is not known whether those small holes existed farther away from the bridge structures.

Besides the fine-scale detail captured by the UAS, another advantage of the UAS is that it could look obliquely under the bridge. Unlike the Jack River and O'Connor Creek, however, this oblique data and product, the point cloud, were not particularly informative. It seems likely that aufeis is so prevalent at this site that the impact of the presence of the bridge is a relatively small factor, whereas the braided gravel geomorphology may be indicative of aufeis driven by permafrost and other subsurface barriers. One possibility here, though, is that aufeis could be contributing to scour around the bridge piers (Beebee et al., 2018).

Peters Creek at Stoltze Road (BN1031)

While the photos captured at Peters Creek do not show aufeis laminations per se, they give some interesting insight into a different process that leads to groundwater-induced flooding at this site. The anchor ice seen in the photos shown in Chapter 2 forms during a cold snap, when the water becomes supercooled and sinks. More information on the formation of anchor ice in this area can be read in Daly et al. (2019) and references therein, but anchor ice adheres to the streambed and to structures like the abutments on this Stoltze Road bridge over Peters Creek. As groundwater continues to feed this creek, which like others is not far from steep terrain (the Chugach Mountains), the anchor ice starts to clog the stream and form a subsurface ice jam. Shelf ice grows and makes conditions worse. This is already a small (80 foot), low bridge with minimal freeboard room. There were also signs of beaver activity including a lodge in this creek, just downstream of the bridge, which would provide another barrier and structure for the anchor ice to adhere to. Anchor ice could be a mechanism that occurs at other sites such as the Jack River and the Robertson River during freeze-up, but it would have been more logistically challenging to capture repeat photography during the exact point of formation at these more remote sites.

The UAS was the right tool to use for this site because the handheld field camera could not see the anchor ice as clearly due to glare off the water. This site was also in an urban location right at the Birchwood Airport, which is uncontrolled. It would be difficult to photograph with a crewed aircraft if other aircraft were trying to land or take off from Birchwood Airport. With the UAS, it was necessary to fly very low (lower than the surrounding trees or <50 feet) to avoid any interference with airport traffic. A handheld aviation radio was also used to listen for traffic. This could potentially be a site for a fixed time-lapse camera with data transmission to detect flood events. However, local residents might express concerns over privacy here.

Anchor River Bridge on the Old Sterling Highway (BN0910)

No detail can be seen with respect to water or ice interacting with the bridge abutments in the Anchor River imagery. For this purpose, a camera would need to be pointed specifically at those bridge structures and would then not be useful for scanning general river conditions. One camera type for such an application could be the so-called 360 cameras deployed by the FAA at remote

airports. These are actually a camera with four fisheye lenses and four separate sensors but may be useful to test in bridge applications. The wide angle, unfortunately, would cause significant distortion like that seen in the handheld GoPro field cameras. The DOT&PF is replacing the Anchor River Bridge during summer 2021 and has deployed a different camera, the Earthcam, with image transmission that, were it to remain in place, could be effective at tracking both ice jams and aufeis-type flooding at this site. However, such a camera would be even more effective if combined, like the one with data shown here, looking upriver. Multiple cameras, look-angles, or lenses may be necessary to paint a full picture of what is happening at this site. Unfortunately, few bridges in Alaska have a readily available power supply that could support heated cameras. Only heaters can keep the lenses clear of moisture and frost buildup.

CHAPTER 4 – CONCLUSIONS AND SUGGESTED RESEARCH

This study made clear that there is no single technology that produces the best imagery for visually studying the impacts of aufeis on bridges. Factors to consider include the height and length of the bridge, the size of the river and watershed, the proximity of the site to terrain, risk for the operator, risk for the aircraft, and the cost of logistics. The UAS was effective at maneuvering close to the ground in tight spaces with a lot of vegetation, like Peters Creek and O'Connor Creek. The crewed aircraft can cover a lot of ground efficiently and capture virtually all the pertinent sites in Interior Alaska in a few hours, whereas capturing more than a couple of sites a day via UAS requires long drives and power management with half a dozen batteries rotating on a vehicle charger. Both the crewed aircraft and the UAS can be impacted by weather, including poor flight visibility, precipitation, winds and temperature; however, the crewed aircraft has a much wider tolerance for winds and temperatures that would simply shut down the UAS. April turned out to be the critical time for acquiring imagery with aufeis features. Daylight in April is long enough to make the light conditions logistically manageable. The field cameras, handheld and fixed, showed a range of possibilities including the recording of fine-scale features like groundwater upwelling through holes in the ice. Fixed field cameras can show general ice conditions on a waterway and potential flood events. However, there are downsides to the wide-angle fisheye optics in terms of distortion, and fixed field cameras are susceptible to moisture buildup and other obscurations.

This study acquired imagery as single frames and some video, but also processed the single frame imagery into sparse and dense point clouds, orthomosaics, and digital elevation models. The point clouds were most useful with small bridges for looking obliquely at the height of ice buildup. The orthomosaics were most useful for large-scale ice features. The single frames were most useful for fine-scale features, and the video captured dynamic water upwelling through holes.

Several topics merit further research following from what was done during this project. No effort here has included satellite analysis of large-scale aufeis features. At this time, there is enough coverage by high-resolution satellites such as Sentinel's Electro-Optical program, LandSat, and commercial spacecraft to look at larger features in Alaska's Interior. Aufeis does provide a unique expression of groundwater at the surface. Good candidates for this type of analysis might be the larger rivers along the Parks, Richardson, Glenn, and Alaska highways including the Jack, Robertson, Gerstle, Johnson, and Gakona rivers. This project was a study in technology application, not the basic science of aufeis, but certainly the latter merits more research. Other expressions of groundwater such as open leads would also benefit from more study in Alaska (Jones et al., 2015).

Another topic of applied research beyond the scope of the current project would be the relationship between sediment transport, aufeis, and scour at these bridges. The work of Dworsky and Conaway (2019) is a good start in this regard. Such a study could also make use of aerial and satellite remote sensing, but more imagery should be captured during the shoulder seasons just after snow/ice melt and just before freeze-up to determine sediment transport and channel dynamics. These studies could certainly make use of in situ sensors as well, including piezometers, to directly measure the movement of groundwater. However, it is very difficult to keep such instrumentation from being destroyed or damaged by ice. This work could also make use of the digital elevation models generated by image processing, where geomorphology emerges quantitatively. Finally, the

physical geography could be quantified and studied in more detail in terms of the relationship between topography and aufeis development for different-sized basins.

The DOT&PF and national transportation entities are developing concepts and protypes for the future of bridge monitoring. An instrumented "smart-bridge" is one of those concepts, and plans are underway to test various types of camera systems on or around bridges. Further afield are ideas of self-inspecting bridges that might house their own UAS in a tiny "hangar" from which the aircraft would emerge on a schedule and look for potential maintenance issues. The Skydio platform, which does not depend on GPS, is particularly promising for very close bridge inspection, where electro-magnetic interference could cause navigation and control problems for platforms dependent on GPS like the DJI Mavic used by the present study. The most mature technology would be expanded use of fixed field cameras looking not only upstream and downstream, but also straight down at bridge piers.

It could also be useful to measure the strength characteristics of laminated ice formations, either in nature or in a laboratory, relative to other ice formations. Perhaps another study could attempt to measure the forces of ice on bridge structures, building on the mathematical theories developed in Russia (Korzhavin, 1962). This is something a study bridge or "smart-bridge" might be designed to do. Aside from the theoretical work from long ago, much of the work in the field of ice/bridge interaction, and even the most basic understanding of river ice, is highly qualitative at this time (Beltaos, 2003; Hains and Zabilansky, 2006; Hicks, 2013 and 2016). More recent work using computational models is starting to emerge (Lamontagne-Hallé et al., 2020), but little so far in cold regions where hydroclimate systems have more complexity. Finally, difficult problems require creative approaches. Huryn et al. (2020) recently showed that aufeis fields have their own unique invertebrate ecosystems. It could be that these ecosystems will tell us more about how arctic groundwater works than we can measure through classic hydrologic methods.

To reiterate a few of these points as a final take-away:

-UAS and hand-held field cameras are typically the better tool for very small creeks, especially in confined locations. Neither UAS nor hand-held cameras are the best tool for a very large rivers in cold conditions (colder than 20 deg F): there is a high risk of the battery freezing and the UAS being lost someplace unretrievable.

-April, just before breakup, might typically be the best time to image because of the relatively long day length and aufeis may standout relative to other ice formations. However harsh, direct light or long shadows should be avoided.

-The remotely-sensed nature of imagery makes it difficult to directly measure water upwelling, but the cameras are also not damaged by the ice conditions the way in situ instruments may be.

-Image collection with crewed aircraft may be the most efficient from the point of view of number of sites collected during a two-day campaign, but small-scale features may be missed.

REFERENCES

Beebee, R.A., K.L. Dworsky, and S.J. Knopp, *Streambed scour evaluations and conditions at selected bridge sites in Alaska, 2016–17*, U.S. Geological Survey Scientific Investigations Report 2019-5110 (2018) 32 p., https://doi.org/10.3133/sir20195110.

Beltaos, S., B.C. Burrell, L. Miller, and D. Sullivan, "Hydraulic Interaction Between Ice and Bridges" 12th Workshop on the Hydraulics of Ice Covered Rivers, Edmonton, AB, Canada (2003) 20 pp.

Callegary, J.B., C.P. Kikuchi, J.C. Koch, M.R. Lilly, and S.A. Leake, "Review: Groundwater in Alaska (USA)." *Hydrogeology Journal,* Vol. 21 (2013) pp. 25-39.

Carey, K.L., R.W. Huck, and D.A. Gaskin, *Prevention and control of culvert icings.* U.S. Army Cold Regions Research and Engineering Laboratory Summary Report of Studies FY 1966-1970, Hanover, NH (1975) 84 pp.

Clark, I.D., and B. Lauriol, "Aufeis of the Firth River Basin, Northern Yukon, Canada: Insights into Permafrost Hydrogeology and Karst." *Arctic and Alpine Research*, Vol. 29 (1997) pp. 240-252.

Daly, S.F., *U.S. Army Core of Engineers Course on Ice: Lectures*. Hanover, NH (2017).

Daly, S.F., J.S. Rocks, M. Reilly-Collette, and A.B. Gelvin, *Ice Control to Prevent Flooding in Ship Creek, Alaska*, Engineer Research & Development Center/U.S. Army Corps of Engineers, Technical Report 19-11, Hanover, NH (2019) 80 pp.

Dworsky, K.L., and J.S. Conaway, *Measurement of long-term channel change through repeated cross-section surveys at bridge crossings in Alaska*, U.S. Geological Survey Open-File Report 2019-1028 (2019) 118 pp., https://doi.org/10.3133/ofr20191028.

Hains, D.B., and L.J. Zabilansky, "Scour Under Ice: Potential Contributing Factor in the Schoharie Creek Bridge Collapse" in *Cold Regions Engineering 2006: Current Practices in Cold Regions Engineering*, edited by M. Davies and J.E. Zufelt, American Society of Civil Engineers (2006) 9 pp.

Harden, D., P. Barnes, and E. Reimnitz, "Distribution and Character of Naleds in Northeastern Alaska." *Arctic*, Vol. 30, No. 1 (1977) 14 pp.

Hicks, F., *The Weird and Wonderful World of River Ice*, Self-Published, Edmonton, Canada (2013) 42 pp.

Hicks, F., *An Introduction to River Ice Engineering for Civil Engineers and Geoscientists*, Self-Published, Edmonton, Canada (2016) 159 pp.

Hicks, F., R. Andrishak, and Y. She, "Modeling Thermal and Dynamic River Ice Processes" in *Cold Regions Engineering 2006: Current Practices in Cold Regions Engineering*, edited by M. Davies and J.E. Zufelt, American Society of Civil Engineers (2006) 11 pp.

Huryn, A.D., M.N. Gooseff, P.J. Hendrickson, M.A. Briggs, K.D. Tape, and N.C. Terry, "Aufeis fields as novel groundwater-dependent ecosystems in the arctic cryosphere." *Limnol. Oceanogr*. (2020) pp. 1-18.

Jones, C., K. Kielland, and L. Hinzman, "Modeling Groundwater Upwelling as a Control on River Ice Thickness." *Hydrol. Res.* Vol. 46, No. 4 (2015) pp. 566-577.

Jorgenson, M.T., K. Yoshikawa, V. Romanovsky, J. Brown, M. Kanevskiy, Y. Shur, S. Marchenko, G. Grosse, and B. Jones, "Map of permafrost characteristics in Alaska" Ninth International Conference on Permafrost, Fairbanks, AK (2008) 1 pp.

Kane, D.L., "Physical mechanics of aufeis growth." *Can. J. Civ. Eng.*, Vol. 8 (1981) pp. 186-195.

Korzhavin, K.N., *Action of Ice on Engineering Structures*, Translated by U.S. Joint Publications Research Service for the U.S. Army Cold Regions Research and Engineering Laboratory, Hanover, NH. Original: Publishing House of Siberian Branch of USSR Academy of Sciences (1962) 321 pp.

Lamontagne-Hallé, P., J.M. McKenzie, B.L. Kurylyk, J. Molson, and L.N. Lyon, "Guidelines for cold-regions groundwater numerical modeling." WIREs Water (2020). 26 pp.

Pavelsky, T.M., and J.P. Zarnetske, "Rapid decline in river icings detected in Arctic Alaska: Implications for a changing hydrologic cycle and river ecosystems." *Geophys. Res. Lett.*, Vol. 44 (2016) pp. 3228-3235.

Turcotte, B., K. Alfredsen, S. Beltaos, and B.C. Burrell, "Ice-related Floods and Flood Delineation along Streams and Small Rivers" 19th Workshop on the Hydraulics of Ice Covered Rivers, Whitehorse, YK, Canada (2017) 26 pp.

Veillette, J.J., and R.D. Thomas, "Icings and seepage in frozen glaciofluvial deposits, District of Keewatin, N.W.T." Can. Geotech. J. Vol. 16 (1979) pp. 789-798.

Yoshikawa, K., L.D. Hinzman, and D.L. Kane, "Spring and aufeis (icing) hydrology in Brooks Range, Alaska." J. Geophys. Res. Vol. 112, (2007) 14 pp.

Zabilansky, L.J., D.B. Hains, and J.I. Remus, "Increased Bed Erosion Due to Ice" in *Cold Regions Engineering 2006: Current Practices in Cold Regions Engineering*, edited by M. Davies and J.E. Zufelt, American Society of Civil Engineers (2006) 12 pp.

Zufelt, J.E., C.M. Vuyovich, and T.B. Baldwin, "Modeling of Aufeis-induced Flooding" in *Cold Regions Engineering 2006: Current Practices in Cold Regions Engineering*, edited by M. Davies and J.E. Zufelt, American Society of Civil Engineers (2006) 13 pp.

APPENDIX A: Additional Images of Case Study Bridges

List of Figures

Figure A1: Jack River orthomosaic from imagery collected by UAS in March 2020.
Figure A2: Jack River point cloud from imagery collected by UAS in March 2020.
Figure A3: Jack River point cloud from imagery collected by UAS in March 2020.
Figure A4: Jack River orthomosaic from imagery collected by UAS in April 2020.
Figure A5: Jack River point cloud from imagery collected by UAS in April 2020.
Figure A6: Jack River point cloud from imagery collected by UAS in April 2020.
Figure A7: Jack River single frame photo from imagery collected by UAS in April 2020 showing bridge/ice interface.
Figure A8: Jack River orthomosaic from imagery collected with crewed aircraft in October 2016.
Figure A9: Jack River orthomosaic from imagery collected with crewed aircraft in April 2017.
Figure A10: Jack River point cloud from imagery collected with crewed aircraft in April 2017.
Figure A11: Jack River orthomosaic from imagery collected with crewed aircraft in November 2017.
Figure A12: Jack River orthomosaic detail from imagery collected with crewed aircraft in November 2017.
Figure A13: Jack River orthomosaic from imagery collected with crewed aircraft in March 2018.
Figure A14: Jack River digital elevation model from imagery collected with crewed aircraft in March 2018.
Figure A15: Jack River detail of digital elevation model from imagery collected with crewed aircraft in March 2018.
Figure A16: Jack River still image from handheld field camera showing water upwelling during April 2020.
Figure A17: Jack River satellite imagery as seen in Google Earth.
Figure A18: O'Connor Creek orthomosaic from imagery collected from crewed aircraft in October 2016.
Figure A19: O'Connor Creek orthomosaic from imagery collected from crewed aircraft in December 2016.
Figure A20: O'Connor Creek orthomosaic from imagery collected from crewed aircraft in March 2017.
Figure A21: O'Connor Creek orthomosaic from imagery collected from crewed aircraft in April 2017.
Figure A22: O'Connor Creek orthomosaic from imagery collected from crewed aircraft in October 2017.
Figure A23: O'Connor Creek orthomosaic from imagery collected from crewed aircraft in March 2018.
Figure A24: O'Connor Creek orthomosaic from imagery collected from crewed aircraft in April 2018.
Figure A25: O'Connor Creek orthomosaic from imagery collected from crewed aircraft in March 2019.
Figure A26: O'Connor Creek orthomosaic from imagery collected from crewed aircraft in April 2019.
Figure A27: O'Connor Creek orthomosaic from imagery collected from crewed aircraft in October 2019.

Figure A28: Robertson River orthomosaic from imagery collected from crewed aircraft in October 2016.
Figure A29: Robertson River orthomosaic from imagery collected from crewed aircraft in December 2016.
Figure A30: Robertson River orthomosaic from imagery collected from crewed aircraft in March 2017.
Figure A31: Robertson River orthomosaic from imagery collected from crewed aircraft in April 2017.
Figure A32: Robertson River orthomosaic from imagery collected from crewed aircraft in November 2017.
Figure A33: Robertson River orthomosaic from imagery collected from crewed aircraft in March 2018.
Figure A34: Robertson River orthomosaic from imagery collected from crewed aircraft in April 2018.
Figure A35: Robertson River orthomosaic from imagery collected from crewed aircraft in March 2019.
Figure A36: Robertson River orthomosaic from imagery collected from crewed aircraft in April 2019.
Figure A37: Peters Creek orthomosaic from imagery collected from UAS on December 20, 2019.
Figure A38: Peters Creek orthomosaic from imagery collected from UAS on December 22, 2019.
Figure A39: Peters Creek orthomosaic from imagery collected from UAS on November 4, 2020.
Figure A40: Peters Creek orthomosaic from imagery collected from UAS on November 10, 2020.
Figure A41: Peters Creek orthomosaic from imagery collected from UAS on November 17, 2020.
Figure A42: Anchor River Bridge stationary mounted field camera image showing common problem of moisture on the camera lens.

Jack River Bridge on Parks Highway near Cantwell (BN0302)

From UAS:

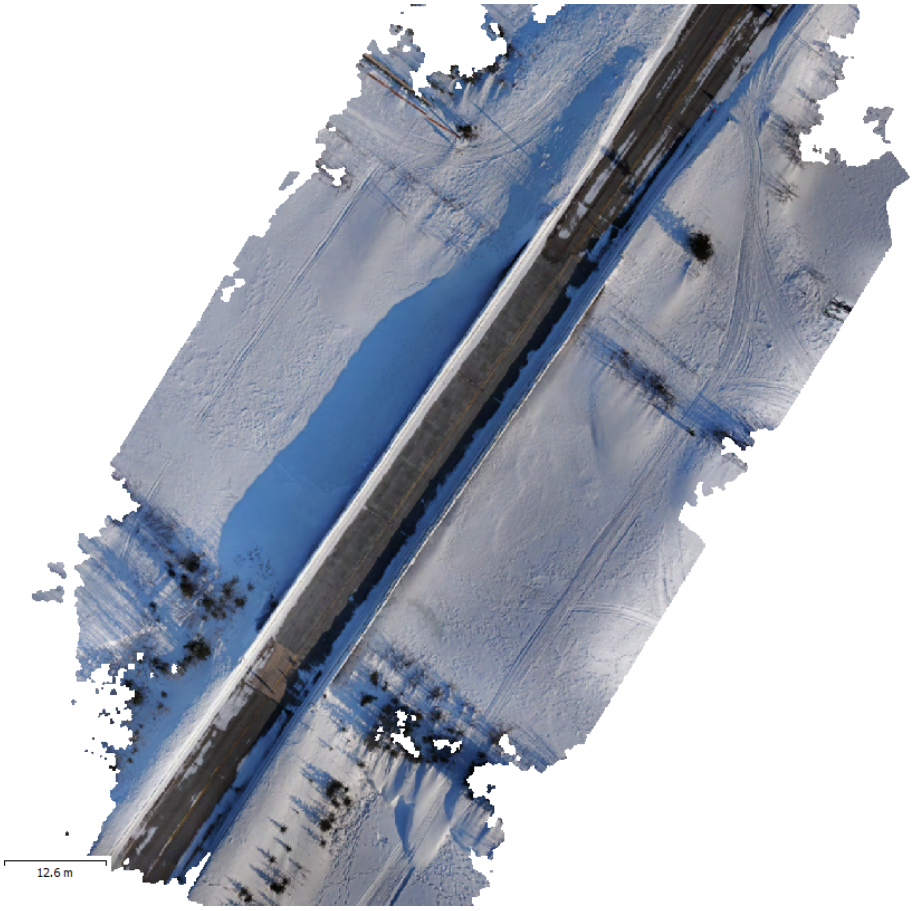

Figure A1: Jack River orthomosaic from imagery collected by UAS in March 2020.

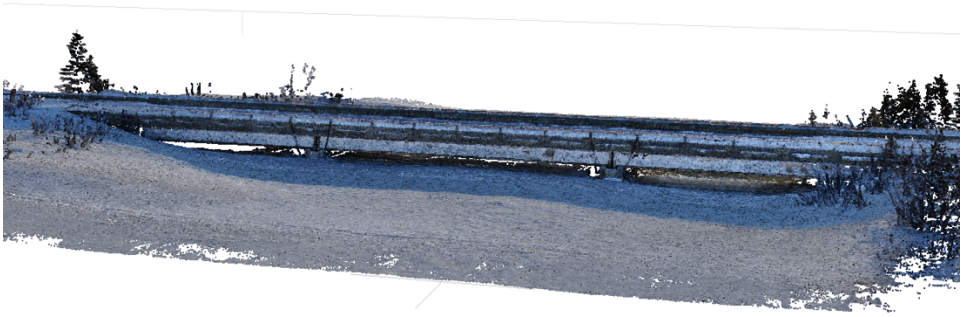

Figure A2: Jack River point cloud from imagery collected by UAS in March 2020.

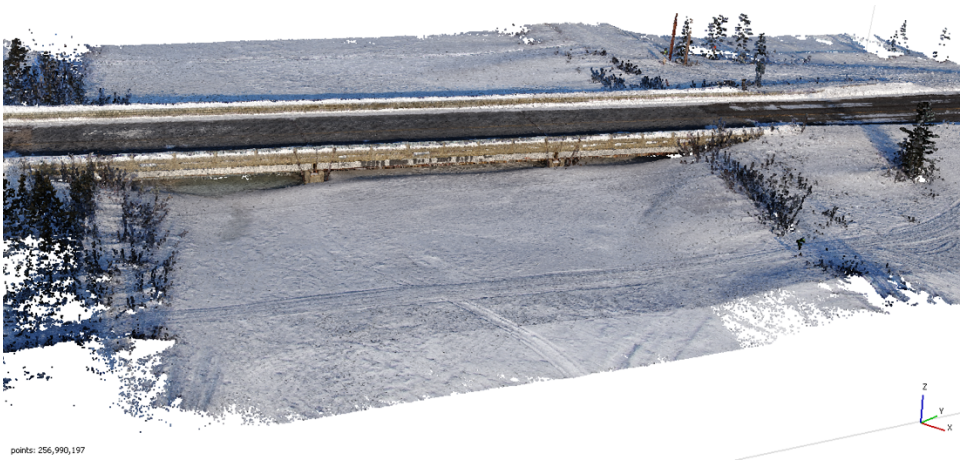

Figure A3: Jack River point cloud from imagery collected by UAS in March 2020.

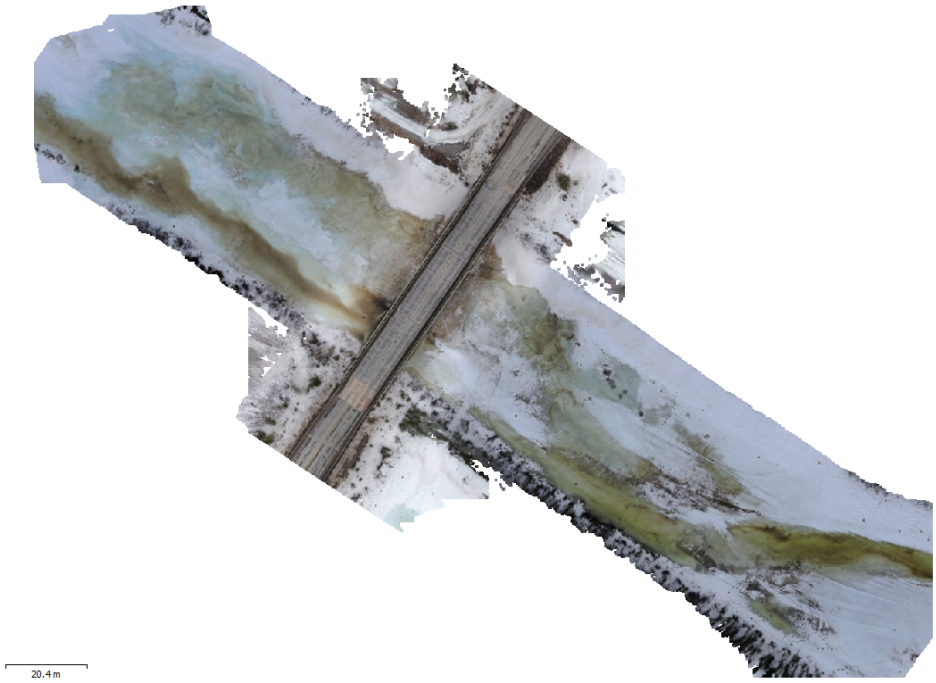

Figure A4: Jack River orthomosaic from imagery collected by UAS in April 2020.



Figure A5: Jack River point cloud from imagery collected by UAS in April 2020.



Figure A6: Jack River point cloud from imagery collected by UAS in April 2020.



Figure A7: Jack River single frame photo from imagery collected by UAS in April 2020 showing bridge/ice interface.

From crewed aircraft:

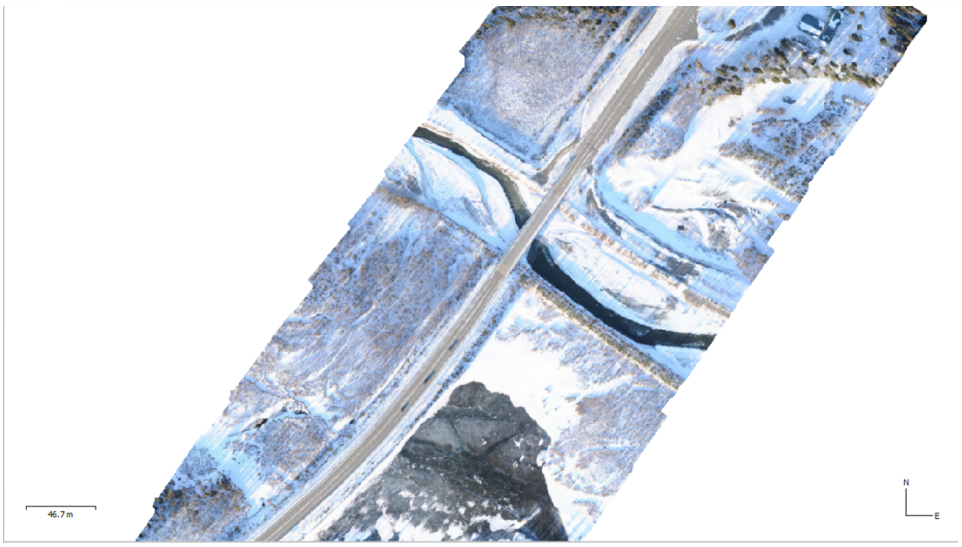

Figure A8: Jack River orthomosaic from imagery collected with crewed aircraft in October 2016.

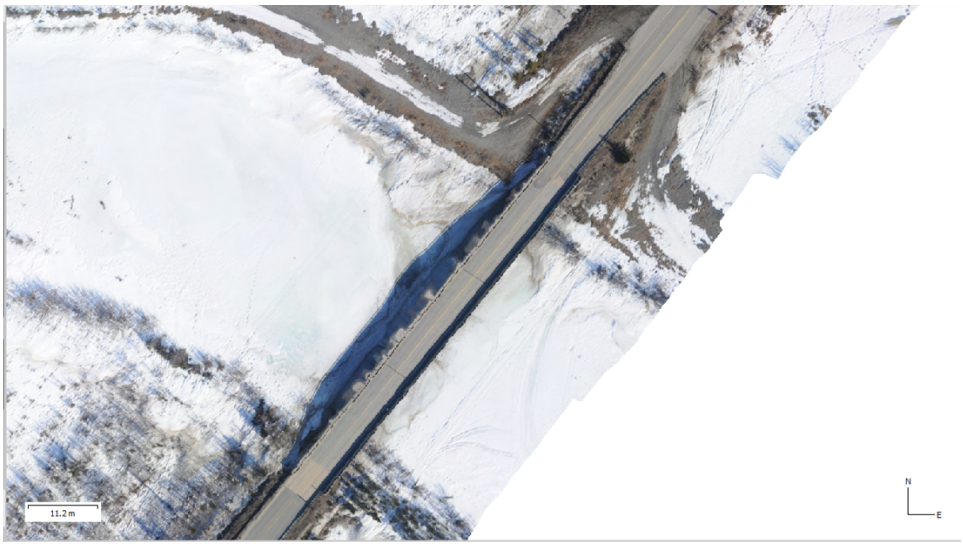

Figure A9: Jack River orthomosaic from imagery collected with crewed aircraft in April 2017.



Figure A10: Jack River point cloud from imagery collected with crewed aircraft in April 2017.

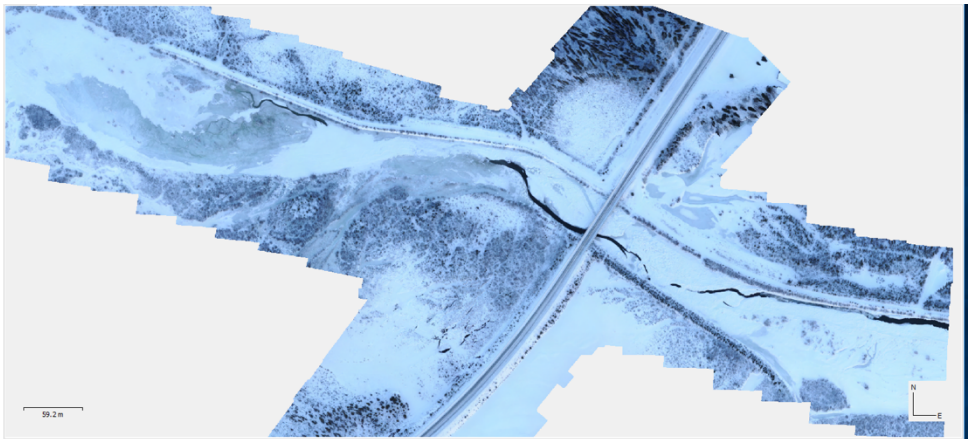

Figure A11: Jack River orthomosaic from imagery collected with crewed aircraft in November, 2017.

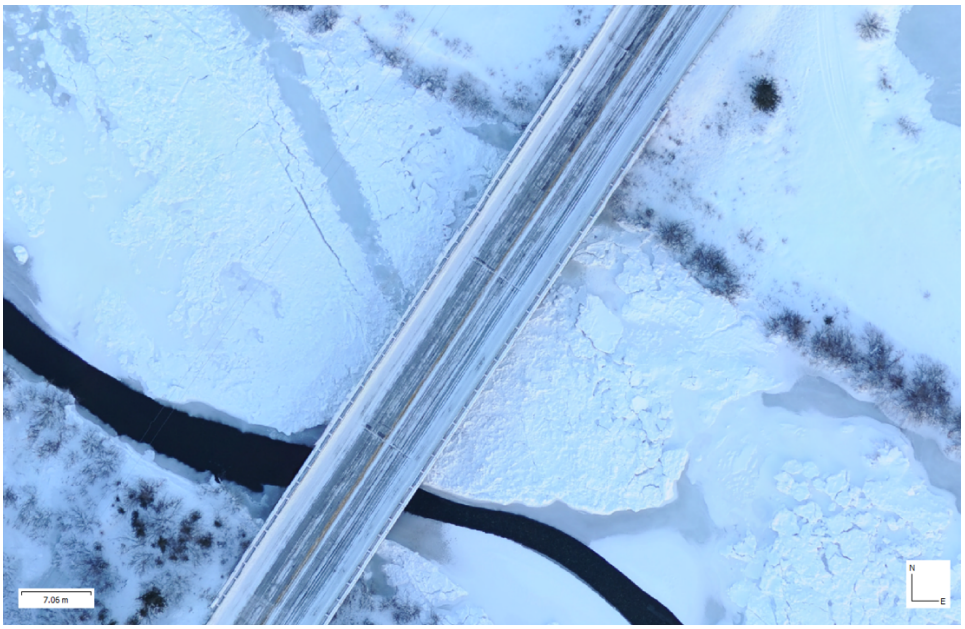

Figure A12: Jack River orthomosaic detail from imagery collected with crewed aircraft in November 2017.

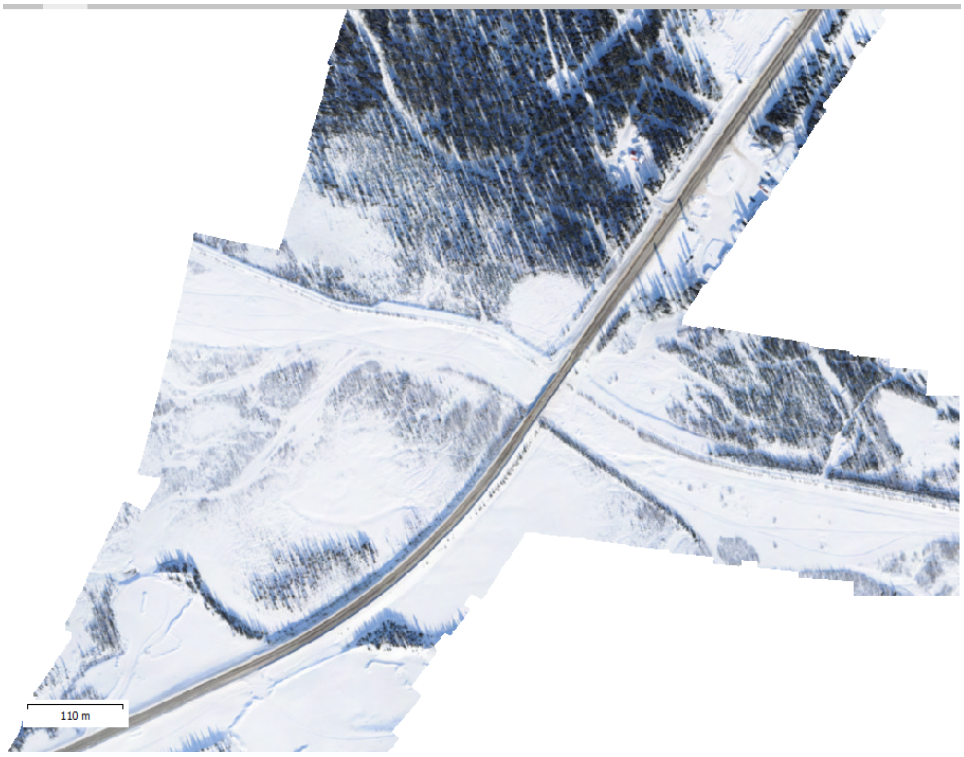

Figure A13: Jack River orthomosaic from imagery collected with crewed aircraft in March 2018.

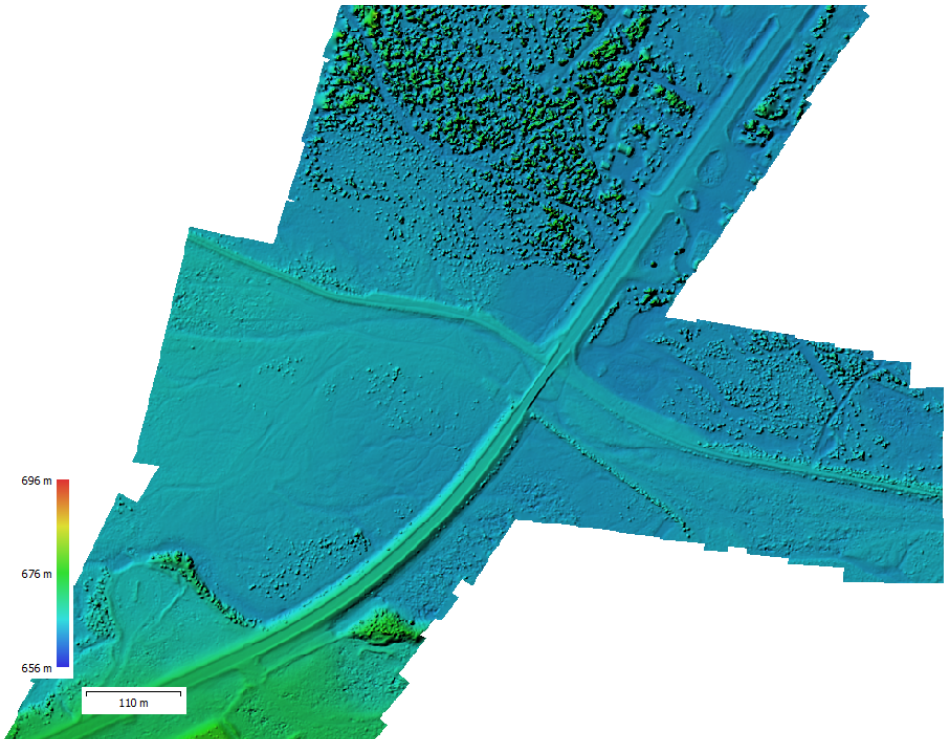

Figure A14: Jack River digital elevation model from imagery collected with crewed aircraft in March 2018.

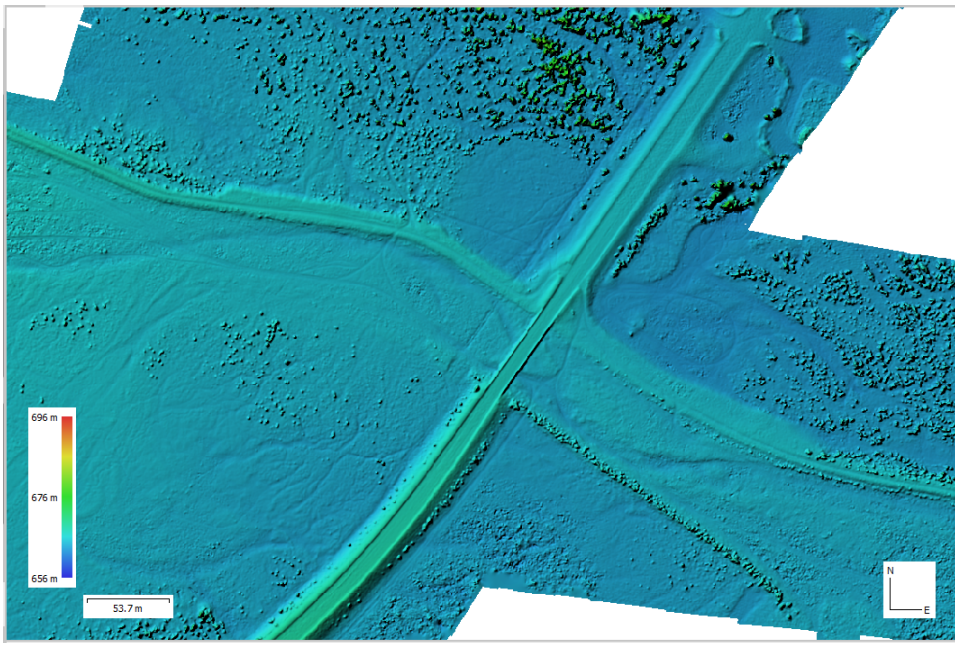

Figure A15: Jack River detail of digital elevation model from imagery collected with crewed aircraft in March 2018.

From handheld field camera:



Figure A16: Jack River still image from handheld field camera showing water upwelling during April 2020.



Figure A17: Jack River satellite imagery as seen in Google Earth. The area shows considerable disturbances in soil and ground cover, as well as water impoundment by the Parks Highway.

O'Connor Creek Bridge on Goldstream Road near Fairbanks (BN0303)

From crewed aircraft:



Figure A18: O'Connor Creek orthomosaic from imagery collected from crewed aircraft in October 2016.

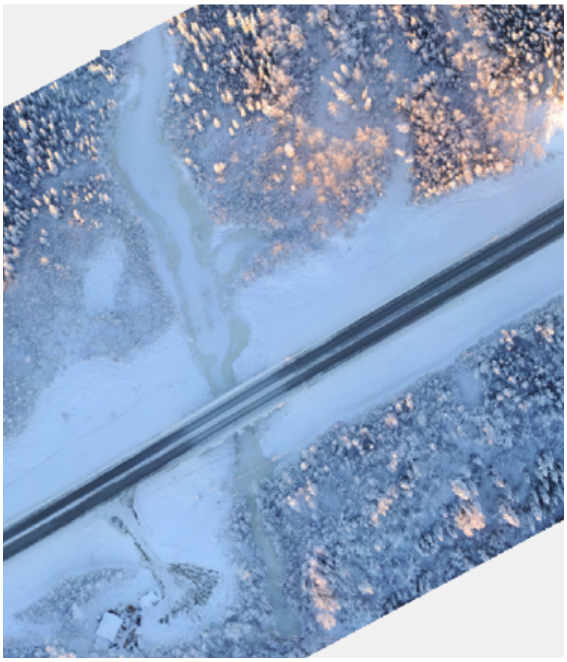

Figure A19: O'Connor Creek orthomosaic from imagery collected from crewed aircraft in December 2016.

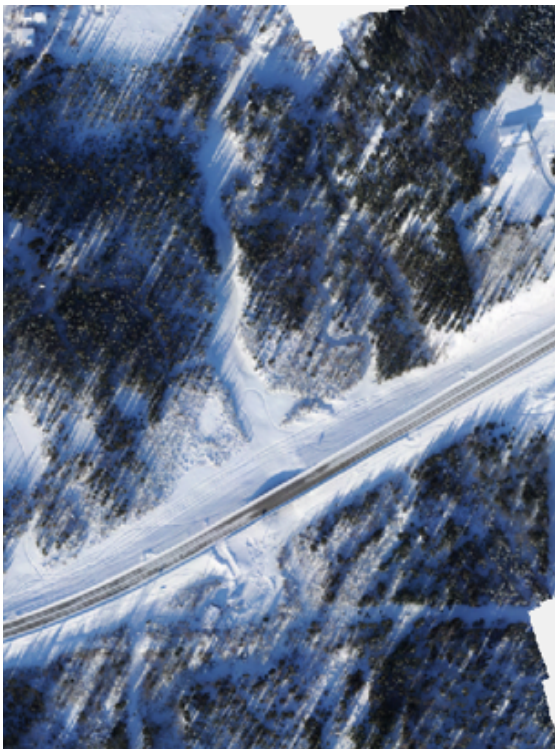

Figure A20: O'Connor Creek orthomosaic from imagery collected from crewed aircraft in March 2017.

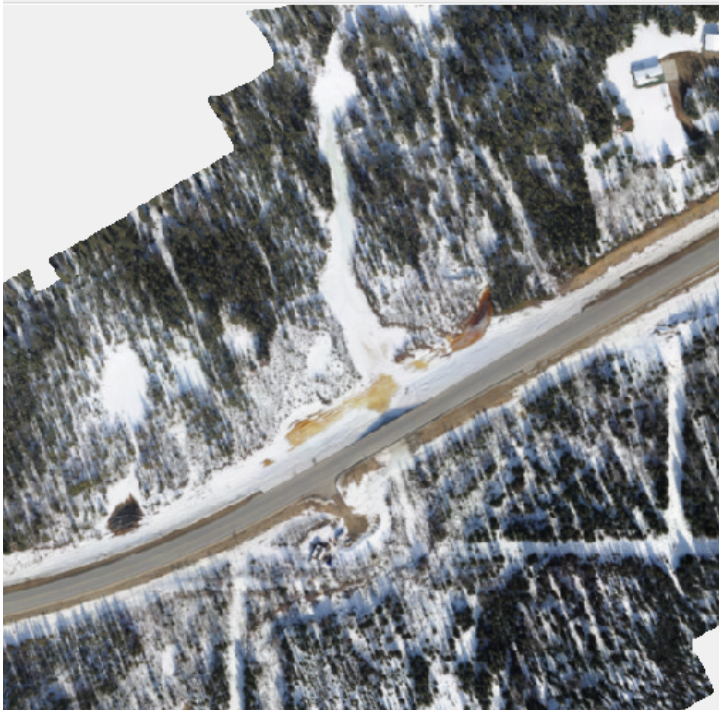

Figure A21: O'Connor Creek orthomosaic from imagery collected from crewed aircraft in April 2017.



Figure A22: O'Connor Creek orthomosaic from imagery collected from crewed aircraft in October 2017.



Figure A23: O'Connor Creek orthomosaic from imagery collected from crewed aircraft in March 2018.



Figure A24: O'Connor Creek orthomosaic from imagery collected from crewed aircraft in April 2018.



Figure A25: O'Connor Creek orthomosaic from imagery collected from crewed aircraft in March 2019.



Figure A26: O'Connor Creek orthomosaic from imagery collected from crewed aircraft in April 2019.

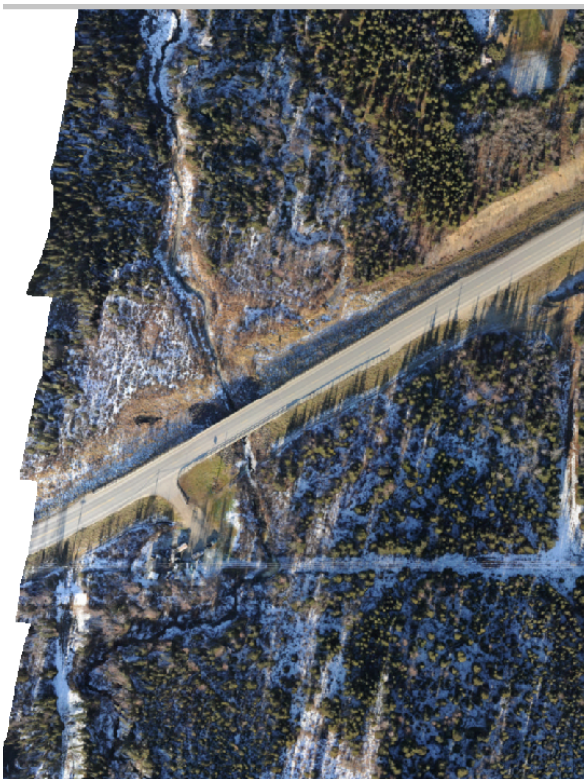

Figure A27: O’Connor Creek orthomosaic from imagery collected from crewed aircraft in October 2019.

Robertson River Bridge on Alaska Highway near Dot Lake (BN0509)

From crewed aircraft:



Figure A28: Robertson River orthomosaic from imagery collected from crewed aircraft in October 2016.

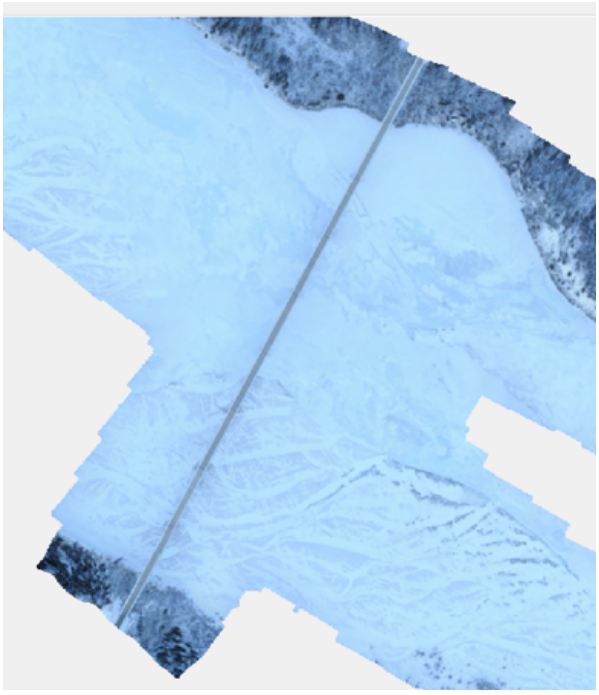

Figure A29: Robertson River orthomosaic from imagery collected from crewed aircraft in December 2016.

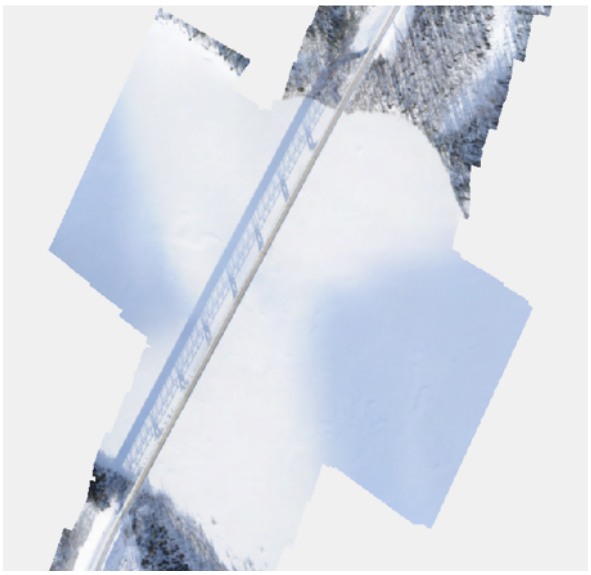

Figure A30: Robertson River orthomosaic from imagery collected from crewed aircraft in March 2017.



Figure A31: Robertson River orthomosaic from imagery collected from crewed aircraft in April 2017.

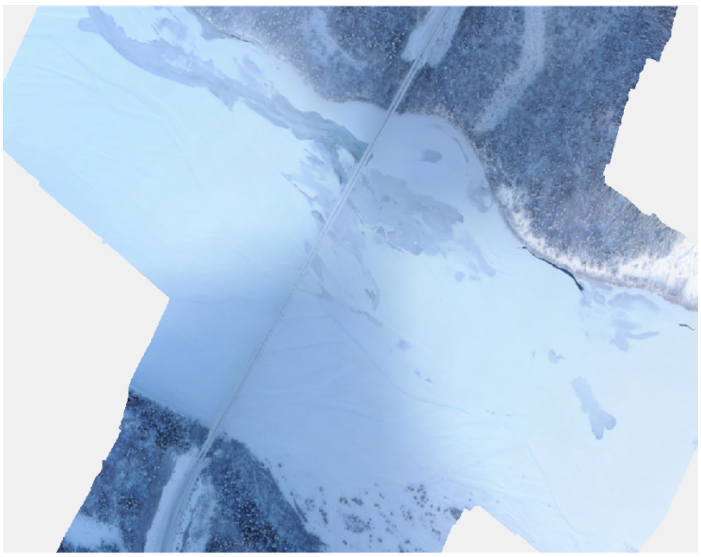

Figure A32: Robertson River orthomosaic from imagery collected from crewed aircraft in November 2017.

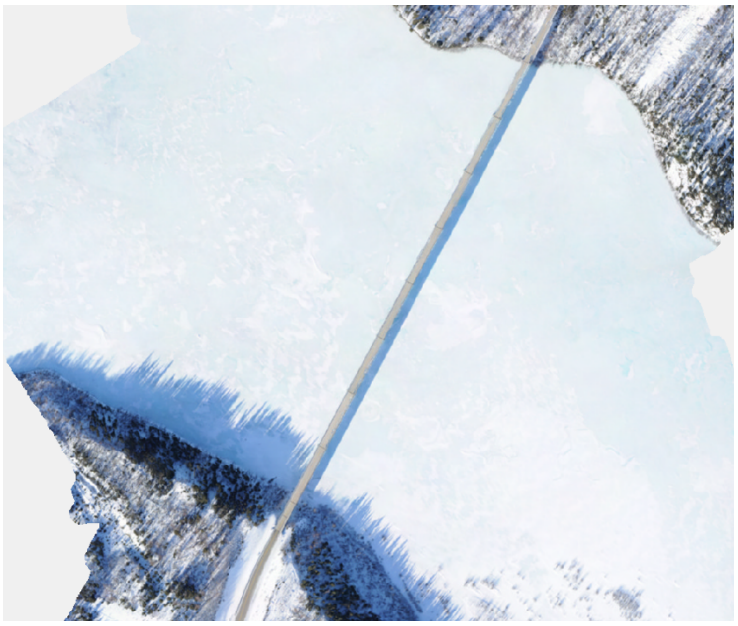

Figure A33: Robertson River orthomosaic from imagery collected from crewed aircraft in March 2018.

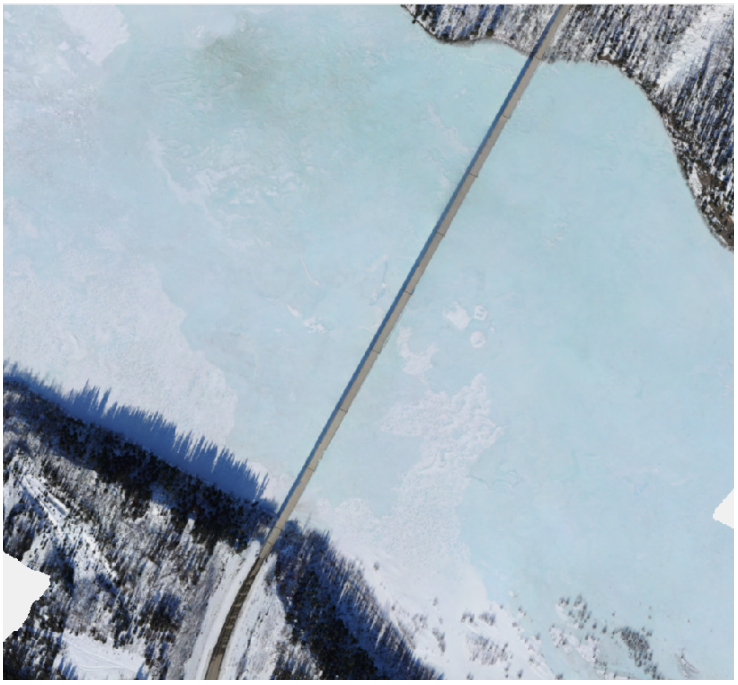

Figure A34: Robertson River orthomosaic from imagery collected from crewed aircraft in April 2018.



Figure A35: Robertson River orthomosaic from imagery collected from crewed aircraft in March 2019.

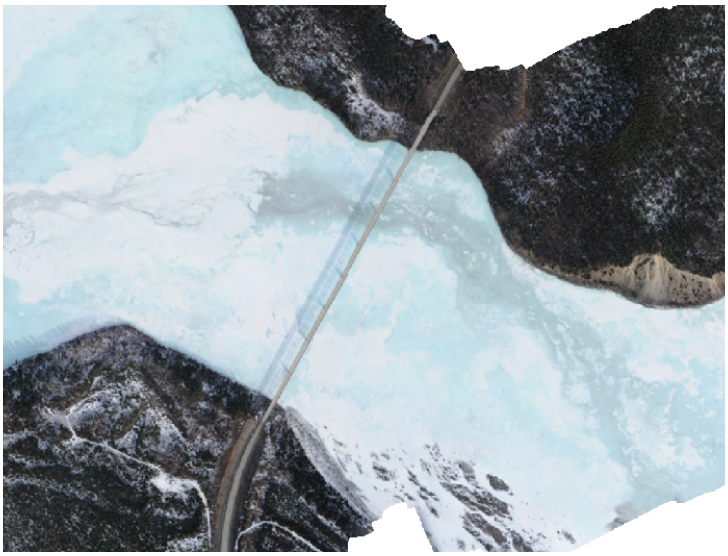

Figure A36: Robertson River orthomosaic from imagery collected from crewed aircraft in April 2019.

Peters Creek at Stoltze Road (BN1031)

Data from UAS:

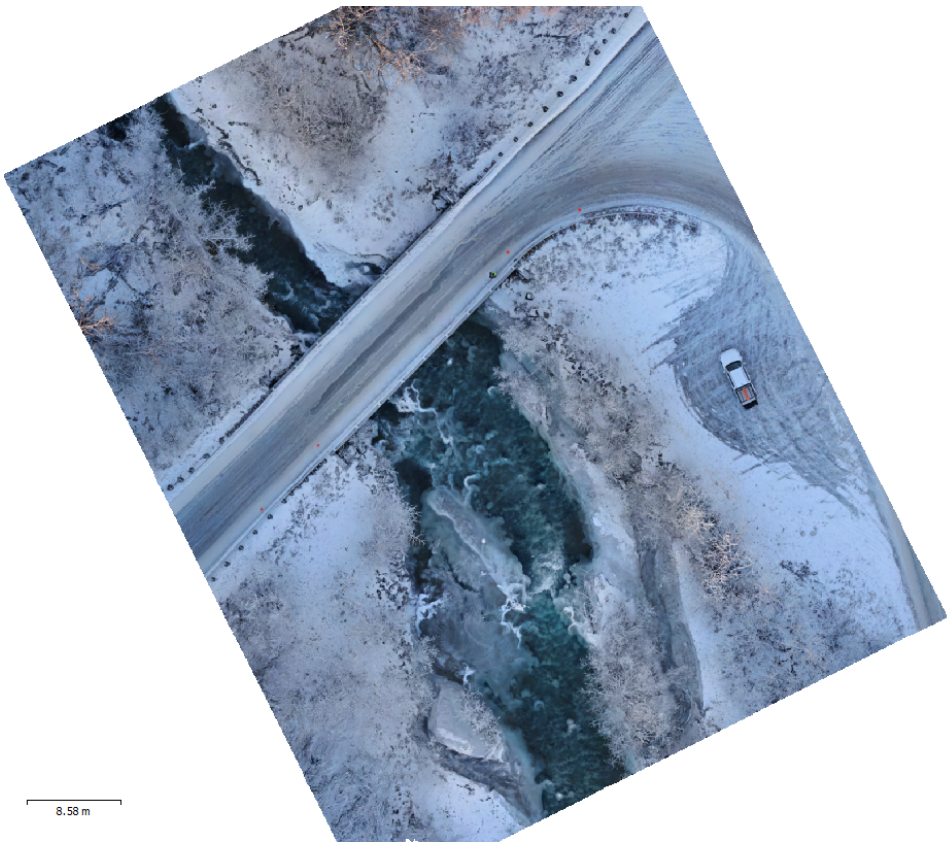

Figure A37: Peters Creek orthomosaic from imagery collected from UAS on December 20, 2019.

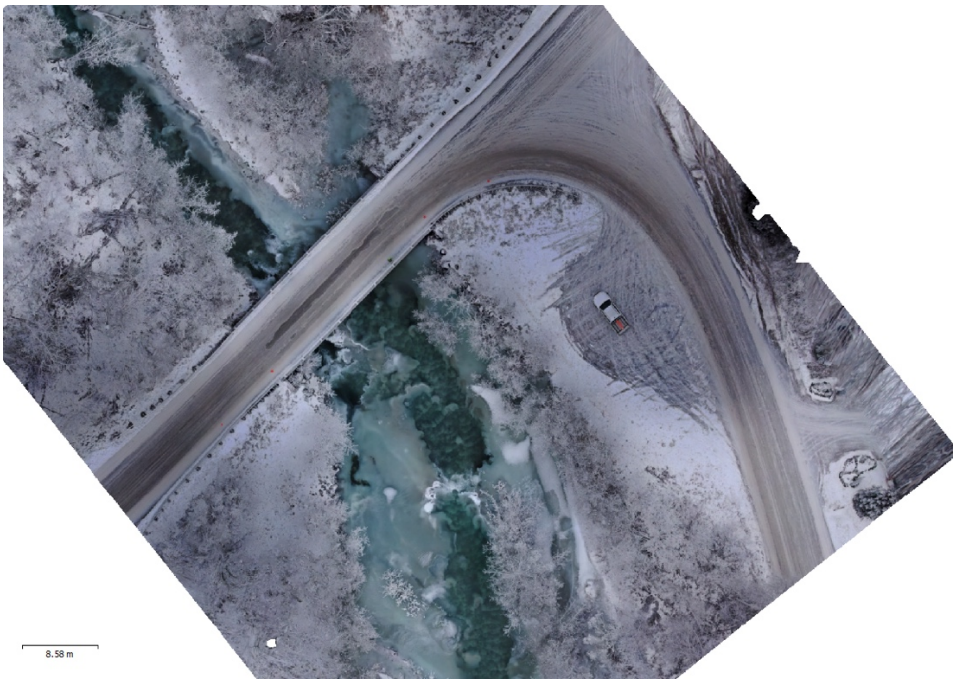

Figure A38: Peters Creek orthomosaic from imagery collected from UAS on December 22, 2019.

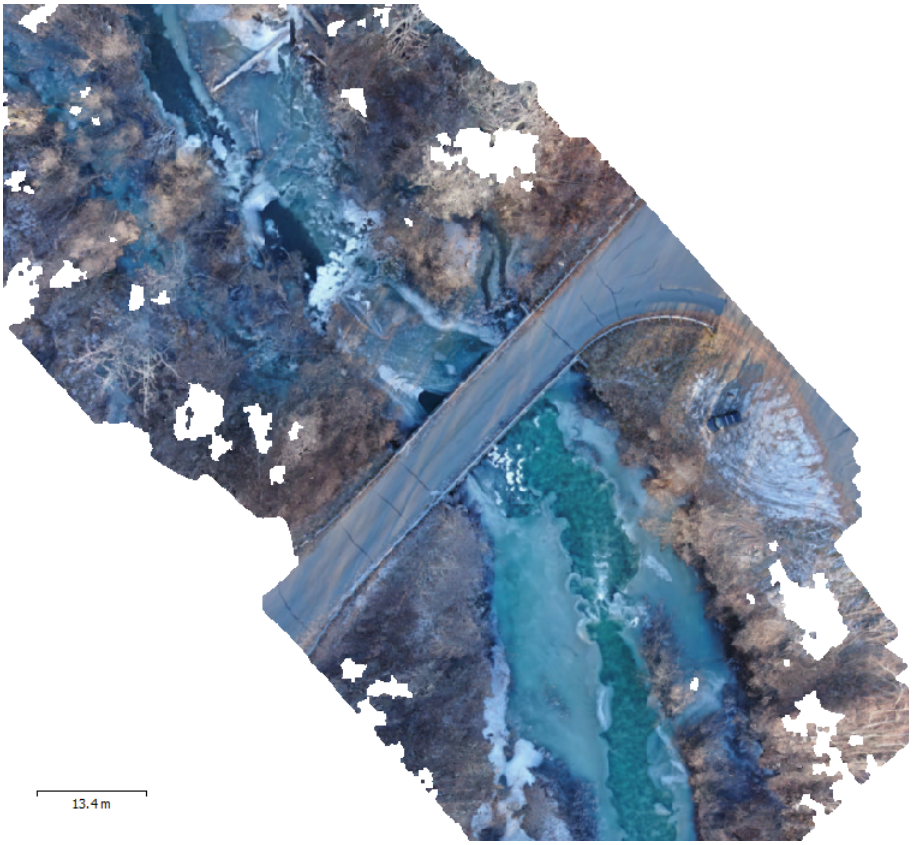

Figure A39: Peters Creek orthomosaic from imagery collected from UAS on November 4, 2020.

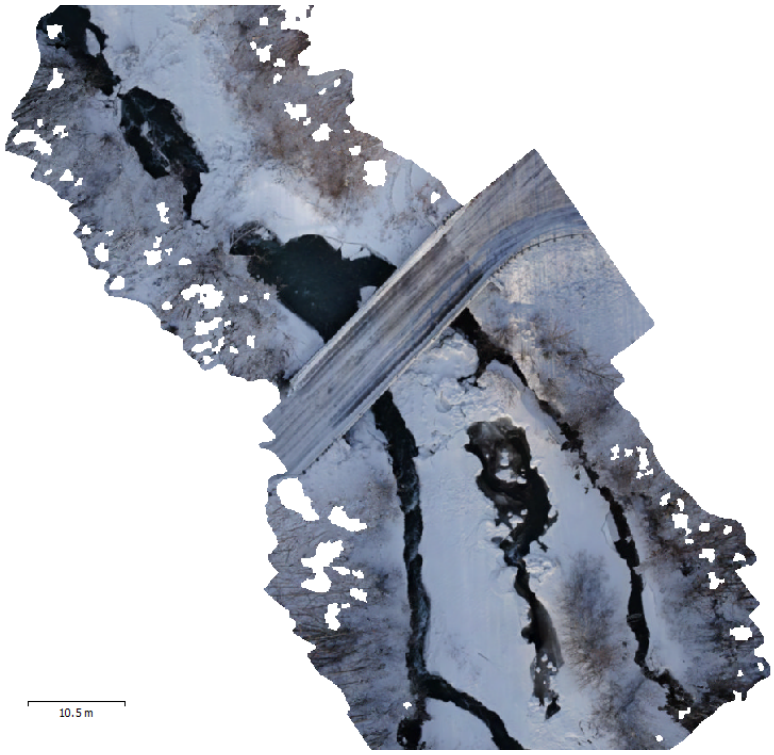

Figure A40: Peters Creek orthomosaic from imagery collected from UAS on November 10, 2020.

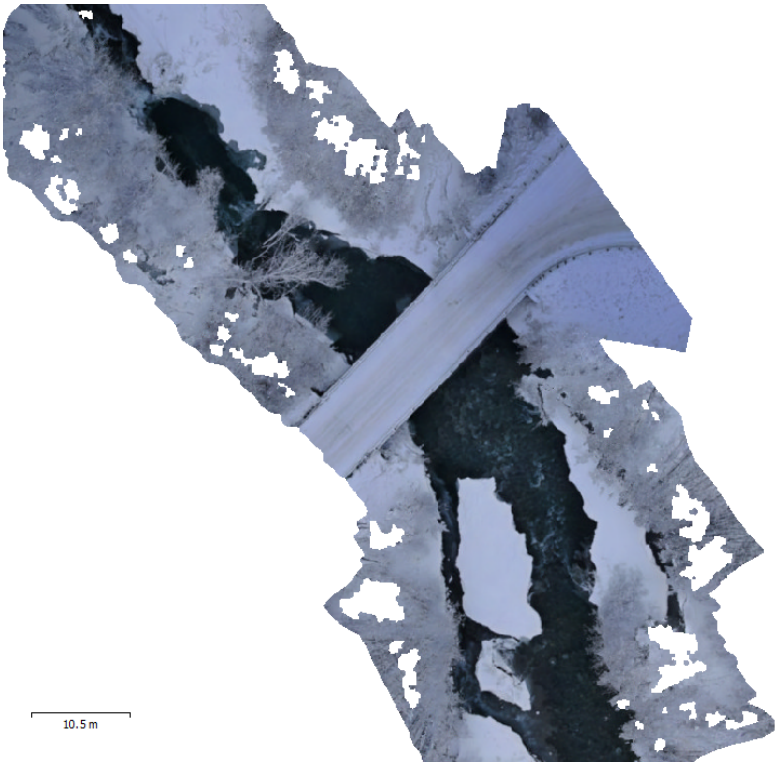

Figure A41: Peters Creek orthomosaic from imagery collected from UAS on November 17, 2020.

Anchor River Bridge on the Old Sterling Highway (BN0910)



Figure A42: Anchor River Bridge stationary mounted field camera image showing common problem of moisture on the camera lens.

APPENDIX B: Sample Images of Other Bridges

List of Figures

Figure B1: Johnson River Bridge orthomosaic from imagery collected by UAS in April 2020.
Figure B2: Johnson River Bridge point cloud from imagery collected by UAS in April 2020.
Figure B3: Johnson River Bridge orthomosaic from imagery collected by crewed aircraft in October 2016.
Figure B4: Johnson River Bridge orthomosaic from imagery collected by crewed aircraft in March 2017.
Figure B5: Johnson River Bridge orthomosaic from imagery collected by crewed aircraft in April 2017.
Figure B6: Johnson River Bridge orthomosaic from imagery collected by crewed aircraft in November 2017.
Figure B7: Johnson River Bridge orthomosaic from imagery collected by crewed aircraft in March 2018.
Figure B8: Johnson River Bridge orthomosaic from imagery collected by crewed aircraft in April 2018.
Figure B9: Johnson River Bridge orthomosaic from imagery collected by crewed aircraft in March 2019.
Figure B10: Johnson River Bridge orthomosaic from imagery collected by crewed aircraft in April 2019.
Figure B11: Gerstle River Bridge orthomosaic from imagery collected by UAS in April 2020.
Figure B12: Gerstle River Bridge orthomosaic detail from imagery collected by UAS in April 2020.
Figure B13: Gerstle River Bridge point cloud from imagery collected by UAS in April 2020.
Figure B14: Gerstle River Bridge orthomosaic from imagery collected by crewed aircraft in March 2017.
Figure B15: Gerstle River Bridge orthomosaic detail from imagery collected by crewed aircraft in March 2017.
Figure B16: Gerstle River Bridge orthomosaic from imagery collected by crewed aircraft in April 2017.
Figure B17: Gerstle River Bridge orthomosaic detail from imagery collected by crewed aircraft in April 2017.
Figure B18: Gerstle River Bridge orthomosaic from imagery collected by crewed aircraft in October 2017.
Figure B19: Gerstle River Bridge orthomosaic from imagery collected by crewed aircraft in November 2017.
Figure B20: Gerstle River Bridge orthomosaic from imagery collected by crewed aircraft in March 2018.
Figure B21: Gerstle River Bridge orthomosaic from imagery collected by crewed aircraft in April 2018.
Figure B22: Gerstle River Bridge orthomosaic from imagery collected by crewed aircraft in March 2019.
Figure B23: Gerstle River Bridge orthomosaic from imagery collected by crewed aircraft in April 2019.
Figure B24: Banner Creek Bridge orthomosaic from imagery collected by UAS in April 2020.

Figure B25: Banner Creek Bridge point cloud from imagery collected by UAS in April 2020.
Figure B26: Banner Creek Bridge point cloud from imagery collected by hand-held field camera in November of 2019.
Figure B27: Banner Creek Bridge orthomosaic from imagery collected by crewed aircraft in October 2016.
Figure B28: Banner Creek Bridge orthomosaic from imagery collected by crewed aircraft in December 2016.
Figure B29: Banner Creek Bridge orthomosaic from imagery collected by crewed aircraft in March 2017.
Figure B30: Banner Creek Bridge point cloud from imagery collected by crewed aircraft in April 2017.
Figure B31: Banner Creek Bridge orthomosaic from imagery collected by crewed aircraft in October 2017.
Figure B32: Banner Creek Bridge orthomosaic from imagery collected by crewed aircraft in November 2017.
Figure B33: Banner Creek Bridge orthomosaic from imagery collected by crewed aircraft in March 2018.
Figure B34: Banner Creek Bridge orthomosaic from imagery collected by crewed aircraft in April 2019.
Figure B35: Gulkana River Bridge orthomosaic from imagery collected by UAS in March 2020.
Figure B36: Gulkana River Bridge orthomosaic from imagery collected by UAS in April 2020.
Figure B37: Gulkana River Bridge point cloud from imagery collected by UAS in April 2020.
Figure B38: Gulkana River Bridge orthomosaic from imagery collected by crewed aircraft in October 2016.
Figure B39: Gulkana River Bridge orthomosaic detail from imagery collected by crewed aircraft in October 2016.
Figure B40: Gulkana River Bridge orthomosaic from imagery collected by crewed aircraft in December 2016.
Figure B41: Gulkana River Bridge orthomosaic from imagery collected by crewed aircraft in April 2017.
Figure B42: Gulkana River Bridge orthomosaic from imagery collected by crewed aircraft in November 2017.
Figure B43: Gulkana River Bridge orthomosaic from imagery collected by crewed aircraft in March 2018.
Figure B44: Gulkana River Bridge orthomosaic from imagery collected by crewed aircraft in April 2018.
Figure B45: Gunnysack Creek Bridge orthomosaic from imagery collected by UAS in April 2020.
Figure B46: Gunnysack Creek Bridge point cloud from imagery collected by UAS in April 2020.
Figure B47: Gunnysack Creek Bridge point cloud from imagery collected by UAS in April 2020.
Figure B48: Gunnysack Creek Bridge orthomosaic from imagery collected by crewed aircraft in October 2016.
Figure B49: Gunnysack Creek Bridge orthomosaic from imagery collected by crewed aircraft in April 2017.
Figure B50: Ruby Creek Bridge orthomosaic from imagery collected by UAS in April 2020.
Figure B51: Ruby Creek Bridge point cloud from imagery collected by UAS in April 2020.

Figure B52: Ruby Creek Bridge point cloud from imagery collected by hand-held field camera in November 2019.
Figure B53: Ruby Creek Bridge orthomosaic from imagery collected by crewed aircraft in October 2016.
Figure B54: Jarvis Creek Bridge orthomosaic from imagery collected by UAS in April 2020.
Figure B55: Jarvis Creek Bridge point cloud from imagery collected by hand-held field camera in March 2020.
Figure B56: Jarvis Creek Bridge point cloud from imagery collected by hand-held field camera in April 2020.
Figure B57: Jarvis Creek Bridge orthomosaic from imagery collected by crewed in October 2016.
Figure B58: Jarvis Creek Bridge orthomosaic from imagery collected by crewed aircraft in December 2016.
Figure B59: Jarvis Creek Bridge orthomosaic from imagery collected by crewed aircraft in March 2017.
Figure B60: Jarvis Creek Bridge orthomosaic from imagery collected by crewed aircraft in April 2017.
Figure B61: Jarvis Creek Bridge orthomosaic from imagery collected by crewed aircraft in October 2017.
Figure B62: Jarvis Creek Bridge orthomosaic from imagery collected by crewed aircraft in March 2018.
Figure B63: Jarvis Creek Bridge orthomosaic from imagery collected by crewed aircraft in April 2018.
Figure B64: Jarvis Creek Bridge orthomosaic from imagery collected by crewed aircraft in March 2019.
Figure B65: Jarvis Creek Bridge orthomosaic from imagery collected by crewed aircraft in April 2019.
Figure B66: Gakona Bridge orthomosaic from imagery collected by UAS in April 2020.
Figure B67: Gakona Bridge point cloud from imagery collected by UAS in April 2020.
Figure B68: Gakona Bridge orthomosaic from imagery collected by UAS in November 2019.
Figure B69: Gakona Bridge orthomosaic from imagery collected by crewed aircraft in October 2016.
Figure B70: Gakona Bridge orthomosaic from imagery collected by crewed aircraft in December 2016.
Figure B71: Gakona Bridge orthomosaic from imagery collected by crewed aircraft in April 2017.
Figure B72: Gakona Bridge orthomosaic from imagery collected by crewed aircraft in November 2017.
Figure B73: Gakona Bridge orthomosaic from imagery collected by crewed aircraft in March 2018.
Figure B74: Gakona Bridge orthomosaic from imagery collected by crewed aircraft in April 2018.
Figure B75: Sinona Creek Bridge orthomosaic from imagery collected by UAS in April 2018.
Figure B76: Sinona Creek Bridge point cloud from imagery collected by UAS in April 2018.
Figure B77: Sinona Creek Bridge orthomosaic from imagery collected by crewed aircraft in March 2018.

Figure B78: Sinona Creek Bridge orthomosaic from imagery collected by crewed aircraft in April 2018.
Figure B79: Tok River Bridge orthomosaic from imagery collected by UAS in April 2020.
Figure B80: Tok River Bridge point cloud from imagery collected by UAS in April 2020.
Figure B81: Tok River Bridge point cloud detail from imagery collected by UAS in April 2020.
Figure B82: Tok River Bridge orthomosaic from imagery collected by crewed aircraft in October 2016.
Figure B83: Tok River Bridge orthomosaic from imagery collected by crewed aircraft in April 2017.
Figure B84: Tok River Bridge orthomosaic from imagery collected by crewed aircraft in March 2018.
Figure B85: Tok River Bridge orthomosaic from imagery collected by crewed aircraft in April 2018.
Figure B86: Seattle Creek Bridge orthomosaic from imagery collected by UAS in April 2020.
Figure B87: Seattle Creek Bridge point cloud from imagery collected by UAS in April 2020.
Figure B88: Seattle Creek Bridge orthomosaic from imagery collected by crewed aircraft in October 2016.
Figure B89: Seattle Creek Bridge orthomosaic from imagery collected by crewed aircraft in December 2016.
Figure B90: Seattle Creek Bridge orthomosaic from imagery collected by crewed aircraft in April 2017.
Figure B91: Seattle Creek Bridge orthomosaic from imagery collected by crewed aircraft in November 2017.
Figure B92: Seattle Creek Bridge orthomosaic from imagery collected by crewed aircraft in March 2018.
Figure B93: Seattle Creek Bridge orthomosaic from imagery collected by crewed aircraft in April 2018.
Figure B94: Carlo Creek Bridge orthomosaic from imagery collected by UAS in March 2020.
Figure B95: Carlo Creek Bridge orthomosaic from imagery collected by UAS in April 2020.
Figure B96: Carlo Creek Bridge orthomosaic from imagery collected by crewed aircraft in October 2016.
Figure B97: Carlo Creek Bridge orthomosaic from imagery collected by crewed aircraft in December 2016.
Figure B98: Carlo Creek Bridge orthomosaic from imagery collected by crewed aircraft in April 2017.
Figure B99: Carlo Creek Bridge orthomosaic from imagery collected by crewed aircraft in March 2018.
Figure B100: Carlo Creek Bridge orthomosaic from imagery collected by crewed aircraft in April 2018.
Figure B101: Kingfisher Creek Bridge orthomosaic from imagery collected by UAS in March 2020.
Figure B102: Kingfisher Creek Bridge point cloud from imagery collected by UAS in March 2020.
Figure B103: Kingfisher Creek Bridge orthomosaic from imagery collected by UAS in April 2020.

Figure B104: Kingfisher Creek Bridge point cloud from imagery collected by UAS in April 2020.
Figure B105: Kingfisher Creek Bridge orthomosaic from imagery collected by crewed aircraft in April 2017.
Figure B106: Kingfisher Creek Bridge orthomosaic from imagery collected by crewed aircraft in November 2017.
Figure B107: Kingfisher Creek Bridge orthomosaic from imagery collected by crewed aircraft in March 2018.
Figure B108: Kingfisher Creek Bridge orthomosaic from imagery collected by crewed aircraft in April 2018.
Figure B109: Goldstream Creek Bridge orthomosaic from imagery collected by UAS in March 2020.
Figure B110: Goldstream Creek Bridge point cloud from imagery collected by UAS in March 2020.
Figure B111: Goldstream Creek Bridge point cloud from imagery collected by UAS in March 2020.
Figure B112: Goldstream Creek Bridge orthomosaic from imagery collected by crewed aircraft in October 2016.
Figure B113: Goldstream Creek Bridge orthomosaic from imagery collected by crewed aircraft in December 2016.
Figure B114: Goldstream Creek Bridge orthomosaic detail from imagery collected by crewed aircraft in December 2016.
Figure B115: Goldstream Creek Bridge orthomosaic from imagery collected by crewed aircraft in March 2017.
Figure B116: Goldstream Creek Bridge orthomosaic from imagery collected by crewed aircraft in April 2017.
Figure B117: Goldstream Creek Bridge orthomosaic from imagery collected by crewed aircraft in October 2017.
Figure B118: Goldstream Creek Bridge point cloud from imagery collected by crewed aircraft in October 2017.
Figure B119: Goldstream Creek Bridge orthomosaic from imagery collected by crewed aircraft in March 2018.
Figure B120: Goldstream Creek Bridge orthomosaic from imagery collected by crewed aircraft in April 2018.
Figure B121: Goldstream Creek Bridge orthomosaic from imagery collected by crewed aircraft in March 2019.
Figure B122: Goldstream Creek Bridge orthomosaic from imagery collected by crewed aircraft in April 2019.
Figure B123: Goldstream Creek Bridge orthomosaic from imagery collected by crewed aircraft in October 2019.
Figure B124: Dragonfly Creek Bridge orthomosaic from imagery collected by UAS in March 2020.
Figure B125: Dragonfly Creek Bridge orthomosaic from imagery collected by UAS in April 2020.
Figure B126: Dragonfly Creek Bridge point cloud from imagery collected by UAS in April 2020.

Figure B127: Dragonfly Creek Bridge orthomosaic from imagery collected by crewed aircraft in April 2017.
Figure B128: Dragonfly Creek Bridge orthomosaic from imagery collected by crewed aircraft in March 2018.
Figure B129: Fox Creek Bridge orthomosaic from imagery collected by UAS in March 2020.
Figure B130: Fox Creek Bridge point cloud from imagery collected by UAS in March 2020.
Figure B131: Fox Creek Bridge point cloud from imagery collected by UAS in March 2020.
Figure B132: Fox Creek Bridge orthomosaic from imagery collected by UAS in April 2020.
Figure B133: Fox Creek Bridge point cloud from imagery collected by UAS in April 2020.
Figure B134: Fox Creek Bridge point cloud from imagery collected by crewed aircraft in November 2017.
Figure B135: Tulsona Creek Bridge orthomosaic from imagery collected by UAS in April 2020.
Figure B136: Tulsona Creek Bridge orthomosaic from imagery collected by crewed aircraft in October 2016.
Figure B137: Tulsona Creek Bridge orthomosaic from imagery collected by crewed aircraft in April 2017.
Figure B137: Tulsona Creek Bridge orthomosaic detail from imagery collected by crewed aircraft in April 2017.
Figure B138: Tulsona Creek Bridge orthomosaic detail from imagery collected by crewed aircraft in November 2017.
Figure B139: Tulsona Creek Bridge orthomosaic detail from imagery collected by crewed aircraft in March 2018.
Figure B140: Tulsona Creek Bridge orthomosaic detail from imagery collected by crewed aircraft in April 2018.

Johnson River Bridge on the Alaska Highway (BN0518)

From UAS:



Figure B1: Johnson River Bridge orthomosaic from imagery collected by UAS in April 2020.



Figure B2: Johnson River Bridge point cloud from imagery collected by UAS in April 2020.

From crewed aircraft:

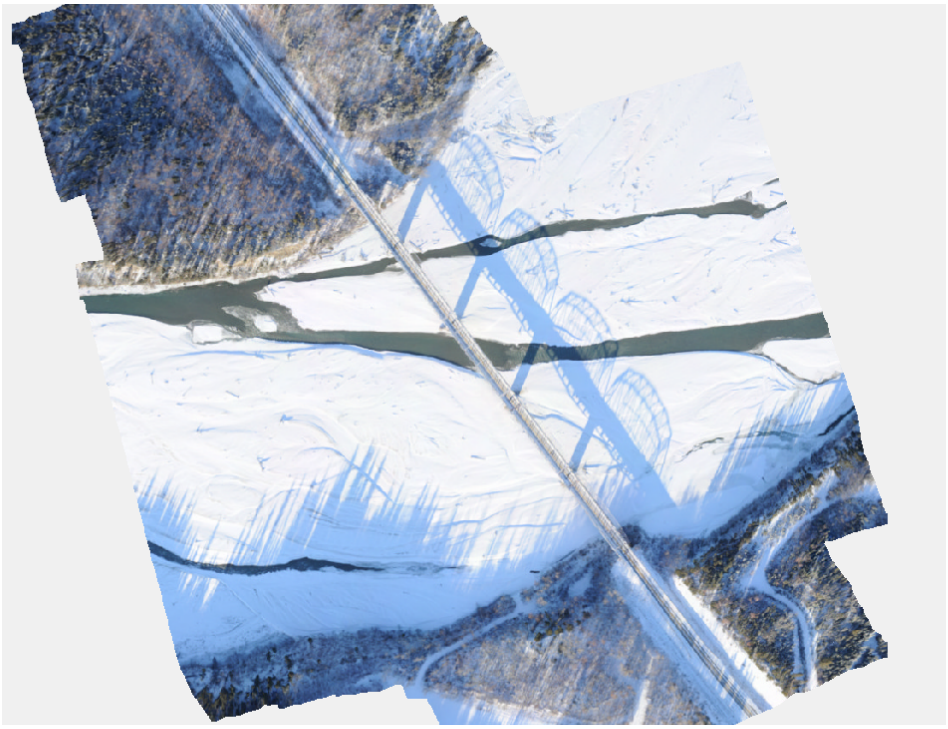
Figure B3: Johnson River Bridge orthomosaic from imagery collected by crewed aircraft in October 2016.

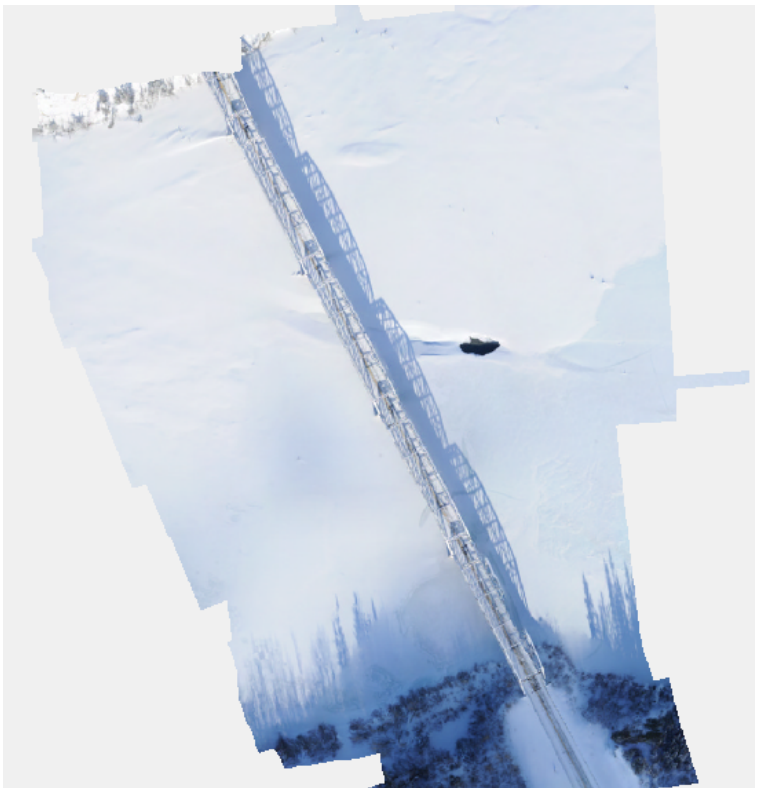

Figure B4: Johnson River Bridge orthomosaic from imagery collected by crewed aircraft in March 2017.



Figure B5: Johnson River Bridge orthomosaic from imagery collected by crewed aircraft in April 2017.

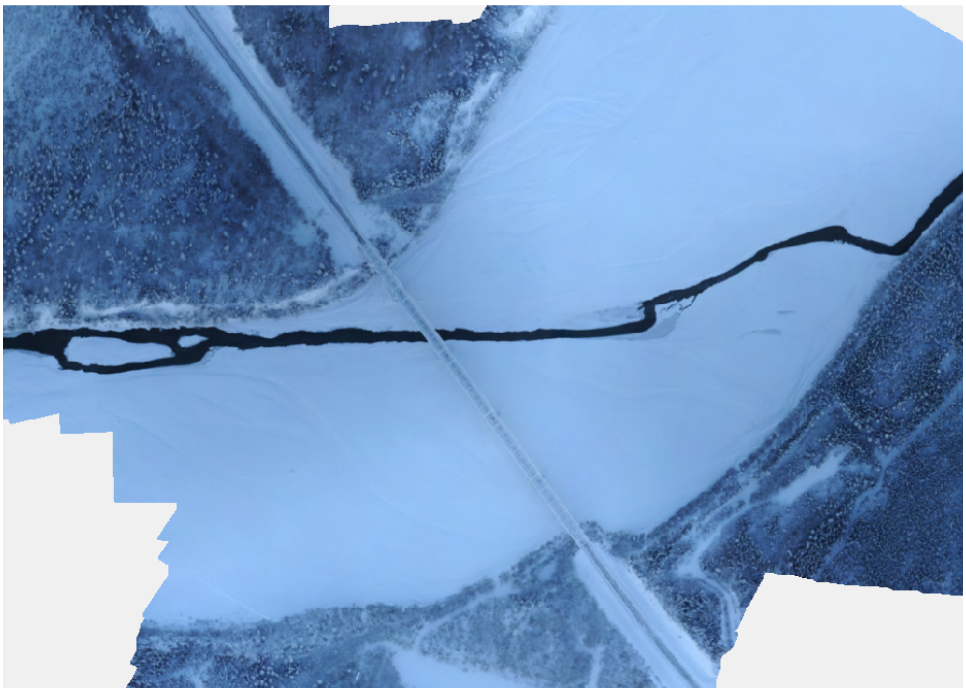

Figure B6: Johnson River Bridge orthomosaic from imagery collected by crewed aircraft in November 2017.

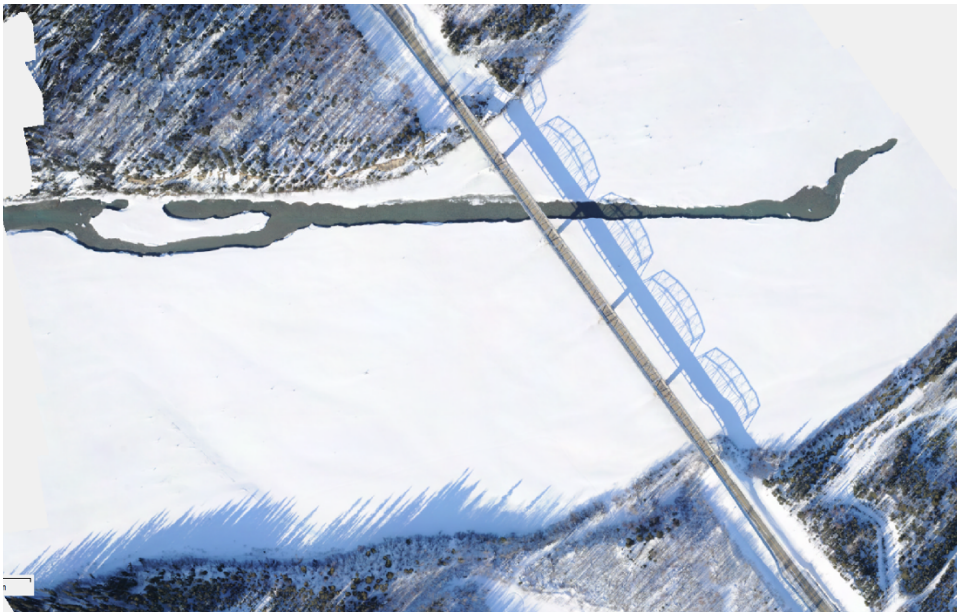

Figure B7: Johnson River Bridge orthomosaic from imagery collected by crewed aircraft in March 2018.

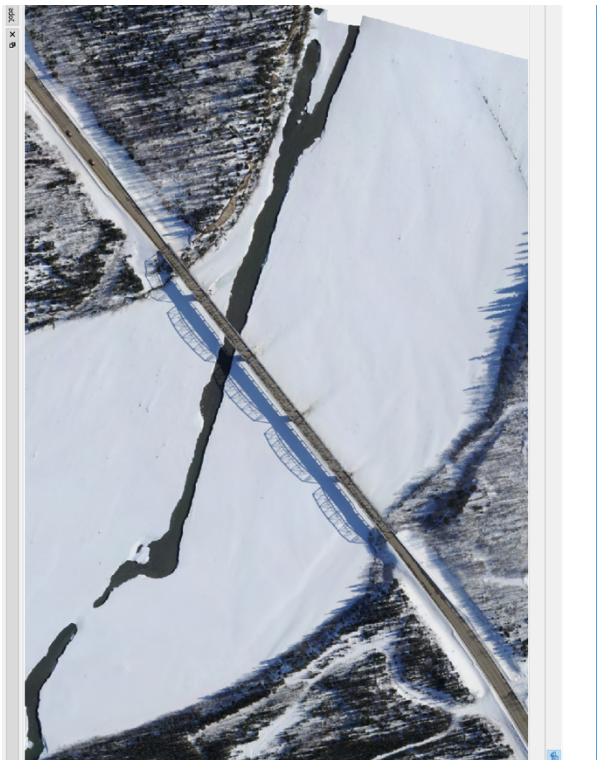

Figure B8: Johnson River Bridge orthomosaic from imagery collected by crewed aircraft in April 2018.

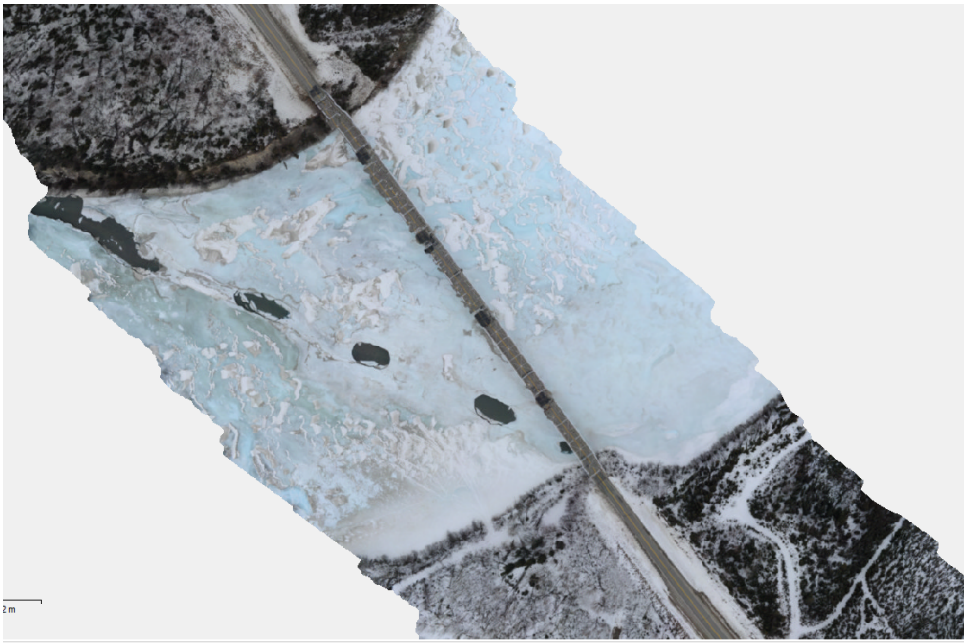

Figure B9: Johnson River Bridge orthomosaic from imagery collected by crewed aircraft in March 2019.

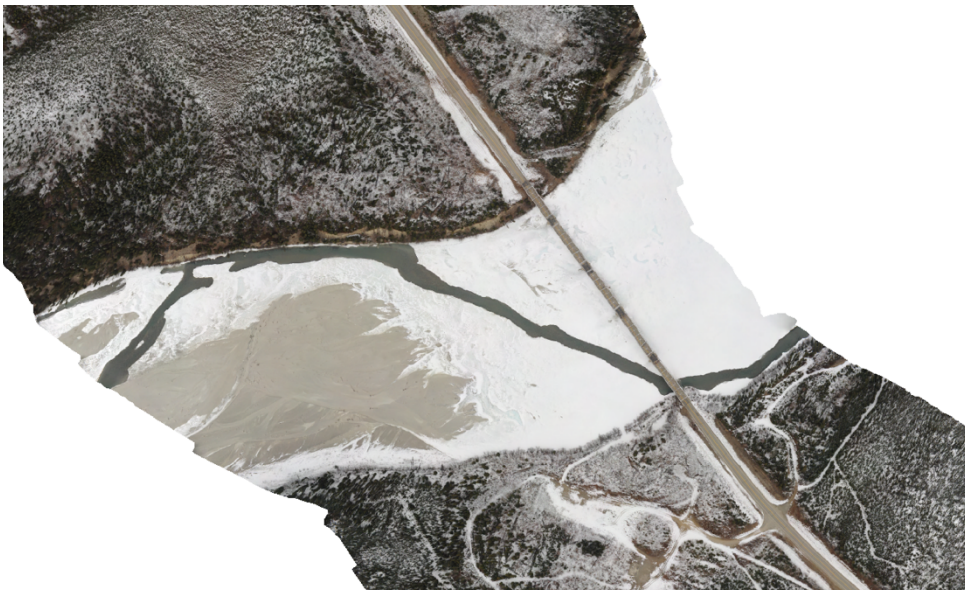

Figure B10: Johnson River Bridge orthomosaic from imagery collected by crewed aircraft in April 2019.

Gerstle River Bridge on the Alaska Highway (BN0520)

From UAS:



Figure B11: Gerstle River Bridge orthomosaic from imagery collected by UAS in April 2020.



Figure B12: Gerstle River Bridge orthomosaic detail from imagery collected by UAS in April 2020.



Figure B13: Gerstle River Bridge point cloud from imagery collected by UAS in April 2020.

From crewed aircraft:



Figure B14: Gerstle River Bridge orthomosaic from imagery collected by crewed aircraft in March 2017.



Figure B15: Gerstle River Bridge orthomosaic detail from imagery collected by crewed aircraft in March 2017.

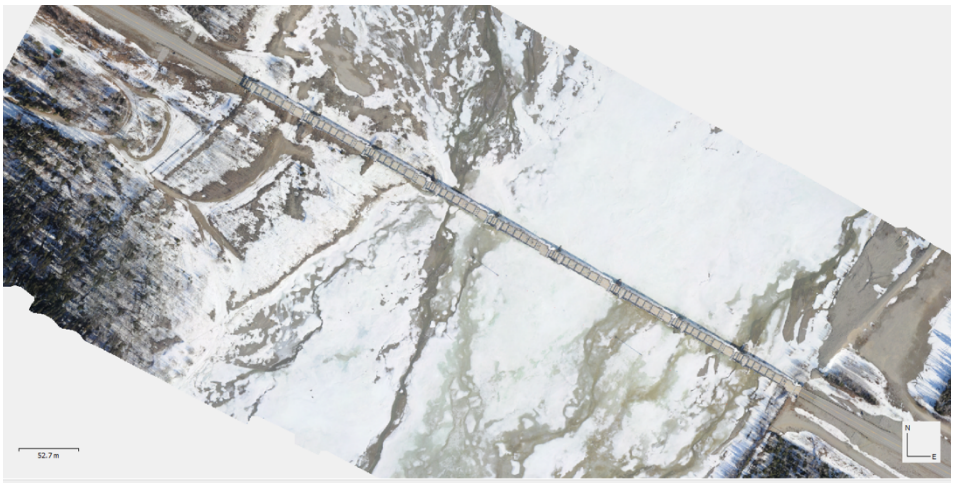

Figure B16: Gerstle River Bridge orthomosaic from imagery collected by crewed aircraft in April 2017.



Figure B17: Gerstle River Bridge orthomosaic detail from imagery collected by crewed aircraft in April 2017.

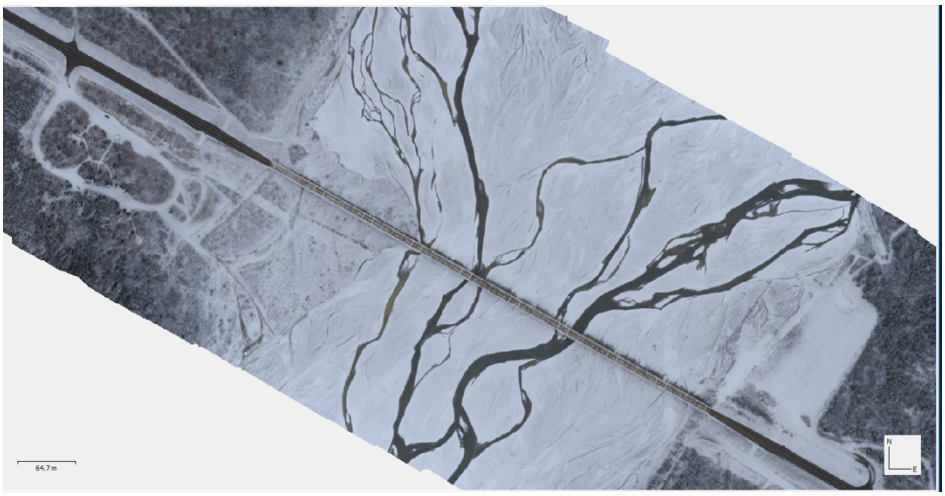

Figure B18: Gerstle River Bridge orthomosaic from imagery collected by crewed aircraft in October 2017.

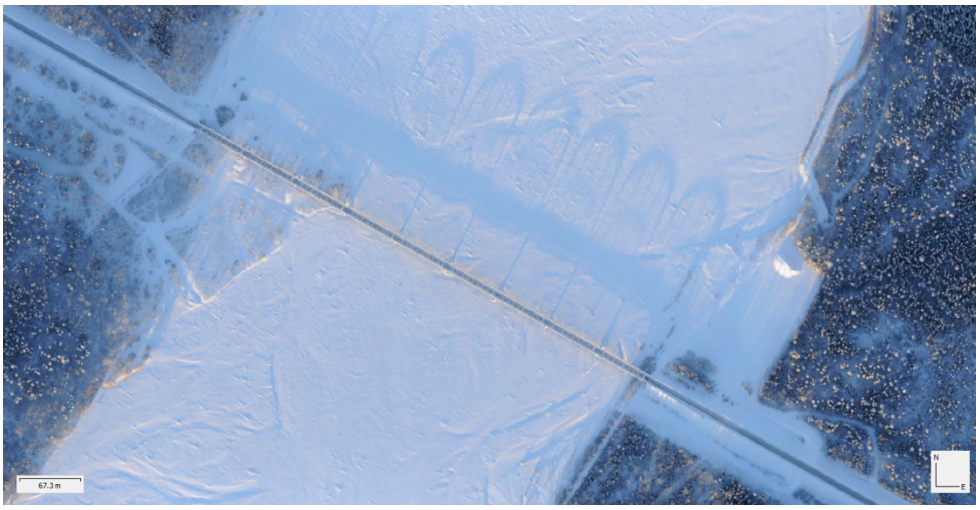

Figure B19: Gerstle River Bridge orthomosaic from imagery collected by crewed aircraft in November 2017.

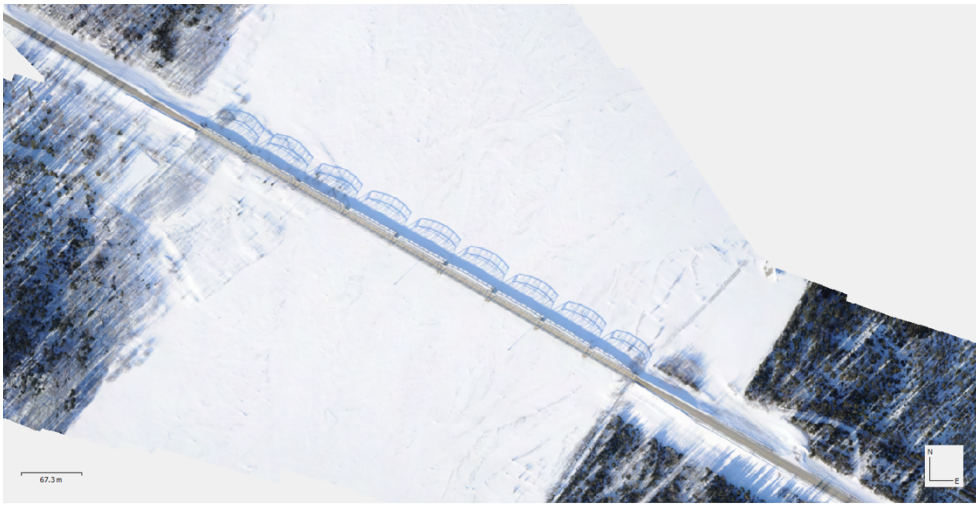

Figure B20: Gerstle River Bridge orthomosaic from imagery collected by crewed aircraft in March 2018.

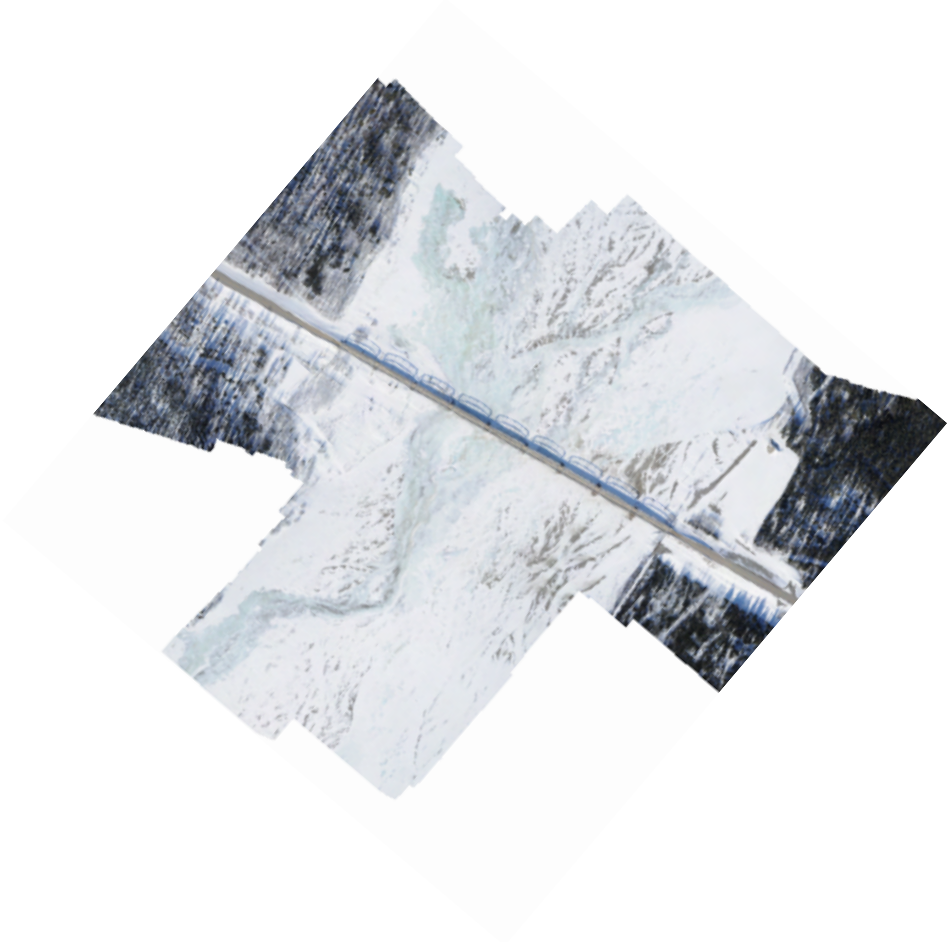

Figure B21: Gerstle River Bridge orthomosaic from imagery collected by crewed aircraft in April 2018.

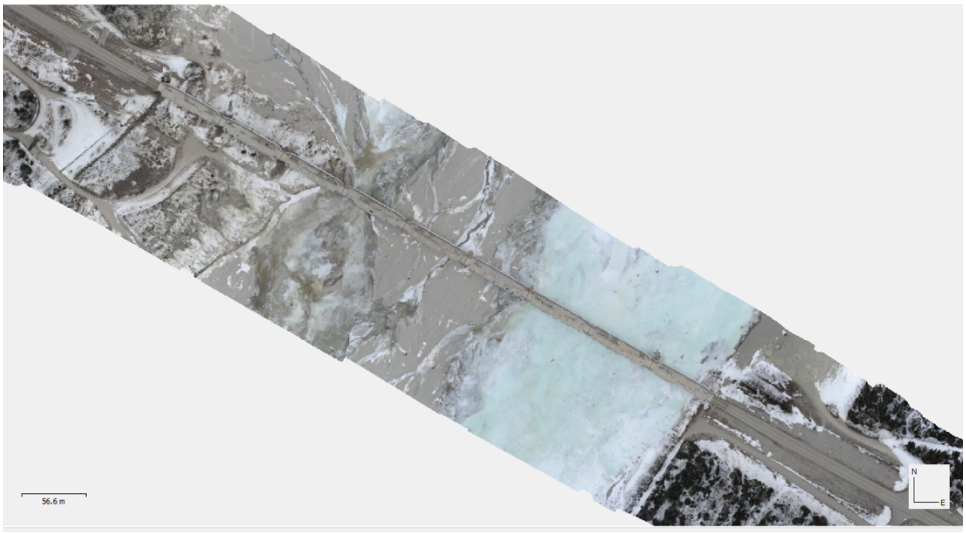

Figure B22: Gerstle River Bridge orthomosaic from imagery collected by crewed aircraft in March 2019.

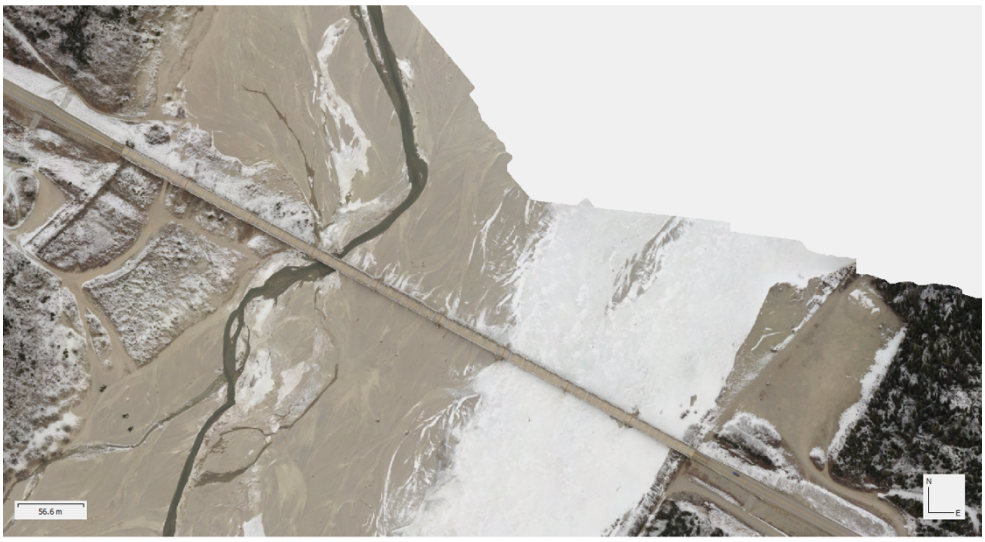

Figure B23: Gerstle River Bridge orthomosaic from imagery collected by crewed aircraft in April 2019.

Banner Creek Bridge on the Richardson Highway (BN0526)

From UAS:

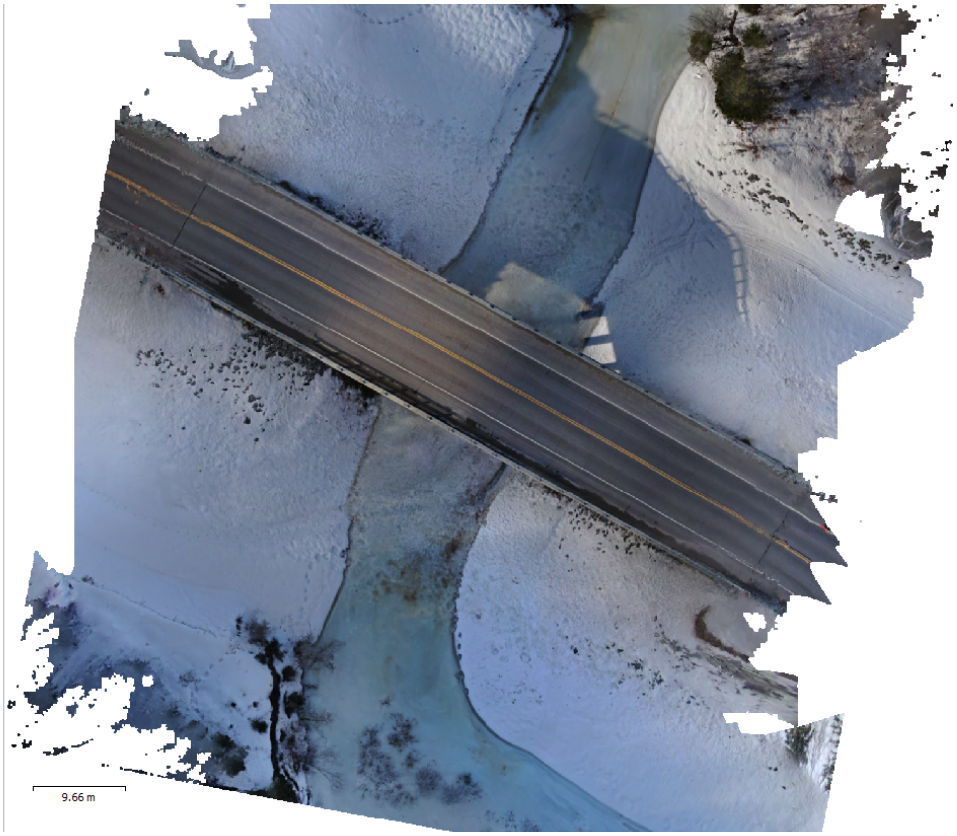

Figure B24: Banner Creek Bridge orthomosaic from imagery collected by UAS in April 2020.



Figure B25: Banner Creek Bridge point cloud from imagery collected by UAS in April 2020.

From hand-held field camera:

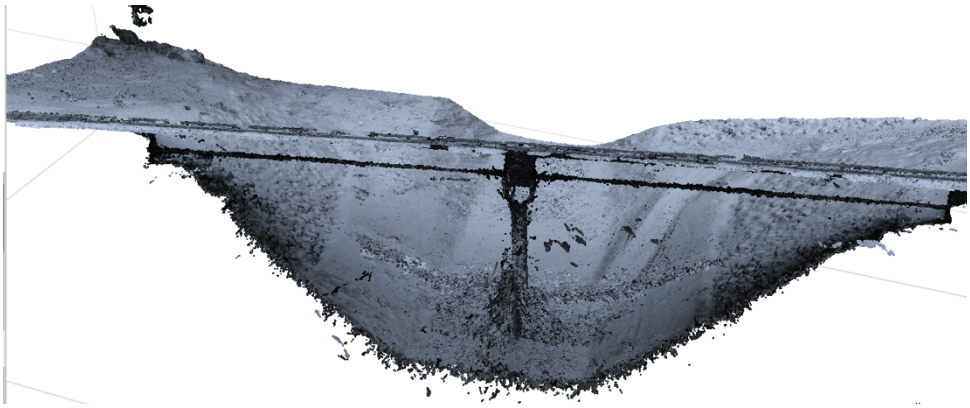

Figure B26: Banner Creek Bridge point cloud from imagery collected by hand-held field camera in November of 2019.

From crewed aircraft:

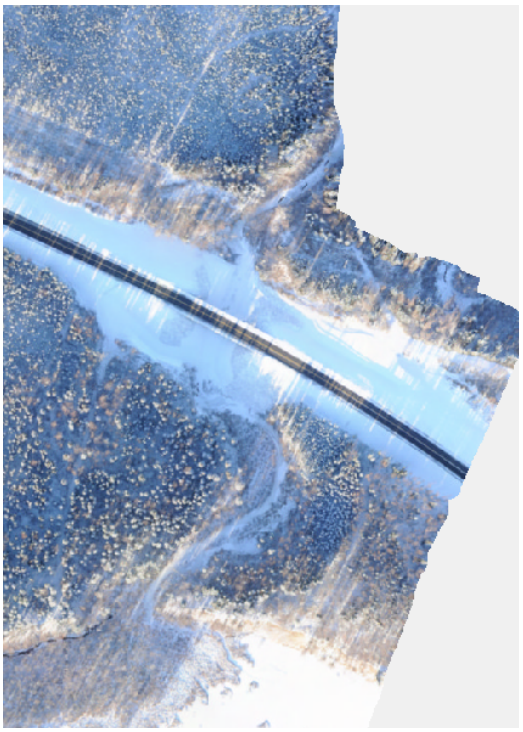

Figure B27: Banner Creek Bridge orthomosaic from imagery collected by crewed aircraft in October 2016.

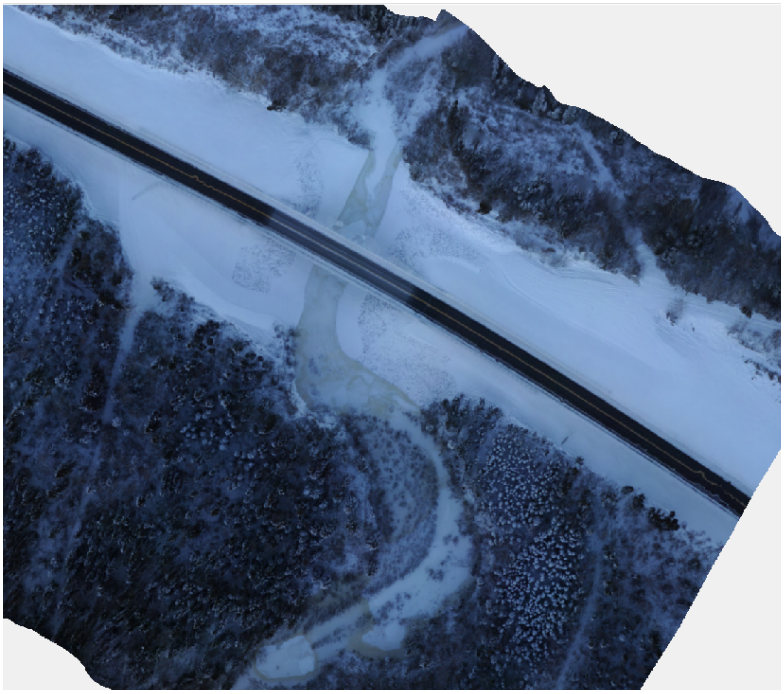

Figure B28: Banner Creek Bridge orthomosaic from imagery collected by crewed aircraft in December 2016.

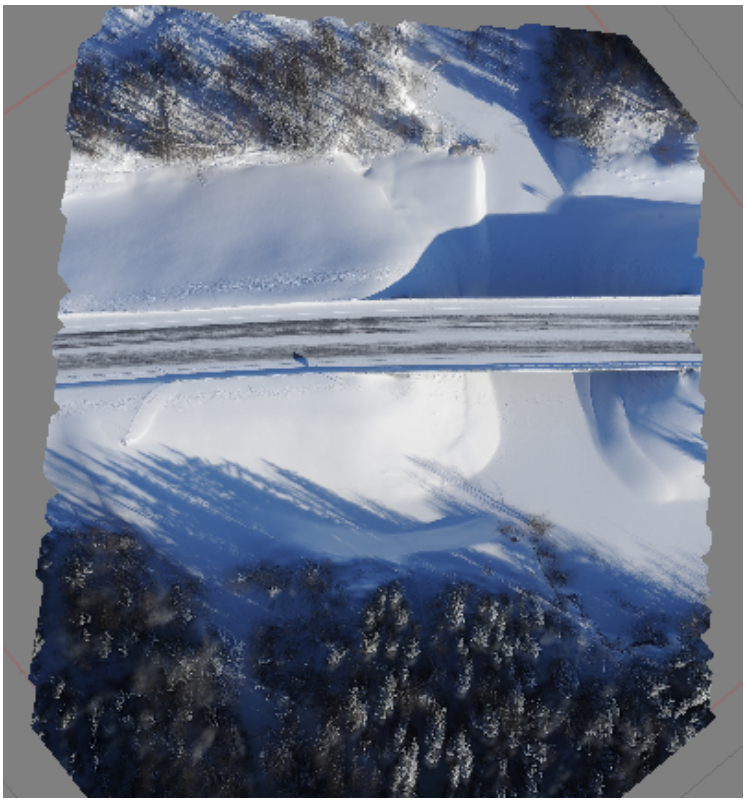

Figure B29: Banner Creek Bridge orthomosaic from imagery collected by crewed aircraft in March 2017.

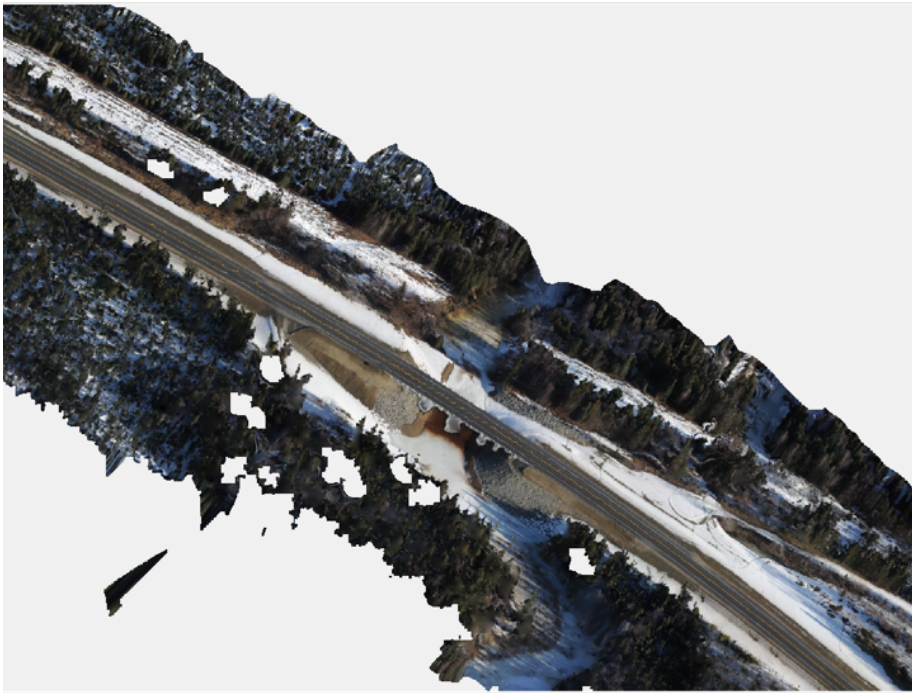

Figure B30: Banner Creek Bridge point cloud from imagery collected by crewed aircraft in April 2017.



Figure B31: Banner Creek Bridge orthomosaic from imagery collected by crewed aircraft in October 2017.

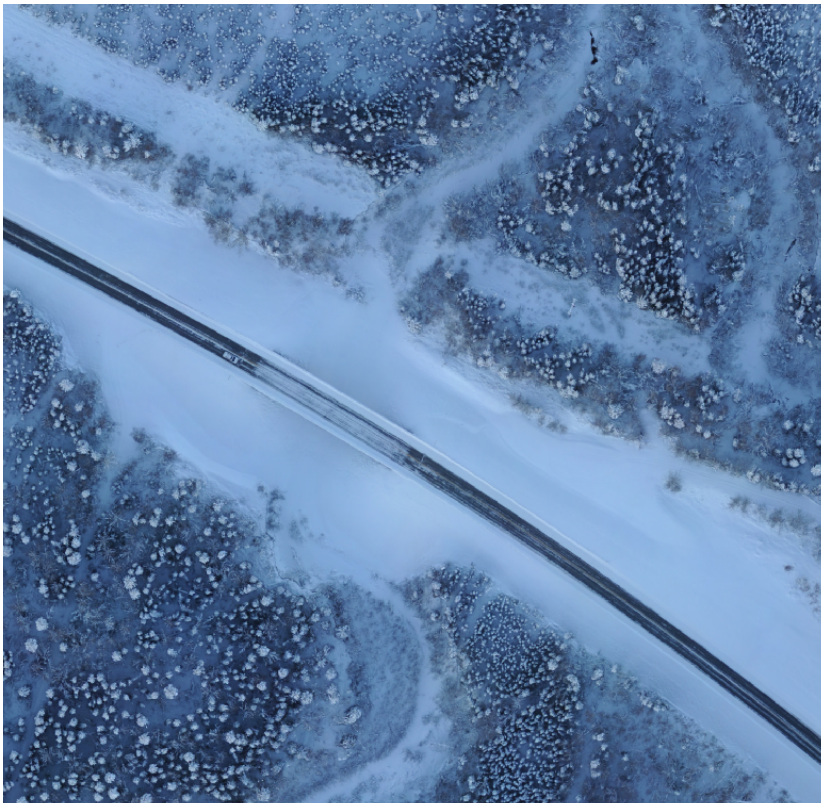

Figure B32: Banner Creek Bridge orthomosaic from imagery collected by crewed aircraft in November 2017.



Figure B33: Banner Creek Bridge orthomosaic from imagery collected by crewed aircraft in March 2018.



Figure B34: Banner Creek Bridge orthomosaic from imagery collected by crewed aircraft in April 2019.

Gulkana River Bridge on the Richardson Highway (BN0574)

From UAS:

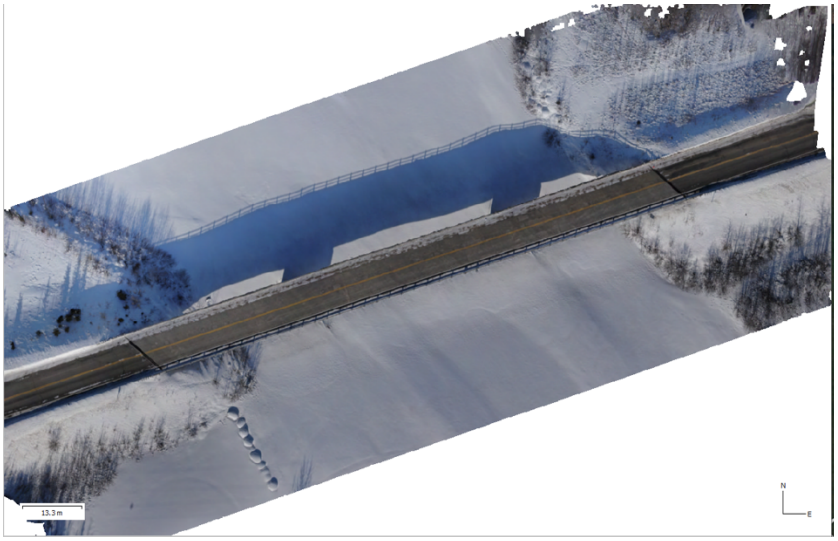

Figure B35: Gulkana River Bridge orthomosaic from imagery collected by UAS in March 2020.

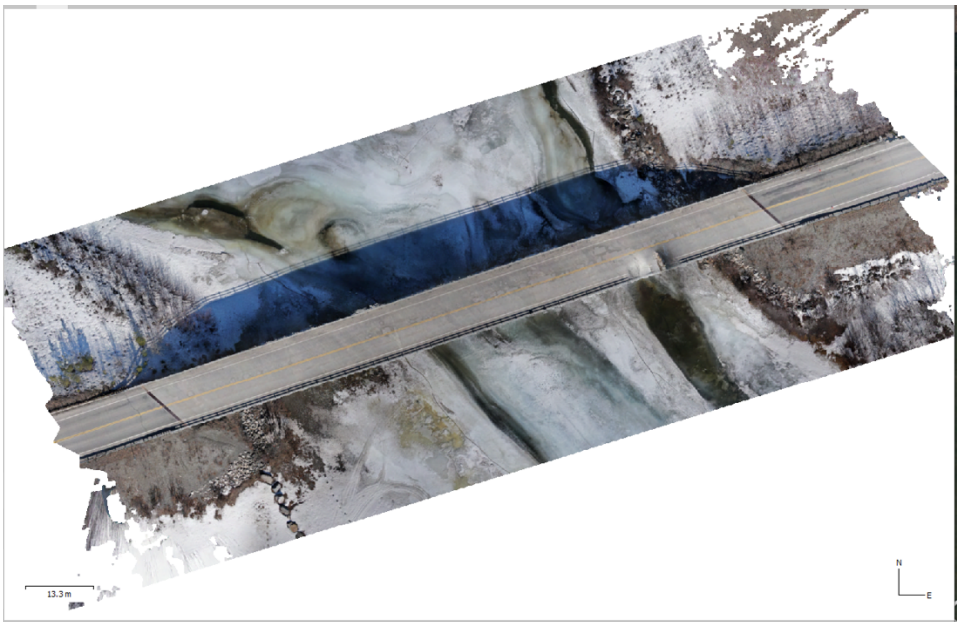

Figure B36: Gulkana River Bridge orthomosaic from imagery collected by UAS in April 2020.

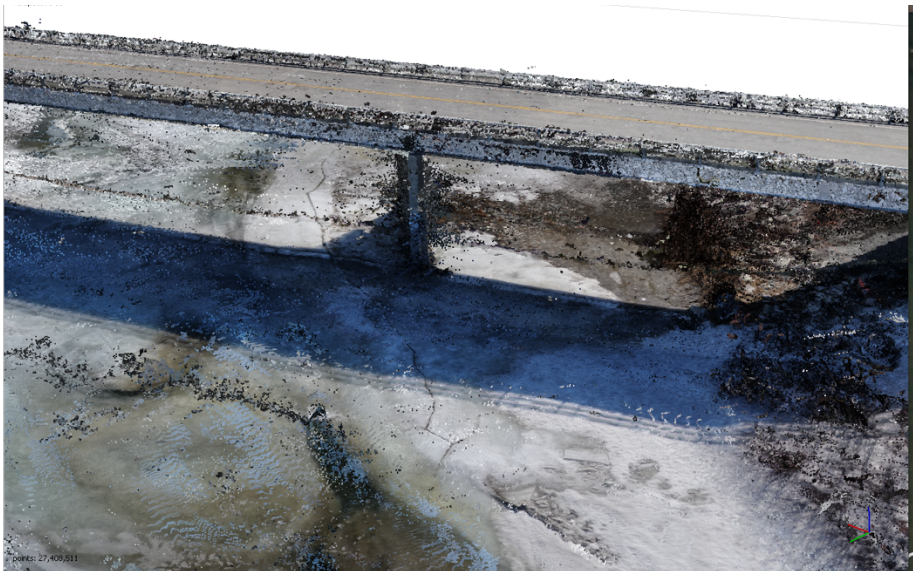

Figure B37: Gulkana River Bridge point cloud from imagery collected by UAS in April 2020.

From crewed aircraft:

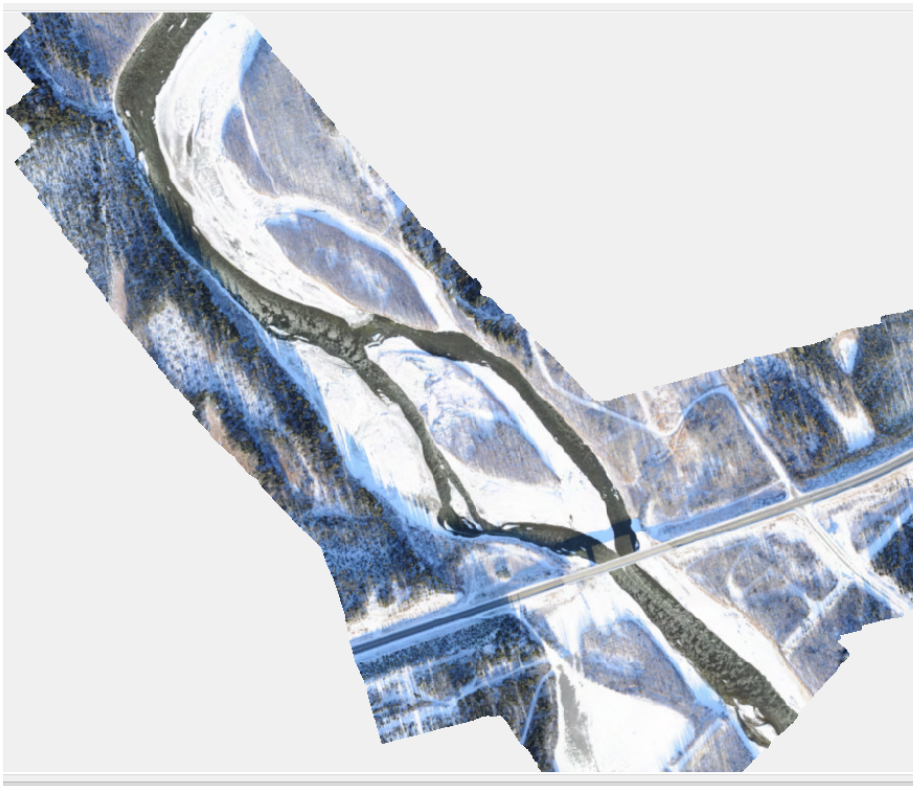

Figure B38: Gulkana River Bridge orthomosaic from imagery collected by crewed aircraft in October 2016.

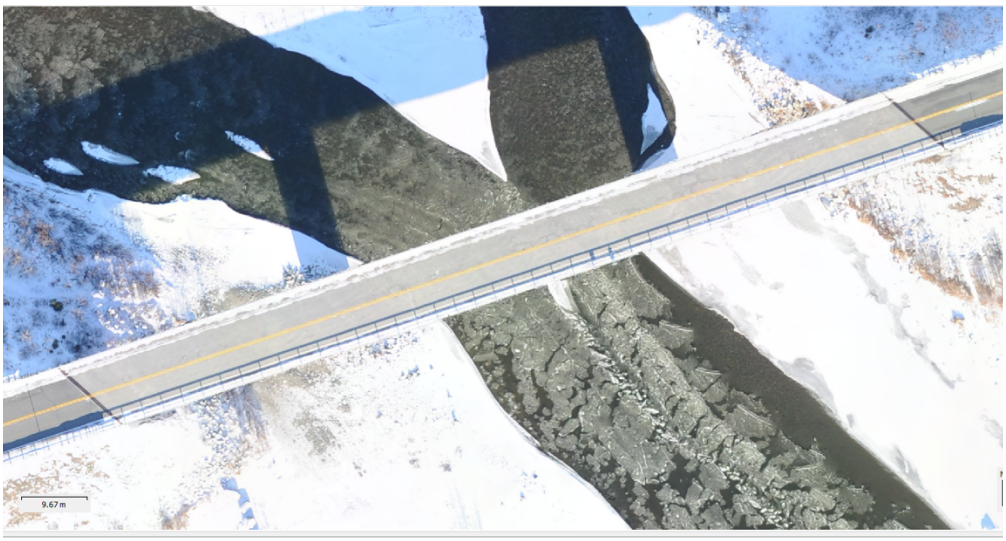

Figure B39: Gulkana River Bridge orthomosaic detail from imagery collected by crewed aircraft in October 2016.

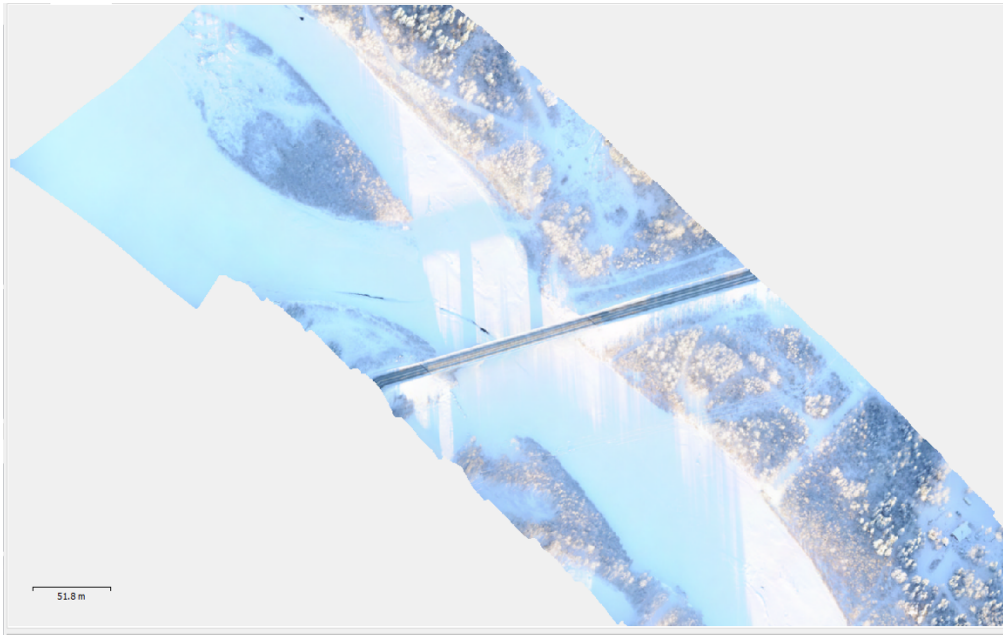

Figure B40: Gulkana River Bridge orthomosaic from imagery collected by crewed aircraft in December 2016.

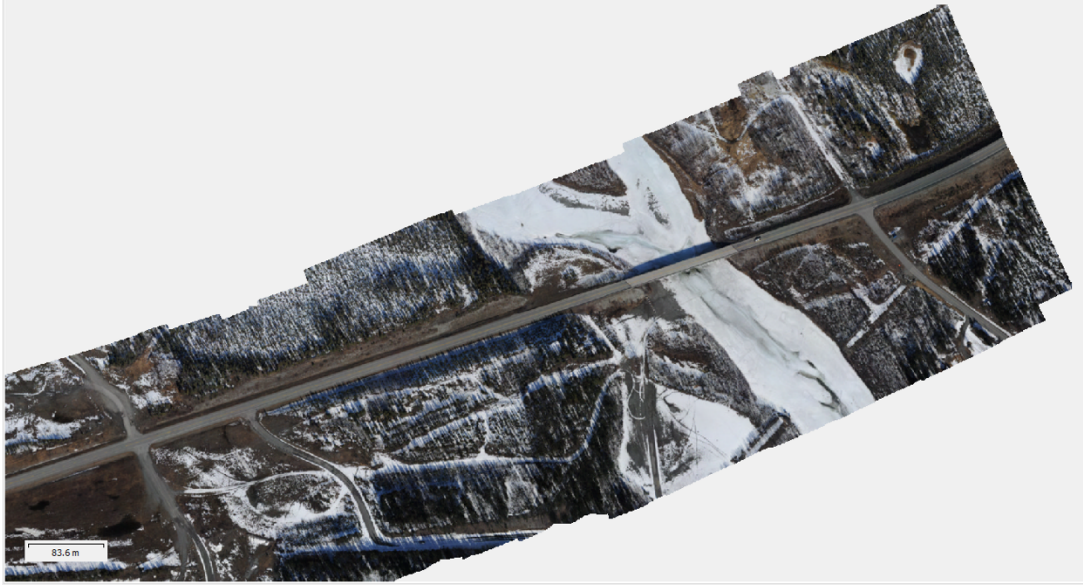

Figure B41: Gulkana River Bridge orthomosaic from imagery collected by crewed aircraft in April 2017.



Figure B42: Gulkana River Bridge orthomosaic from imagery collected by crewed aircraft in November 2017.



Figure B43: Gulkana River Bridge orthomosaic from imagery collected by crewed aircraft in March 2018.



Figure B44: Gulkana River Bridge orthomosaic from imagery collected by crewed aircraft in April 2018.

Gunnysack Creek Bridge on the Richardson Highway (BN0590)

From UAS:

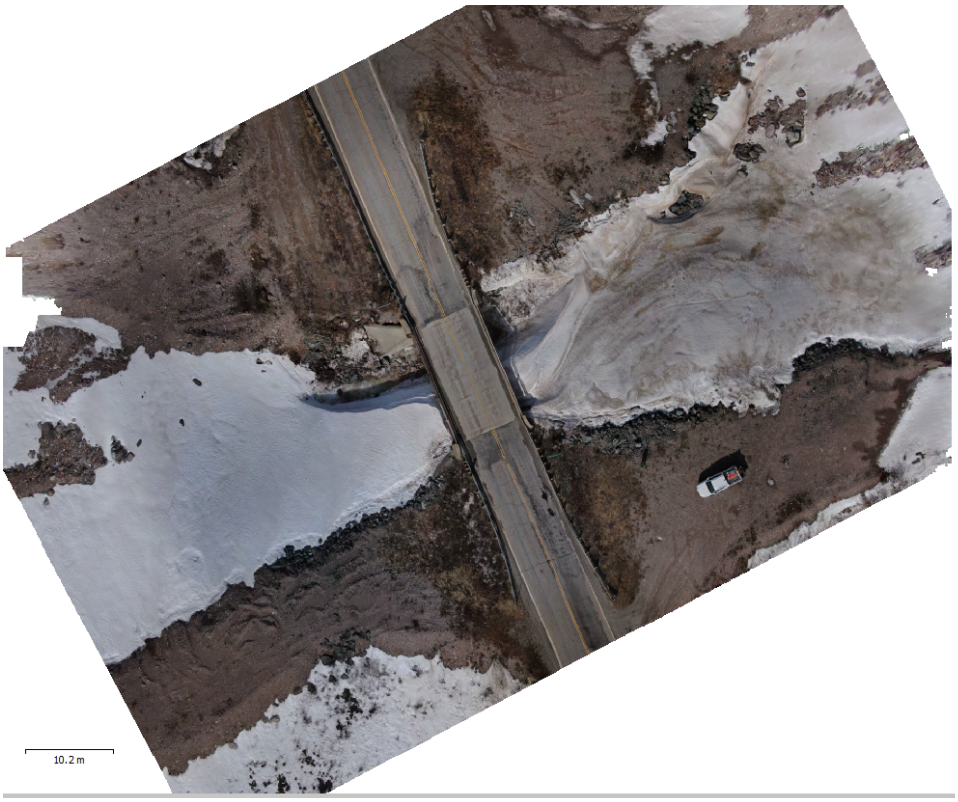

Figure B45: Gunnysack Creek Bridge orthomosaic from imagery collected by UAS in April 2020.



Figure B46: Gunnysack Creek Bridge point cloud from imagery collected by UAS in April 2020.

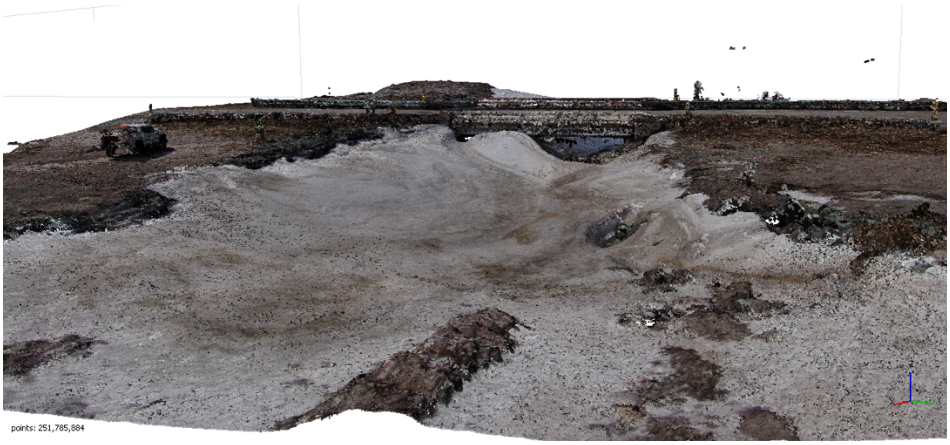

Figure B47: Gunnysack Creek Bridge point cloud from imagery collected by UAS in April 2020.

From crewed aircraft:

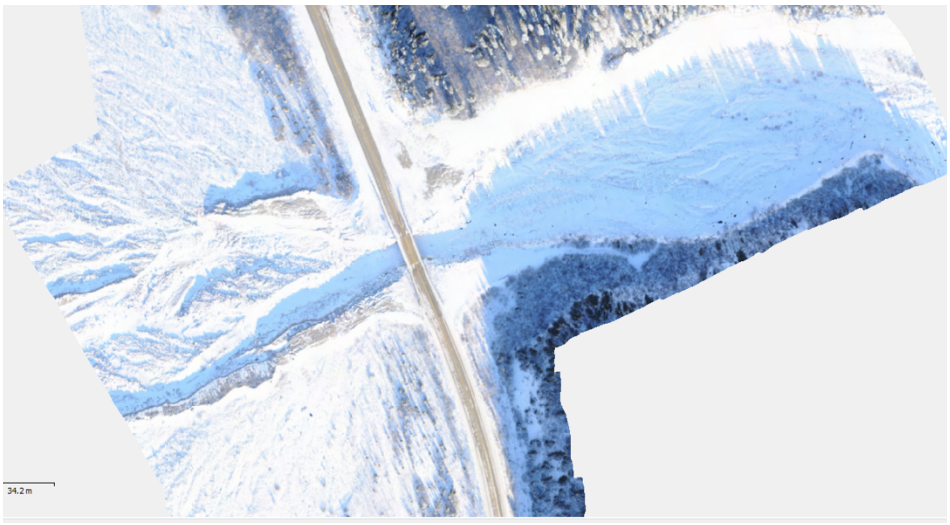

Figure B48: Gunnysack Creek Bridge orthomosaic from imagery collected by crewed aircraft in October 2016.

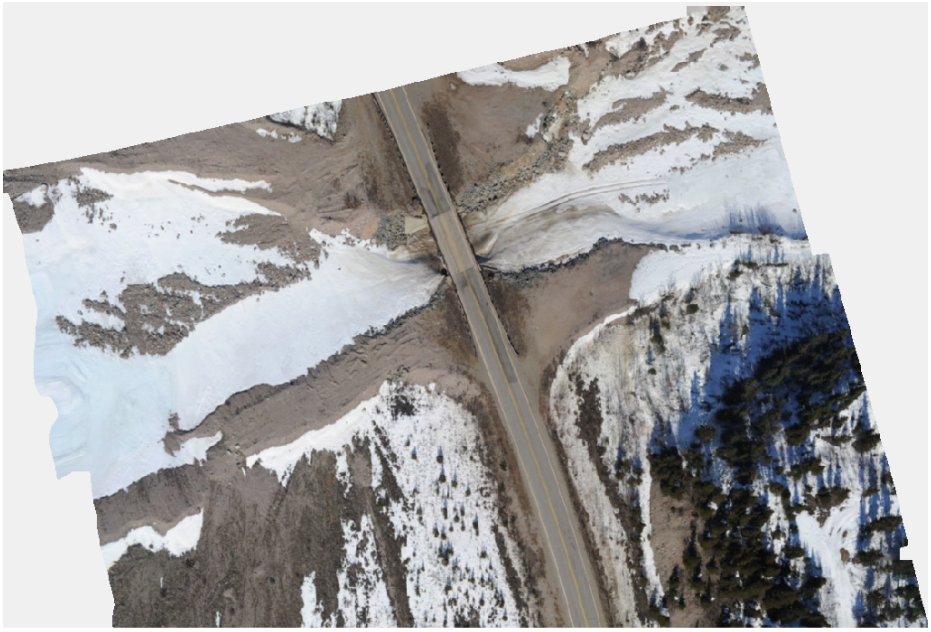

Figure B49: Gunnysack Creek Bridge orthomosaic from imagery collected by crewed aircraft in April 2017.

Ruby Creek Bridge on the Richardson Highway (BN0594)

From UAS:

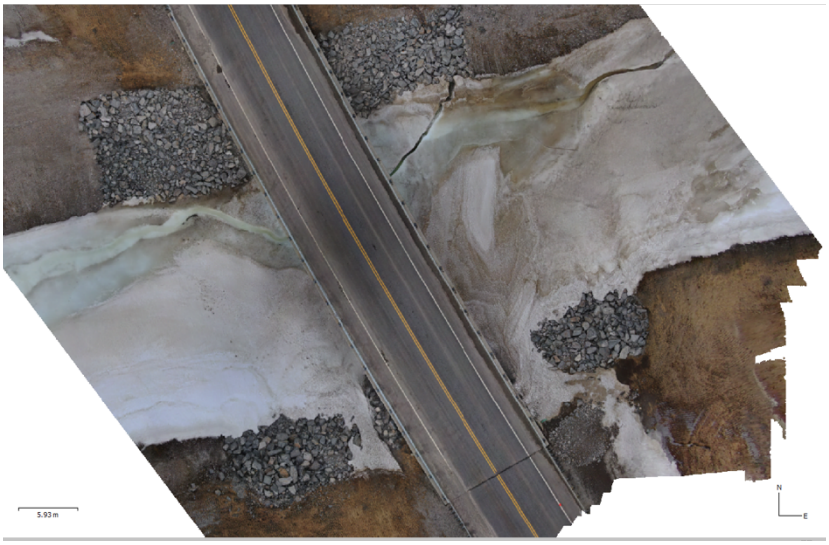

Figure B50: Ruby Creek Bridge orthomosaic from imagery collected by UAS in April 2020.



Figure B51: Ruby Creek Bridge point cloud from imagery collected by UAS in April 2020.

From hand-held field camera:

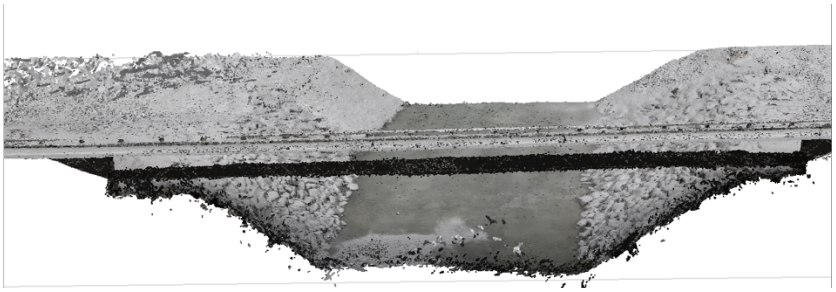

Figure B52: Ruby Creek Bridge point cloud from imagery collected by hand-held field camera in November 2019.

From crewed aircraft:

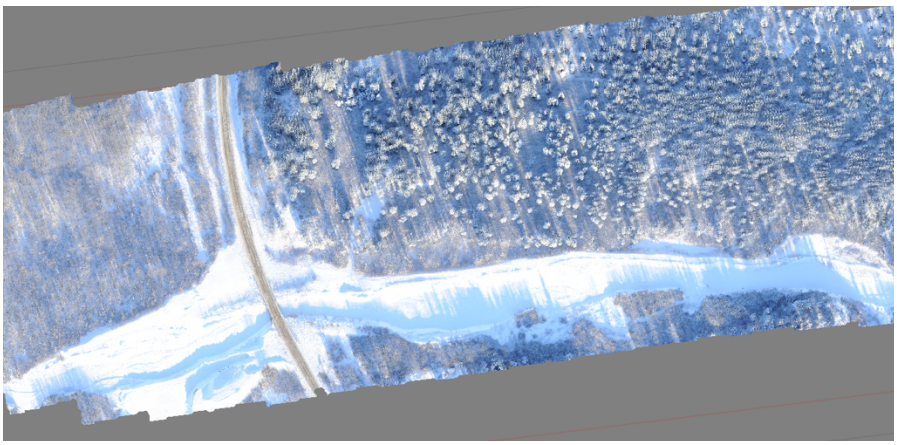

Figure B53: Ruby Creek Bridge orthomosaic from imagery collected by crewed aircraft in October 2016.

Jarvis Creek Bridge on the Richardson Highway (BN0595)

From UAS:



Figure B54: Jarvis Creek Bridge orthomosaic from imagery collected by UAS in April 2020.

From hand-held field camera:

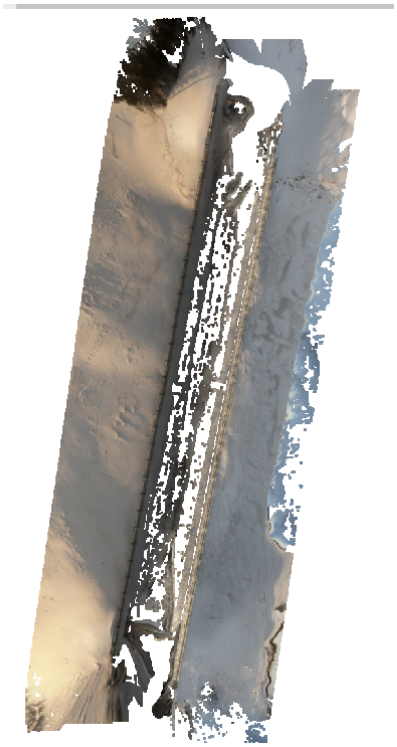

Figure B55: Jarvis Creek Bridge point cloud from imagery collected by hand-held field camera in March 2020.



Figure B56: Jarvis Creek Bridge point cloud from imagery collected by hand-held field camera in April 2020.

From crewed aircraft:

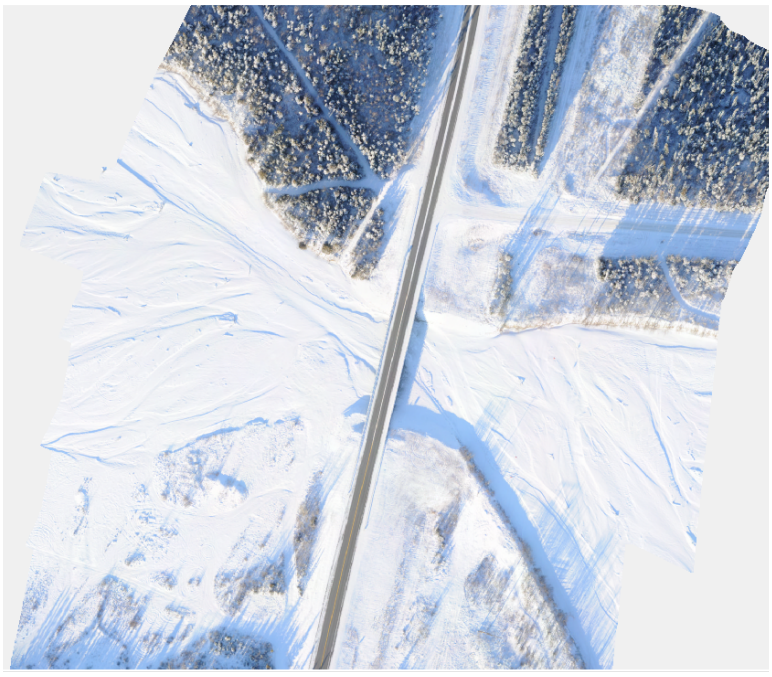

Figure B57: Jarvis Creek Bridge orthomosaic from imagery collected by crewed in October 2016.

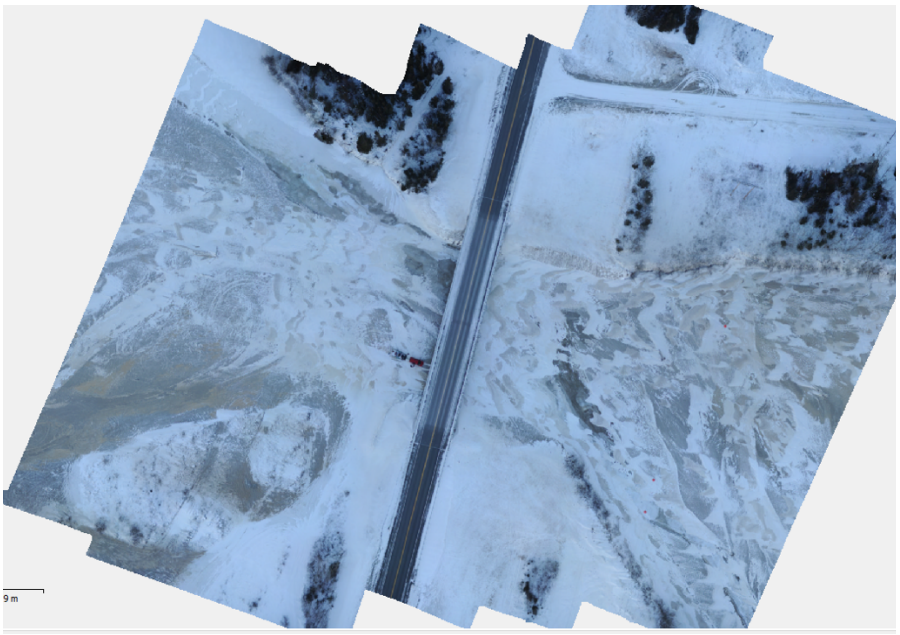

Figure B58: Jarvis Creek Bridge orthomosaic from imagery collected by crewed aircraft in December 2016.

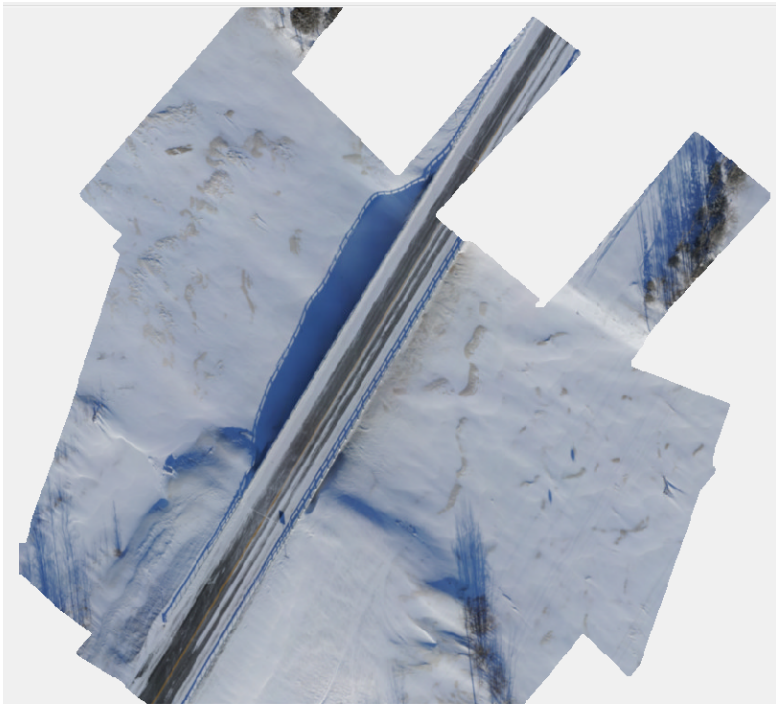

Figure B59: Jarvis Creek Bridge orthomosaic from imagery collected by crewed aircraft in March 2017.

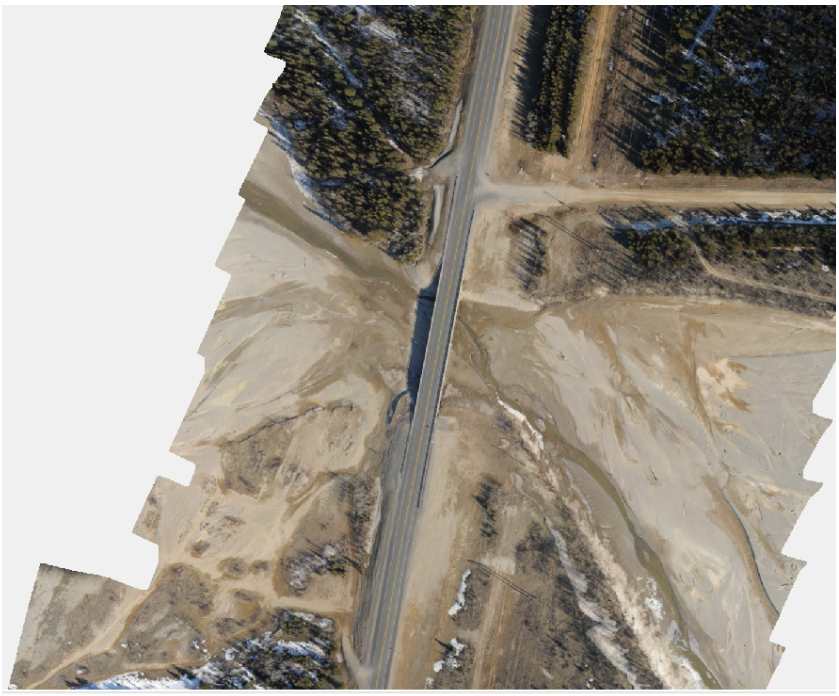

Figure B60: Jarvis Creek Bridge orthomosaic from imagery collected by crewed aircraft in April 2017.

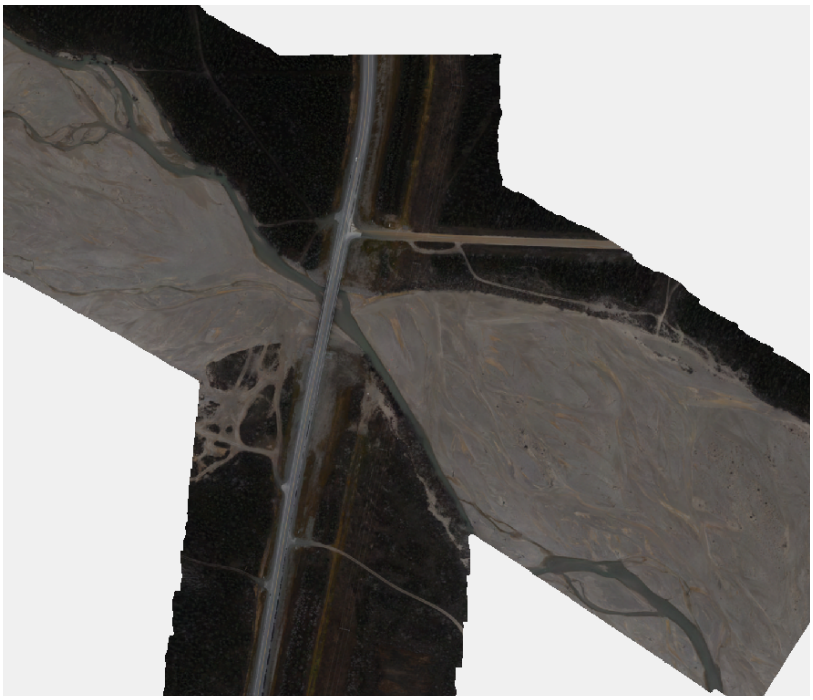

Figure B61: Jarvis Creek Bridge orthomosaic from imagery collected by crewed aircraft in October 2017.

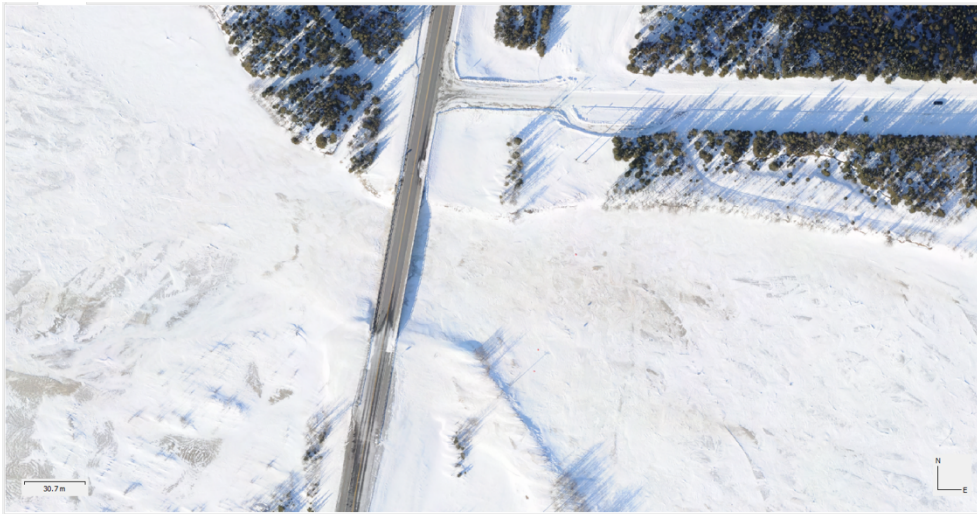

Figure B62: Jarvis Creek Bridge orthomosaic from imagery collected by crewed aircraft in March 2018.


Figure B63: Jarvis Creek Bridge orthomosaic from imagery collected by crewed aircraft in April 2018.



Figure B64: Jarvis Creek Bridge orthomosaic from imagery collected by crewed aircraft in March 2019.

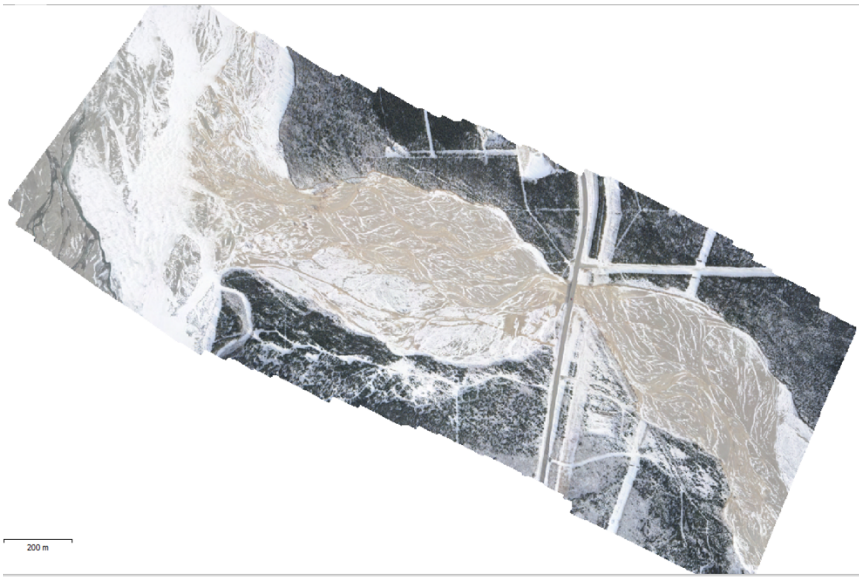

Figure B65: Jarvis Creek Bridge orthomosaic from imagery collected by crewed aircraft in April 2019.

Gakona River Bridge on the Tok Cutoff (BN0646)

From UAS:



Figure B66: Gakona River Bridge orthomosaic from imagery collected by UAS in April 2020.



Figure B67: Gakona River Bridge point cloud from imagery collected by UAS in April 2020.

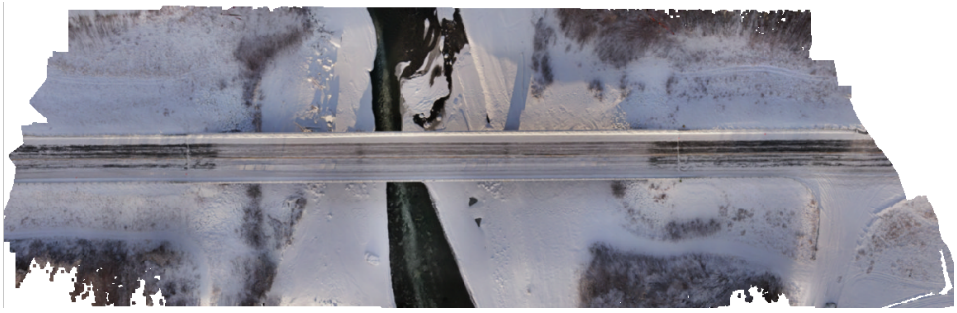

Figure B68: Gakona River Bridge orthomosaic from imagery collected by UAS in November 2019.

From crewed aircraft:

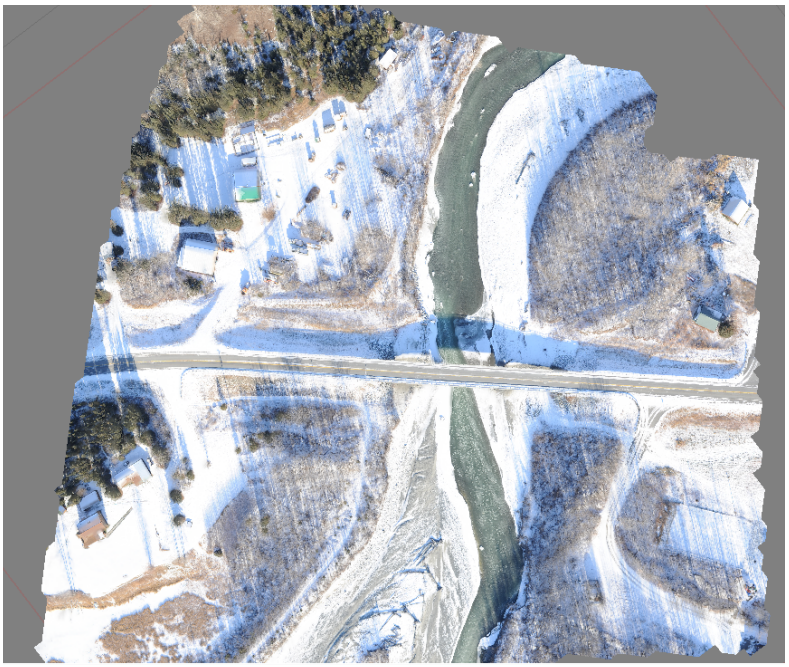

Figure B69: Gakona River Bridge orthomosaic from imagery collected by crewed aircraft in October 2016.

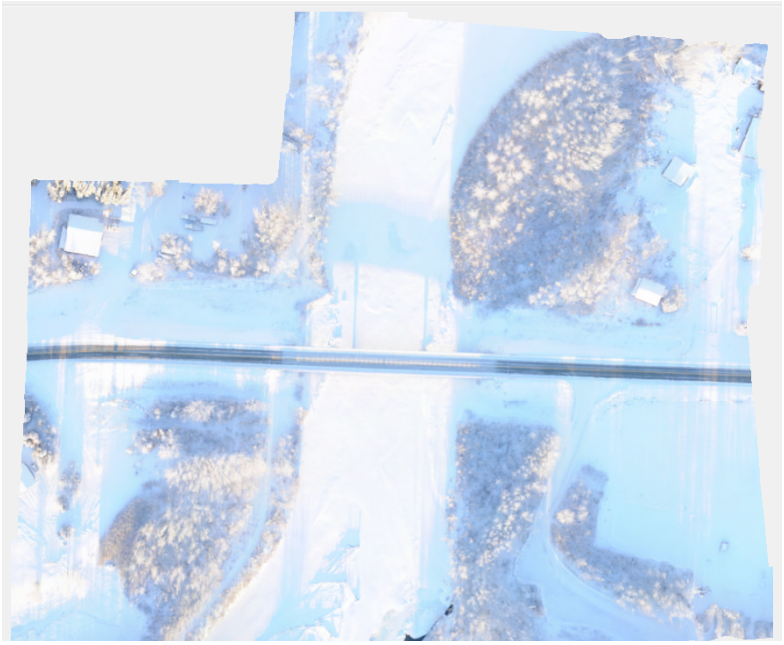

Figure B70: Gakona River Bridge orthomosaic from imagery collected by crewed aircraft in December 2016.



Figure B71: Gakona River Bridge orthomosaic from imagery collected by crewed aircraft in April 2017.

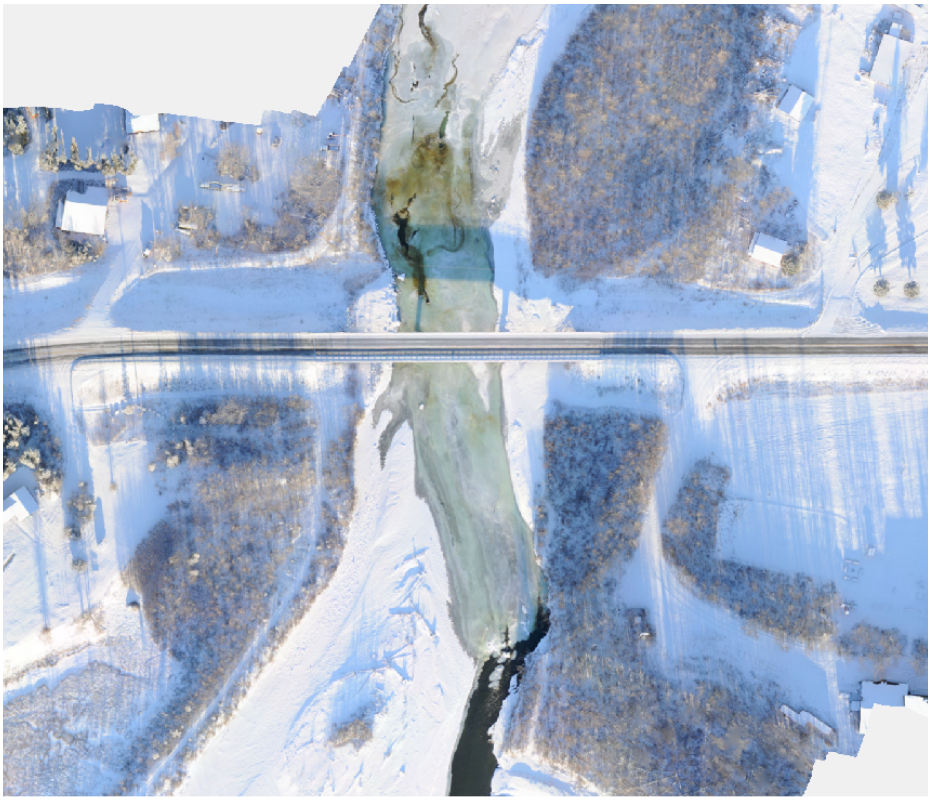

Figure B72: Gakona River Bridge orthomosaic from imagery collected by crewed aircraft in November 2017.



Figure B73: Gakona River Bridge orthomosaic from imagery collected by crewed aircraft in March 2018.



Figure B74: Gakona River Bridge orthomosaic from imagery collected by crewed aircraft in April 2018.

Sinona Creek Bridge on the Tok Cutoff (BN0648)

From UAS:

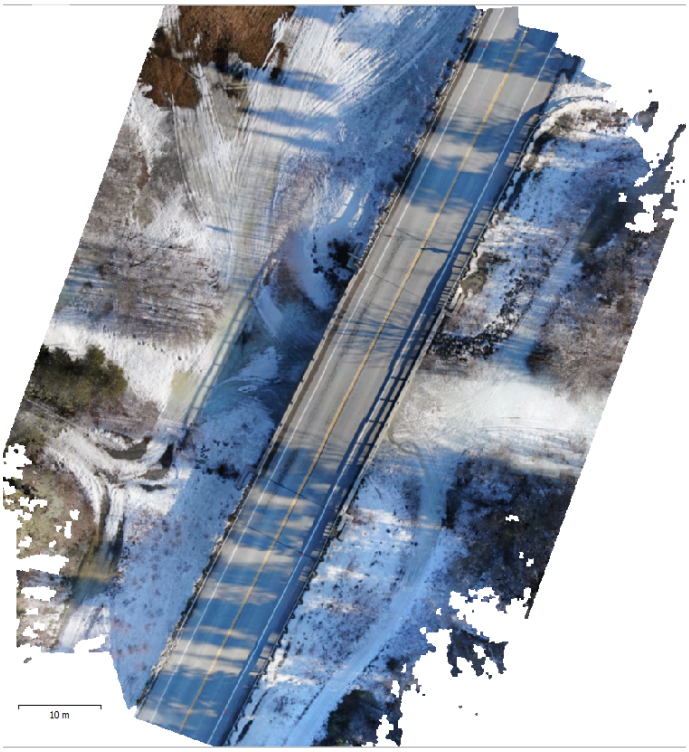

Figure B75: Sinona Creek Bridge orthomosaic from imagery collected by UAS in April 2018.

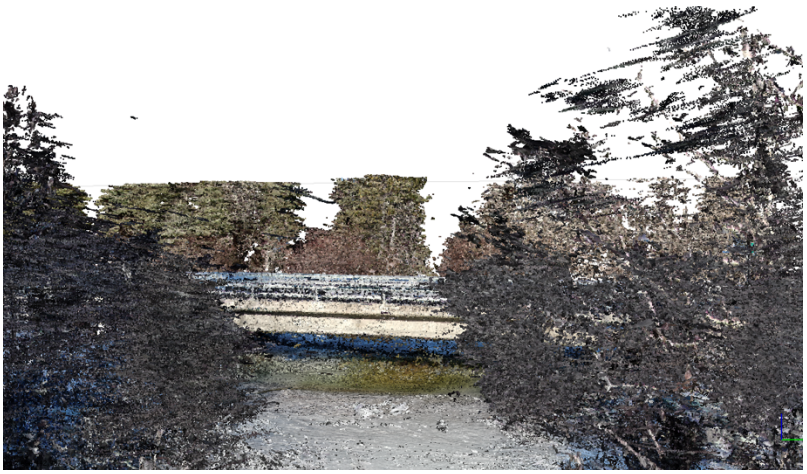

Figure B76: Sinona Creek Bridge point cloud from imagery collected by UAS in April 2018.

From crewed aircraft:

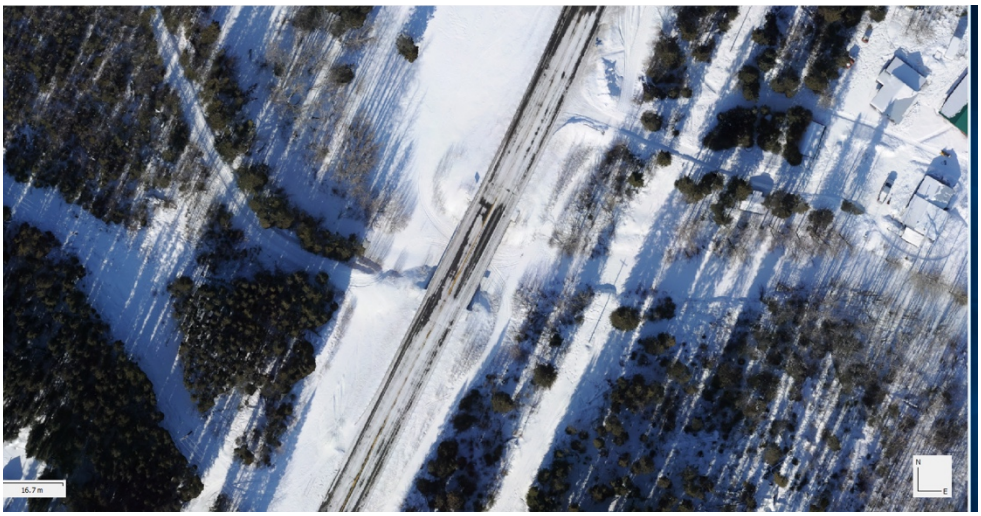

Figure B77: Sinona Creek Bridge orthomosaic from imagery collected by crewed aircraft in March 2018.



Figure B78: Sinona Creek Bridge orthomosaic from imagery collected by crewed aircraft in April 2018.

Tok River Bridge on the Alaska Highway (BN0663)

From UAS:



Figure B79: Tok River Bridge orthomosaic from imagery collected by UAS in April 2020.



Figure B80: Tok River Bridge point cloud from imagery collected by UAS in April 2020.



Figure B81: Tok River Bridge point cloud detail from imagery collected by UAS in April 2020.

From crewed aircraft:

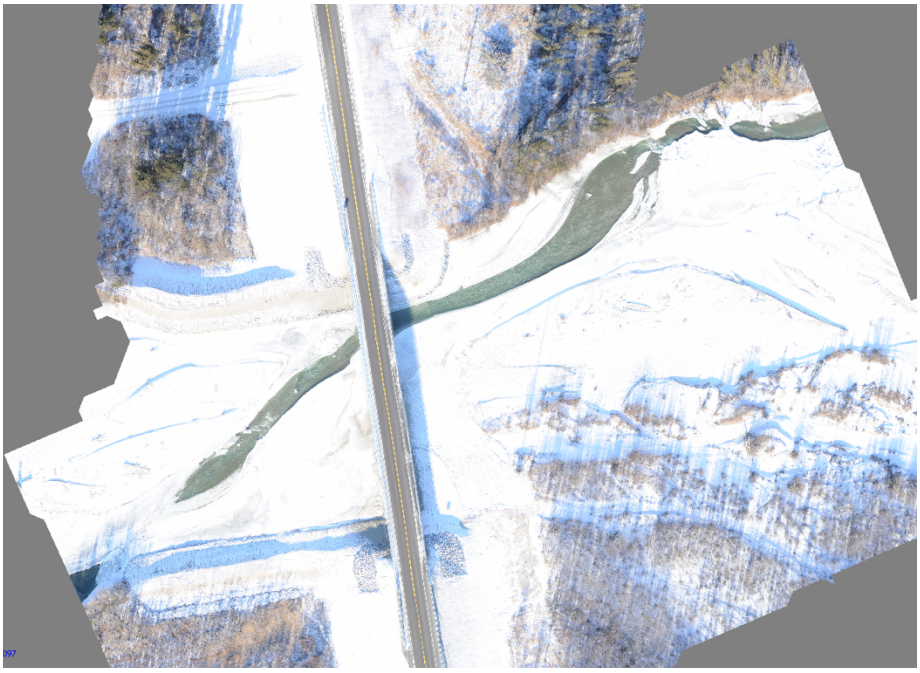

Figure B82: Tok River Bridge orthomosaic from imagery collected by crewed aircraft in October 2016.

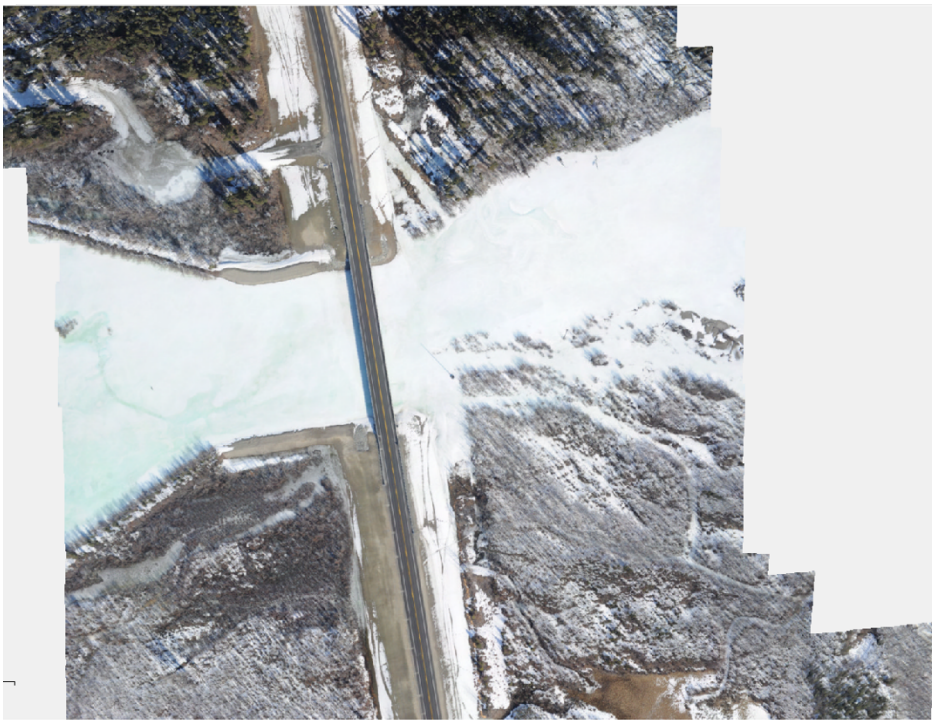

Figure B83: Tok River Bridge orthomosaic from imagery collected by crewed aircraft in April 2017.

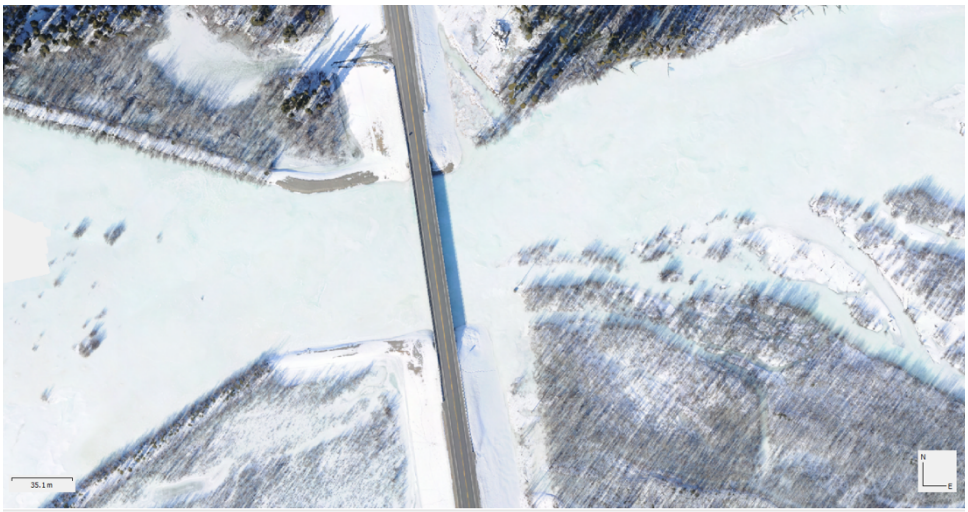

Figure B84: Tok River Bridge orthomosaic from imagery collected by crewed aircraft in March 2018.

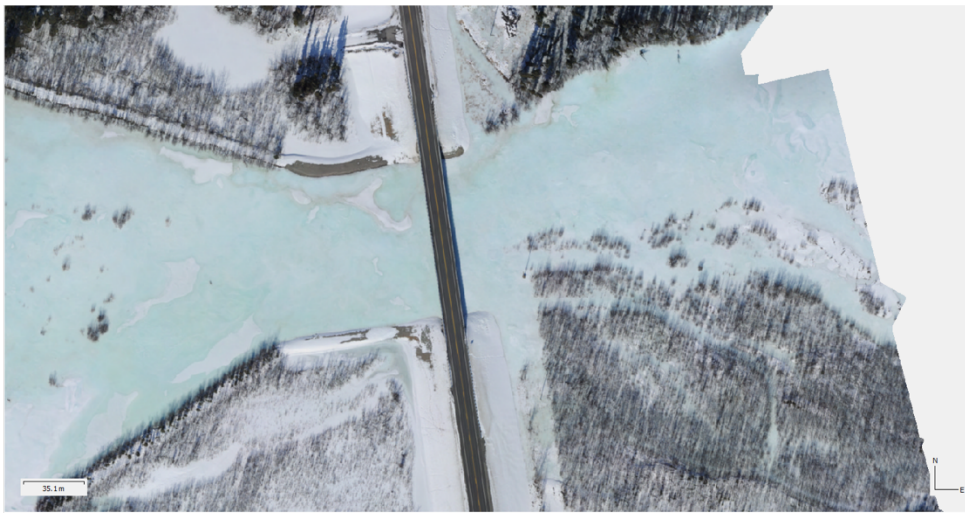

Figure B85: Tok River Bridge orthomosaic from imagery collected by crewed aircraft in April 2018.

Seattle Creek Bridge on the Denali Highway (BN0690)

From UAS:

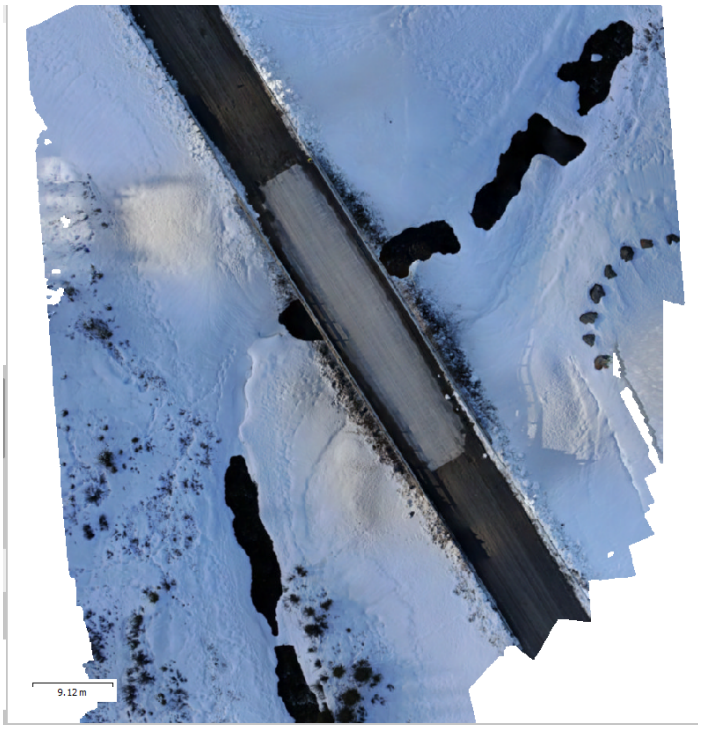

Figure B86: Seattle Creek Bridge orthomosaic from imagery collected by UAS in April 2020.



Figure B87: Seattle Creek Bridge point cloud from imagery collected by UAS in April 2020.

From crewed aircraft:

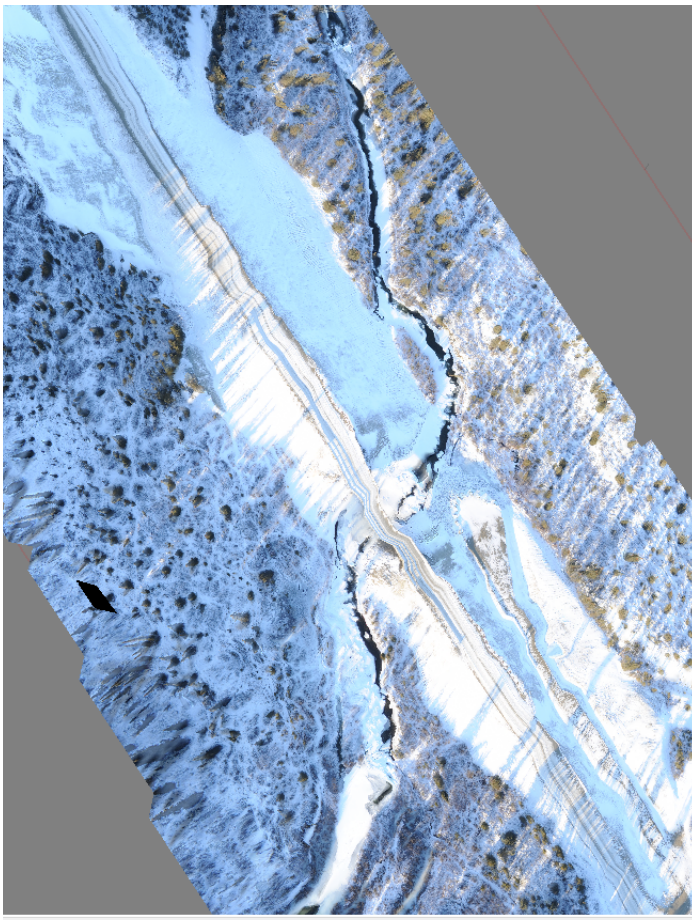

Figure B88: Seattle Creek Bridge orthomosaic from imagery collected by crewed aircraft in October 2016.

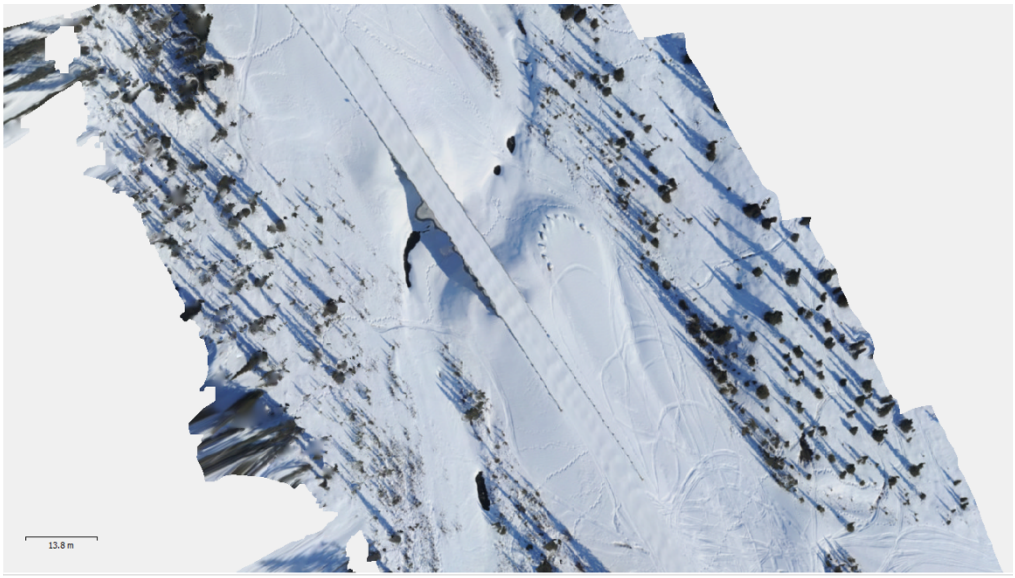

Figure B89: Seattle Creek Bridge orthomosaic from imagery collected by crewed aircraft in December 2016.

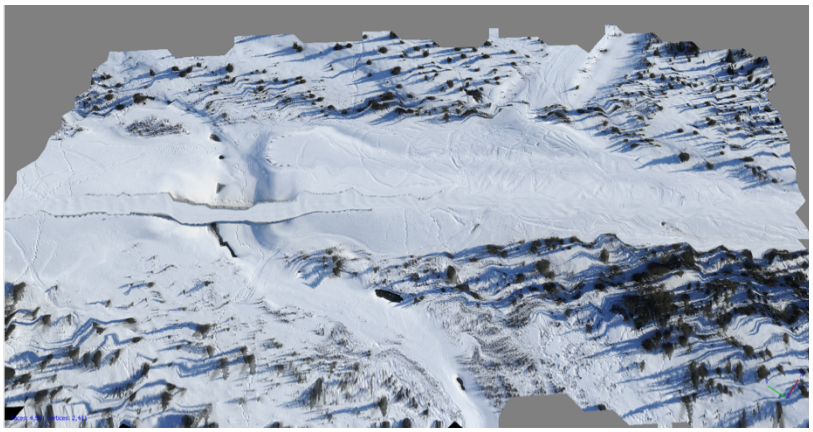

Figure B90: Seattle Creek Bridge orthomosaic from imagery collected by crewed aircraft in April 2017.

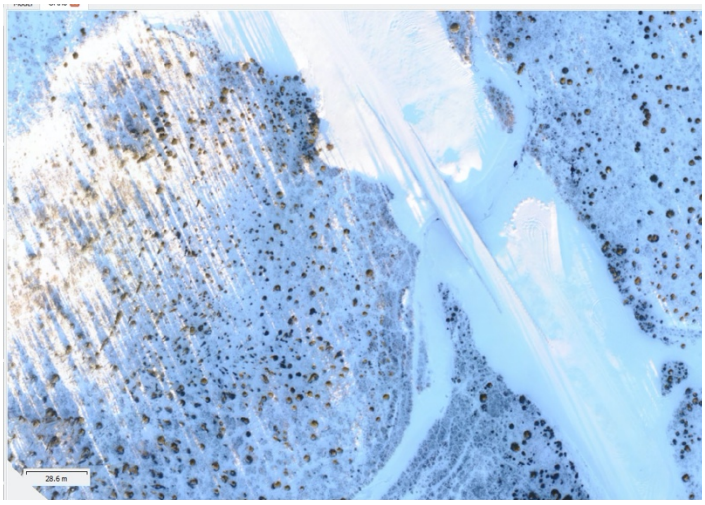

Figure B91: Seattle Creek Bridge orthomosaic from imagery collected by crewed aircraft in November 2017.



Figure B92: Seattle Creek Bridge orthomosaic from imagery collected by crewed aircraft in March 2018.

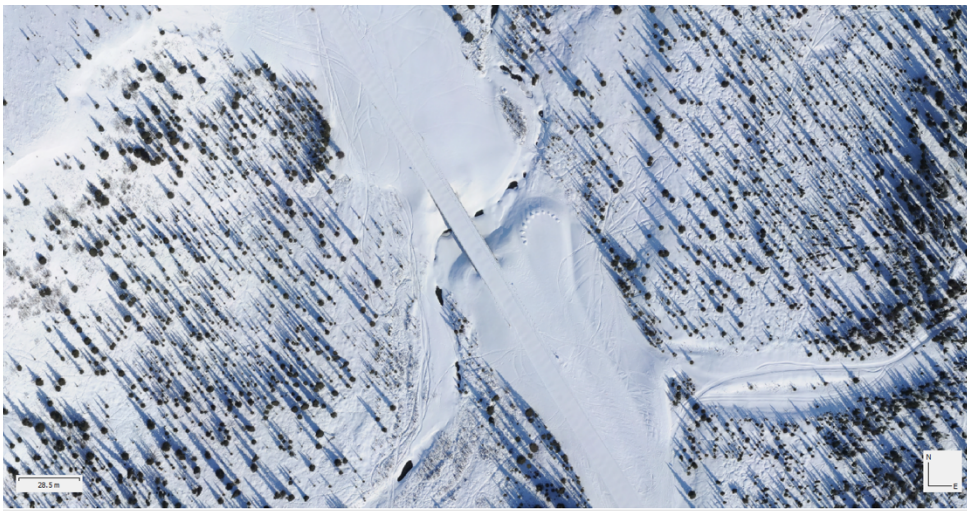

Figure B93: Seattle Creek Bridge orthomosaic from imagery collected by crewed aircraft in April 2018.

Carlo Creek Bridge on the Parks Highway (BN0693)

From UAS:

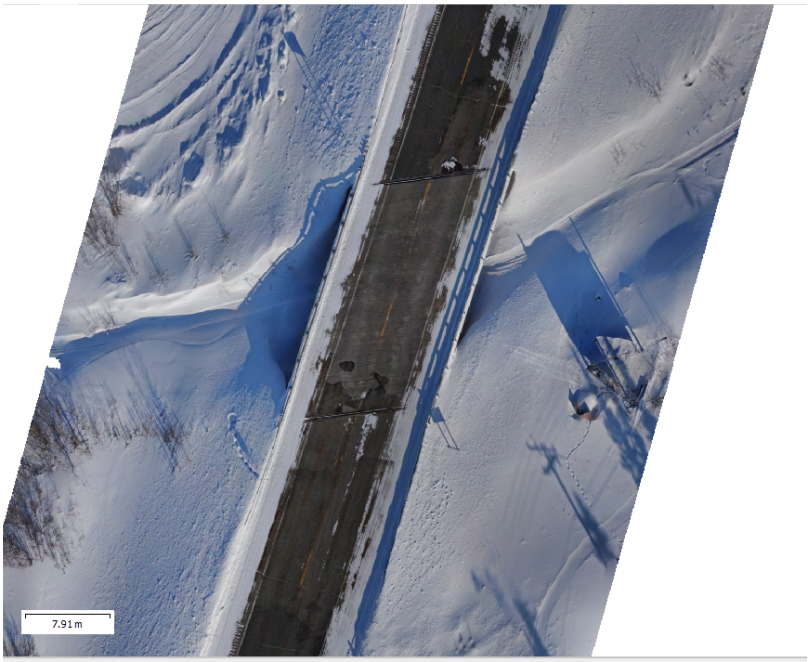

Figure B94: Carlo Creek Bridge orthomosaic from imagery collected by UAS in March 2020.



Figure B95: Carlo Creek Bridge orthomosaic from imagery collected by UAS in April 2020.

From crewed aircraft:

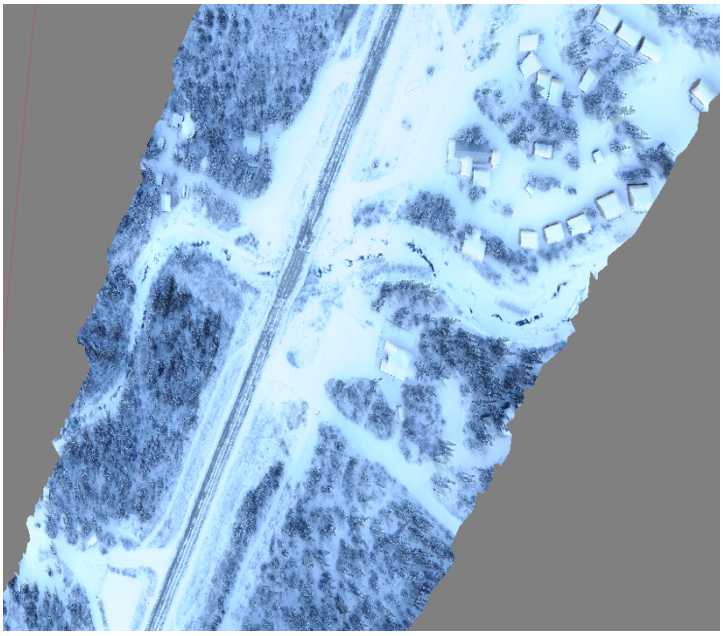
Figure B96: Carlo Creek Bridge orthomosaic from imagery collected by crewed aircraft in October 2016.

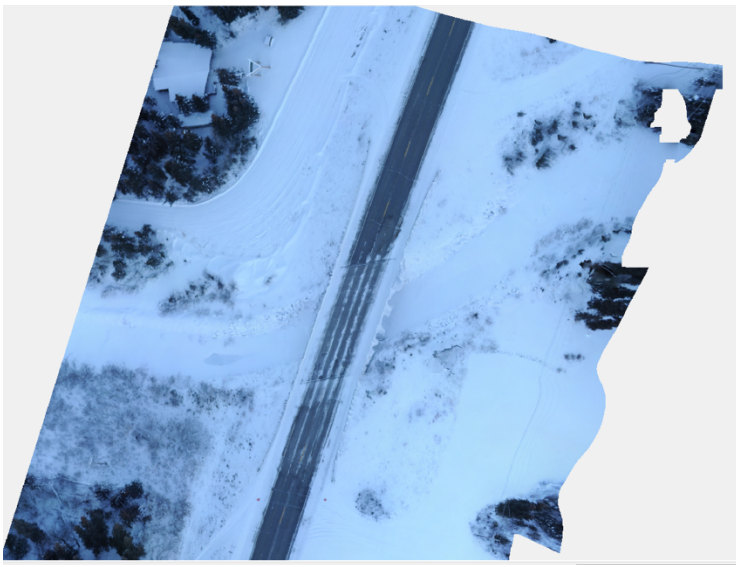

Figure B97: Carlo Creek Bridge orthomosaic from imagery collected by crewed aircraft in December 2016.

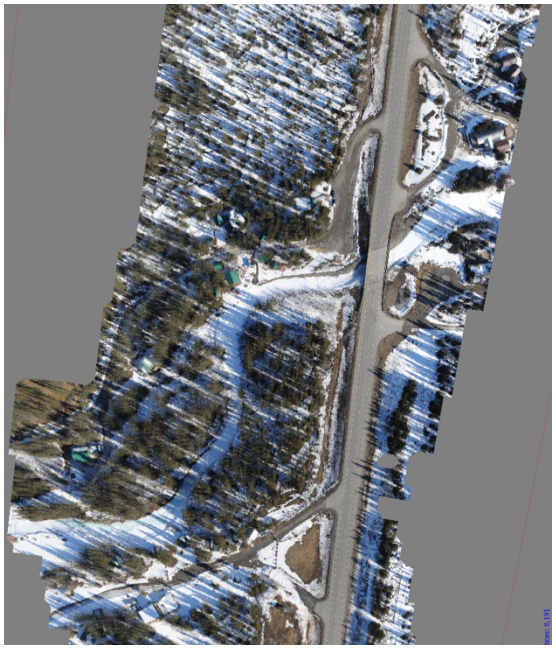

Figure B98: Carlo Creek Bridge orthomosaic from imagery collected by crewed aircraft in April 2017.



Figure B99: Carlo Creek Bridge orthomosaic from imagery collected by crewed aircraft in March 2018.



Figure B100: Carlo Creek Bridge orthomosaic from imagery collected by crewed aircraft in April 2018.

Kingfisher Creek Bridge on the Parks Highway (BN0697)

From UAS:

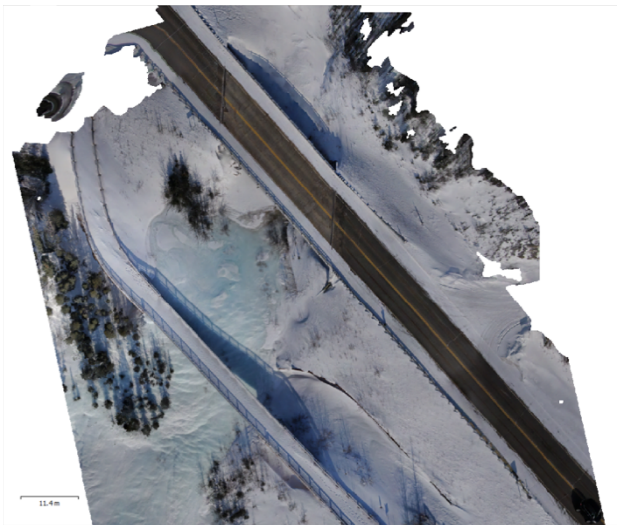

Figure B101: Kingfisher Creek Bridge orthomosaic from imagery collected by UAS in March 2020.

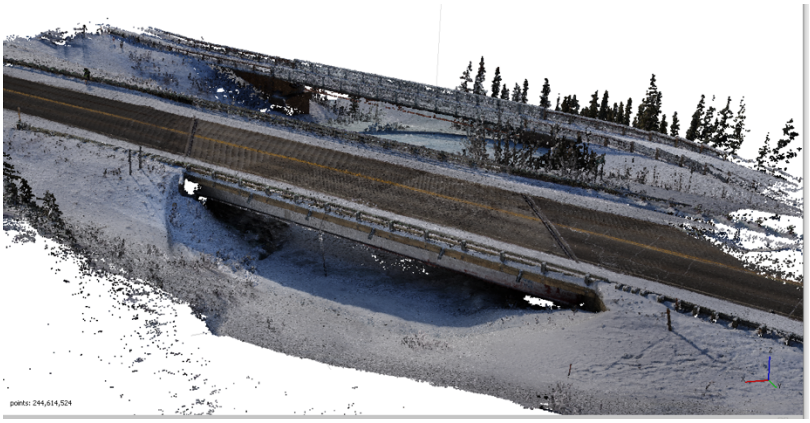

Figure B102: Kingfisher Creek Bridge point cloud from imagery collected by UAS in March 2020.

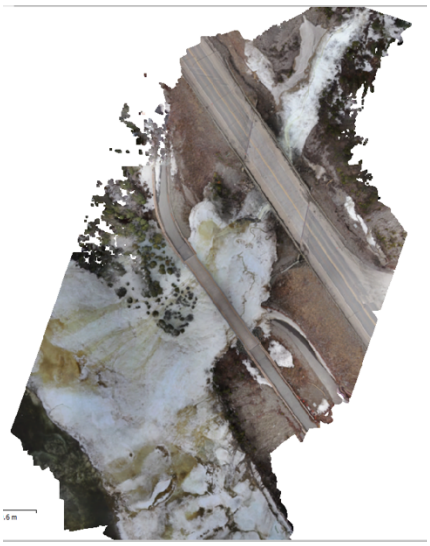

Figure B103: Kingfisher Creek Bridge orthomosaic from imagery collected by UAS in April 2020.



Figure B104: Kingfisher Creek Bridge point cloud from imagery collected by UAS in April 2020.

From crewed aircraft:

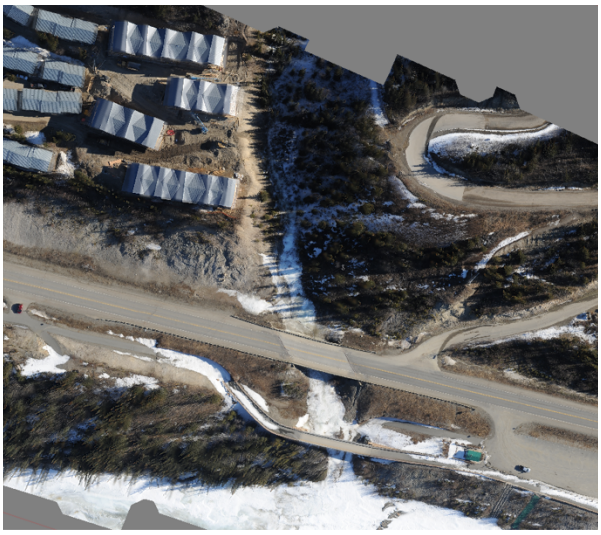

Figure B105: Kingfisher Creek Bridge orthomosaic from imagery collected by crewed aircraft in April 2017.



Figure B106: Kingfisher Creek Bridge orthomosaic from imagery collected by crewed aircraft in November 2017.



Figure B107: Kingfisher Creek Bridge orthomosaic from imagery collected by crewed aircraft in March 2018.



Figure B108: Kingfisher Creek Bridge orthomosaic from imagery collected by crewed aircraft in April 2018.

Goldstream Creek Bridge on Ballaine Road (BN1009)

From UAS:

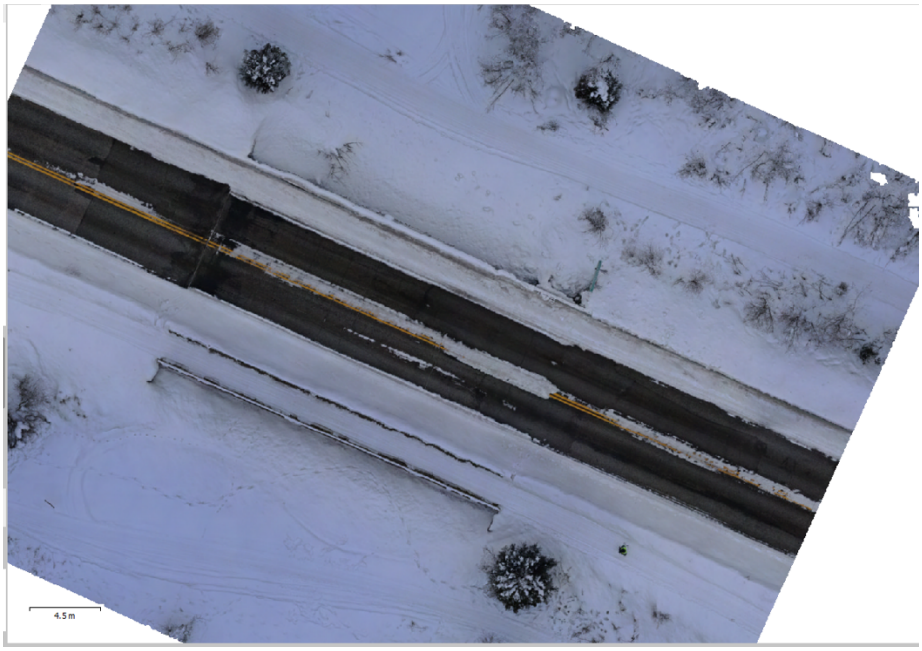

Figure B109: Goldstream Creek Bridge orthomosaic from imagery collected by UAS in March 2020.



Figure B110: Goldstream Creek Bridge point cloud from imagery collected by UAS in March 2020.



Figure B111: Goldstream Creek Bridge point cloud from imagery collected by UAS in March 2020.

From crewed aircraft:



Figure B112: Goldstream Creek Bridge orthomosaic from imagery collected by crewed aircraft in October 2016.

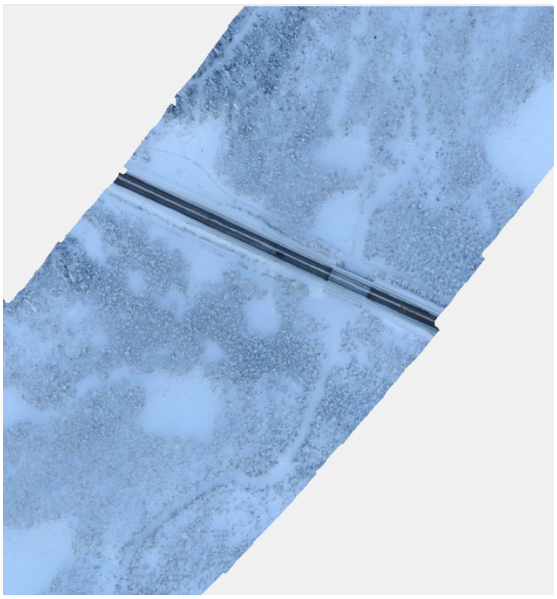

Figure B113: Goldstream Creek Bridge orthomosaic from imagery collected by crewed aircraft in December 2016.

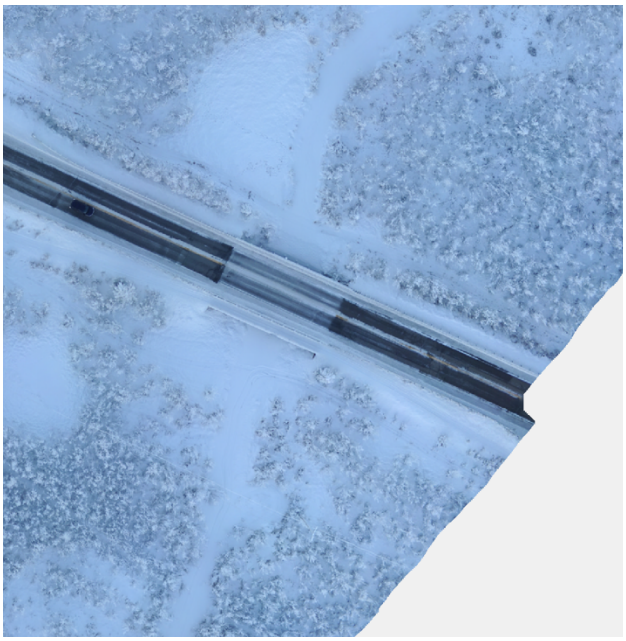

Figure B114: Goldstream Creek Bridge orthomosaic detail from imagery collected by crewed aircraft in December 2016.

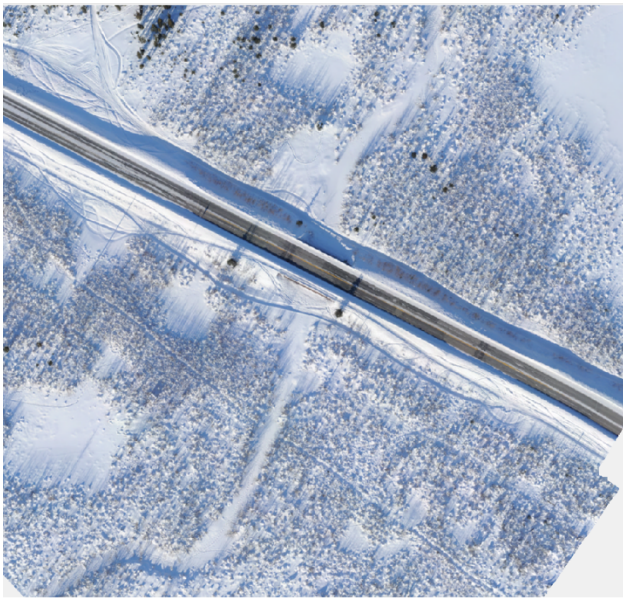

Figure B115: Goldstream Creek Bridge orthomosaic from imagery collected by crewed aircraft in March 2017.



Figure B116: Goldstream Creek Bridge orthomosaic from imagery collected by crewed aircraft in April 2017.

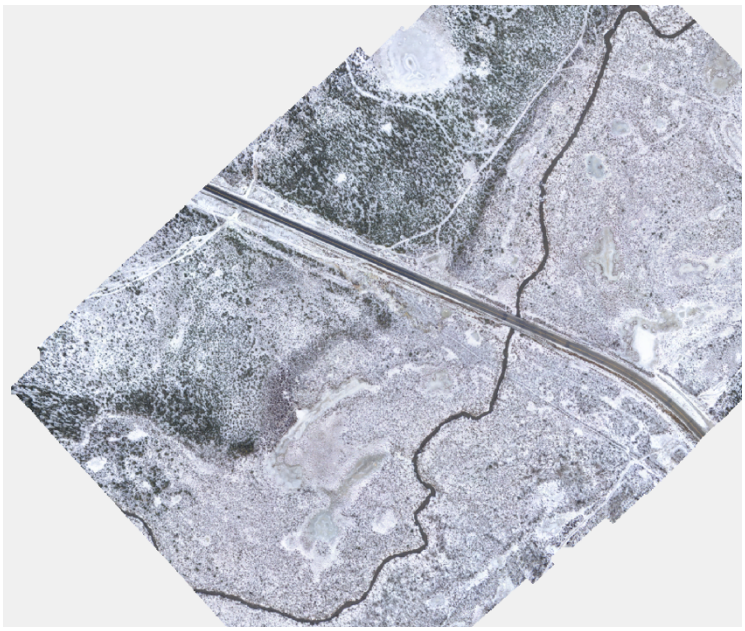

Figure B117: Goldstream Creek Bridge orthomosaic from imagery collected by crewed aircraft in October 2017.

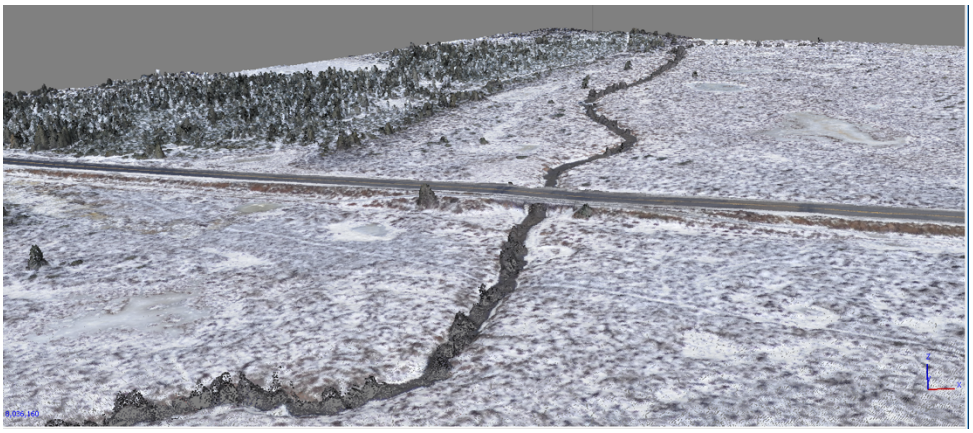

Figure B118: Goldstream Creek Bridge point cloud from imagery collected by crewed aircraft in October 2017.



Figure B119: Goldstream Creek Bridge orthomosaic from imagery collected by crewed aircraft in March 2018.



Figure B120: Goldstream Creek Bridge orthomosaic from imagery collected by crewed aircraft in April 2018.



Figure B121: Goldstream Creek Bridge orthomosaic from imagery collected by crewed aircraft in March 2019.



Figure B122: Goldstream Creek Bridge orthomosaic from imagery collected by crewed aircraft in April 2019.

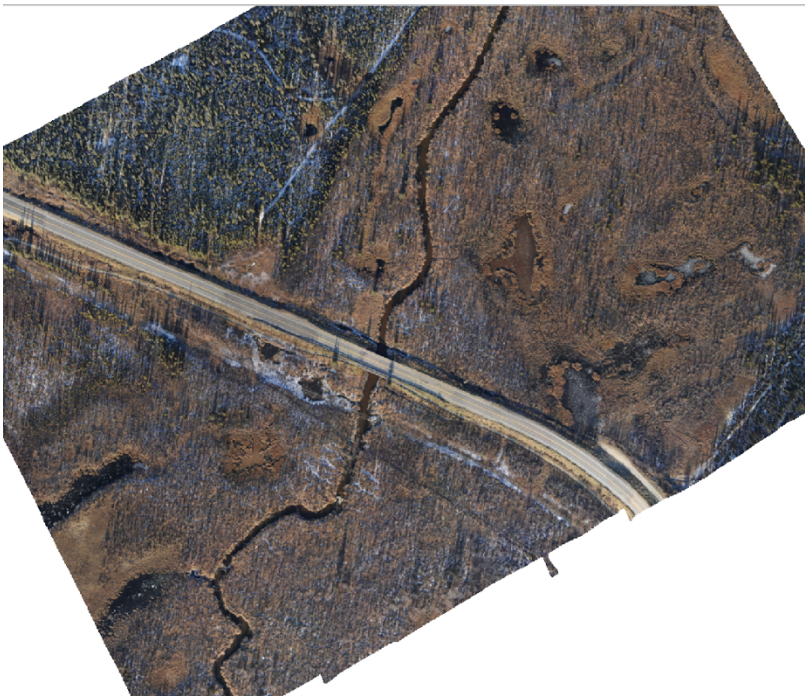
Figure B123: Goldstream Creek Bridge orthomosaic from imagery collected by crewed aircraft in October 2019.

Dragonfly Creek Bridge on the Parks Highway (BN1075)

From UAS:

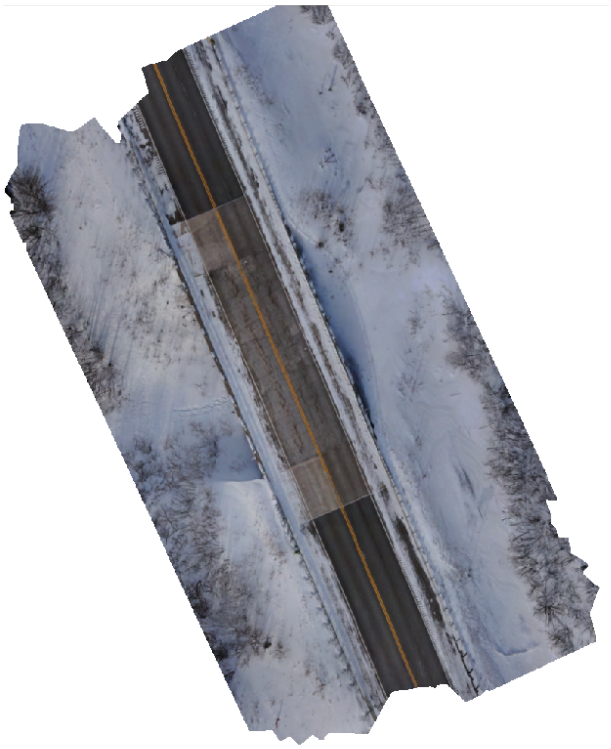

Figure B124: Dragonfly Creek Bridge orthomosaic from imagery collected by UAS in March 2020.



Figure B125: Dragonfly Creek Bridge orthomosaic from imagery collected by UAS in April 2020.



Figure B126: Dragonfly Creek Bridge point cloud from imagery collected by UAS in April 2020.

From crewed aircraft:

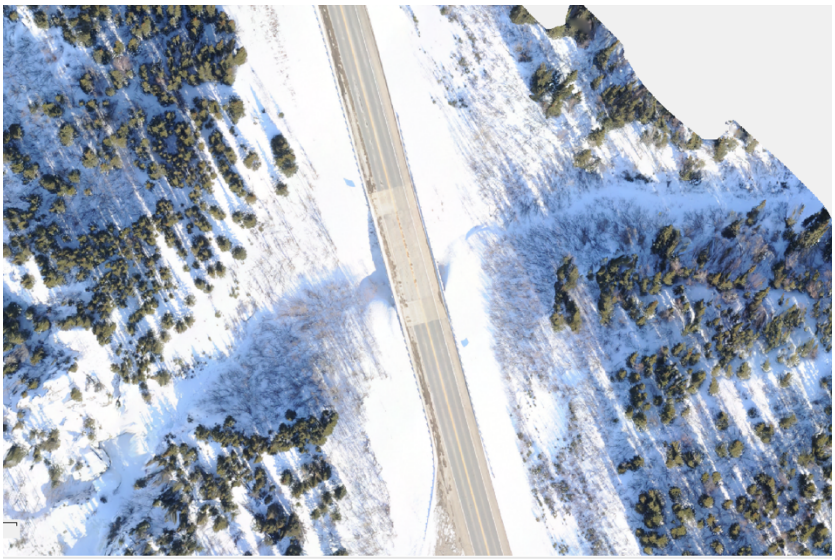
Figure B127: Dragonfly Creek Bridge orthomosaic from imagery collected by crewed aircraft in April 2017.



Figure B128: Dragonfly Creek Bridge orthomosaic from imagery collected by crewed aircraft in March 2018.

Fox Creek Bridge on the Parks Highway (BN1144)

From UAS:

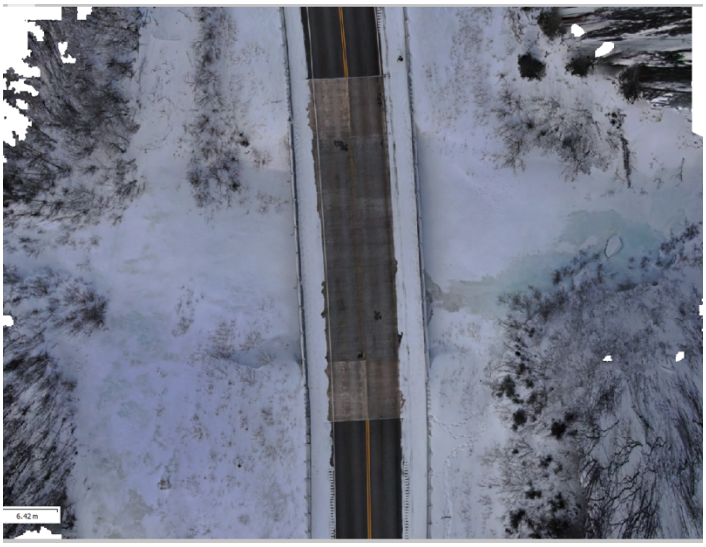

Figure B129: Fox Creek Bridge orthomosaic from imagery collected by UAS in March 2020.


Figure B130: Fox Creek Bridge point cloud from imagery collected by UAS in March 2020.

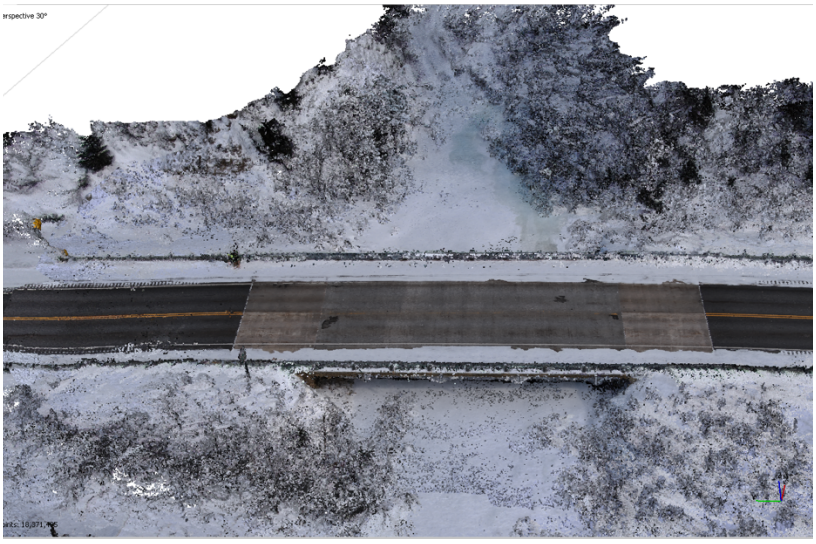
Figure B131: Fox Creek Bridge point cloud from imagery collected by UAS in March 2020.



Figure B132: Fox Creek Bridge orthomosaic from imagery collected by UAS in April 2020.



Figure B133: Fox Creek Bridge point cloud from imagery collected by UAS in April 2020.

From crewed aircraft:



Figure B134: Fox Creek Bridge point cloud from imagery collected by crewed aircraft in November 2017.

Tulsona Creek Bridge on the Tok Cutoff (BN1250)

From UAS:

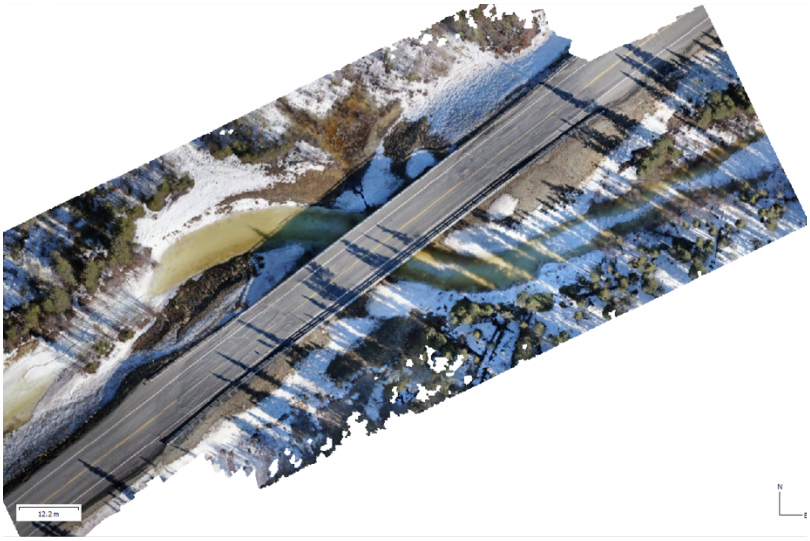

Figure B135: Tulsona Creek Bridge orthomosaic from imagery collected by UAS in April 2020.

From crewed aircraft:

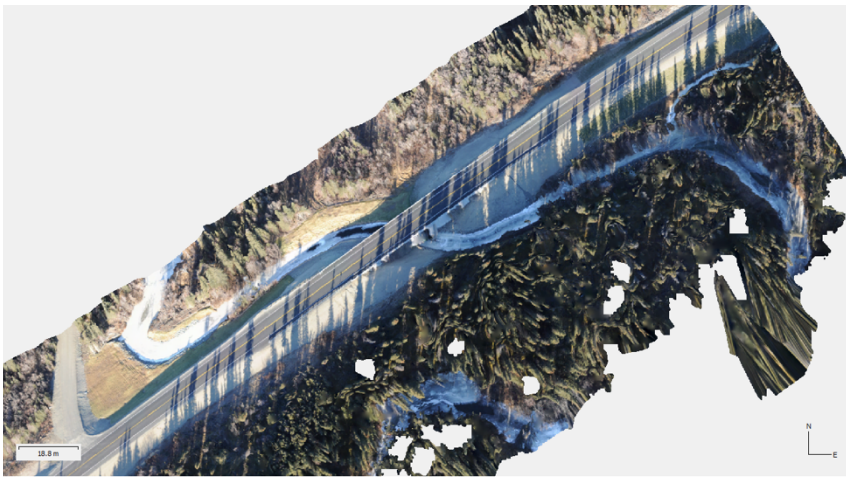

Figure B136: Tulsona Creek Bridge orthomosaic from imagery collected by crewed aircraft in October 2016.

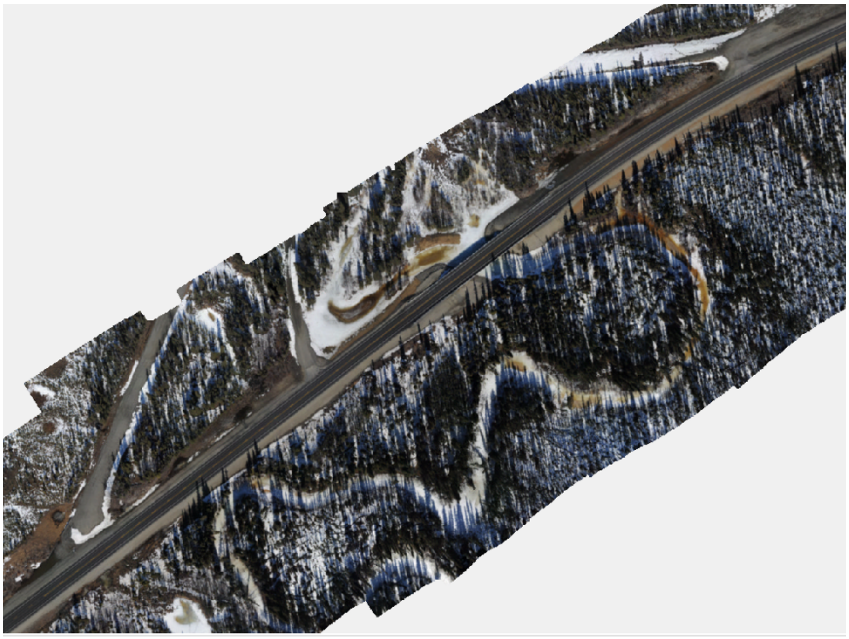

Figure B137: Tulsona Creek Bridge orthomosaic from imagery collected by crewed aircraft in April 2017.



Figure B137: Tulsona Creek Bridge orthomosaic detail from imagery collected by crewed aircraft in April 2017.

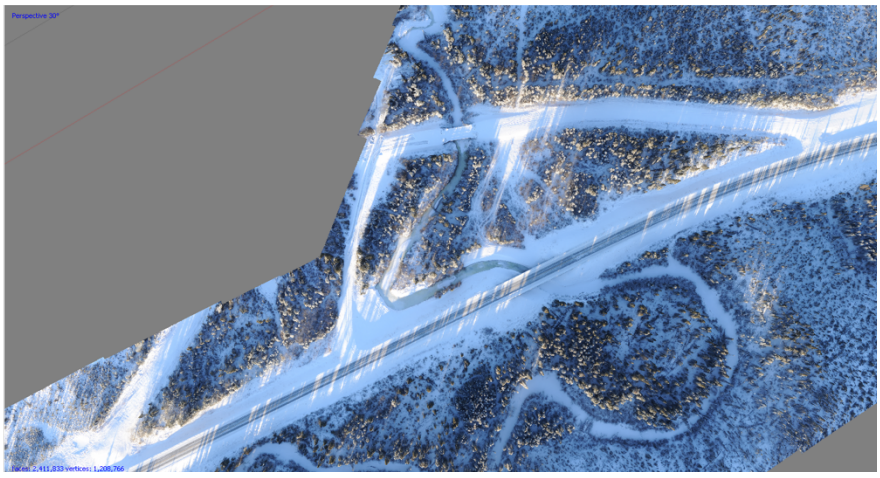

Figure B138: Tulsona Creek Bridge orthomosaic detail from imagery collected by crewed aircraft in November 2017.



Figure B139: Tulsona Creek Bridge orthomosaic detail from imagery collected by crewed aircraft in March 2018.



Figure B140: Tulsona Creek Bridge orthomosaic detail from imagery collected by crewed aircraft in April 2018.